

Solar-Assisted Hybrid Ventilation in an Institutional Building

Eleni Mouriki

A Thesis in the Department of Building, Civil, and Environmental Engineering

Presented in Partial Fulfillment of the Requirements for the Degree of Master
of Applied Science (Building Engineering) at Concordia University

Montreal, Quebec, Canada

May 2009

© Eleni Mouriki, 2009



Library and Archives
Canada

Published Heritage
Branch

395 Wellington Street
Ottawa ON K1A 0N4
Canada

Bibliothèque et
Archives Canada

Direction du
Patrimoine de l'édition

395, rue Wellington
Ottawa ON K1A 0N4
Canada

Your file *Votre référence*
ISBN: 978-0-494-63175-1
Our file *Notre référence*
ISBN: 978-0-494-63175-1

NOTICE:

The author has granted a non-exclusive license allowing Library and Archives Canada to reproduce, publish, archive, preserve, conserve, communicate to the public by telecommunication or on the Internet, loan, distribute and sell theses worldwide, for commercial or non-commercial purposes, in microform, paper, electronic and/or any other formats.

The author retains copyright ownership and moral rights in this thesis. Neither the thesis nor substantial extracts from it may be printed or otherwise reproduced without the author's permission.

In compliance with the Canadian Privacy Act some supporting forms may have been removed from this thesis.

While these forms may be included in the document page count, their removal does not represent any loss of content from the thesis.

AVIS:

L'auteur a accordé une licence non exclusive permettant à la Bibliothèque et Archives Canada de reproduire, publier, archiver, sauvegarder, conserver, transmettre au public par télécommunication ou par l'Internet, prêter, distribuer et vendre des thèses partout dans le monde, à des fins commerciales ou autres, sur support microforme, papier, électronique et/ou autres formats.

L'auteur conserve la propriété du droit d'auteur et des droits moraux qui protègent cette thèse. Ni la thèse ni des extraits substantiels de celle-ci ne doivent être imprimés ou autrement reproduits sans son autorisation.

Conformément à la loi canadienne sur la protection de la vie privée, quelques formulaires secondaires ont été enlevés de cette thèse.

Bien que ces formulaires aient inclus dans la pagination, il n'y aura aucun contenu manquant.


Canada

ABSTRACT

Solar-Assisted Hybrid Ventilation in an Institutional Building

Eleni Mouriki

Natural and mixed mode ventilation systems are now often incorporated in the sustainable design of buildings in order to meet the increasingly stringent energy performance standards. An area of significant interest is the integration of these systems with atria as their large glazed spaces – a widespread feature in modern building design – have an untapped potential to enhance natural/ hybrid ventilation.

This study presents experimental and complementary simulation results based on the long-term monitoring performed in an institutional building. The objective is to evaluate the performance of the building's natural ventilation system, examine its impact on the indoor conditions and assess its night cooling potential.

Long-term monitoring consisted of temperature and airflow measurements at the top atrium of the building, along with pressure difference and airflow measurements at the exterior air inlet grilles in the upper building levels. Experiments also included night-time ventilation rates and slab temperature measurements at lower building levels. A mathematical model was developed to estimate the cooling storage capacity of the slab.

The natural ventilation system at its present operation is able to cover only part of the building's cooling requirements. The application of modified ventilation strategies at night, making use of the building's thermal mass and cool outdoor air, holds a significant cooling potential. In order to achieve optimal performance and to avoid occupants'

discomfort due to overcooling, a predictive control strategy should be implemented in the building. These operating strategies can be generalized for similar hybrid ventilation systems in buildings with high thermal mass.

ACKNOWLEDGMENTS

I would like to thank my supervisors Dr. A.K. Athienitis and Dr. T. Stathopoulos for their advice and support throughout my graduate studies.

I have no words to express my gratitude to Dr. P. Karava for her continuous encouragement, patience and understanding, and her (always) constructive guidance. I am very fortunate to have received her personal and professional support.

Special thanks to Denis Dumont, Luc Demers, Yves Gilbert and Jacques Payer. Their help is greatly appreciated.

I am also thankful to Dr. K.W. Park for his valuable assistance in the experiments and his high quality drawings he provided for my thesis and on every occasion where I needed them.

I am grateful to my good friends and colleagues for their faith in me, their understanding and encouragement. Your friendship and useful advice helped me complete this thesis.

Finally I want to thank my parents and my brother who, even though they are so far away, they never ceased to support me in some many ways throughout the entire length of my studies. This great opportunity to come study in Canada, I owe it to them.

Financial support of this work was provided by NSERC through the Solar Buildings Research Network.

TABLE OF CONTENTS

| | |
|---|-----|
| LIST OF FIGURES | vii |
| LIST OF TABLES | x |
| NOMENCLATURE | xi |
| 1. INTRODUCTION | 1 |
| 1.1. Background and context | 1 |
| 1.2. Objectives and scope | 3 |
| 1.3. Thesis layout | 4 |
| 2. LITERATURE REVIEW | 6 |
| 2.1. Design parameters - flow characteristics, temperature and airflow predictions | 7 |
| 2.1.1. Thermal and airflow studies in natural (wind/ buoyancy forces) or mechanical ventilation | 7 |
| 2.1.2. Flow enhancement in an atrium – single storey configuration | 13 |
| 2.1.3. Opening configurations | 14 |
| 2.2. Simulation programs – limitations, coupling methods, modifications and testing applicability | 15 |
| 2.3. Performance evaluation of mixed mode buildings | 22 |
| 2.3.1. Thermal comfort in naturally ventilated environments | 22 |
| 2.3.2. Thermal performance – impact of climatic conditions and user behaviour | 23 |
| 2.3.3. Thermal performance of naturally ventilated atrium buildings – simulation and monitoring studies | 28 |
| 2.4. Summary | 30 |
| 3. EXPERIMENTAL SETUP | 31 |
| 3.1. Building description | 31 |
| 3.2. Hybrid ventilation system | 33 |
| 3.3. Natural ventilation system performance | 36 |
| 3.3.1. Initial short-term measurements | 37 |
| 3.3.2. Thermal and airflow monitoring in the atrium | 38 |
| 3.3.3. Airflow monitoring at the corridor grilles | 41 |
| 3.4. Installation | 44 |
| 4. HYBRID VENTILATION SYSTEM PERFORMANCE | 46 |
| 4.1. Natural ventilation system operation hours | 46 |
| 4.2. Temperature Measurements | 50 |
| 4.2.1. Natural ventilation system in operation | 50 |

| | |
|---|-----|
| 4.2.2. Natural ventilation system not in operation | 57 |
| 4.3. Airflow measurements | 62 |
| 4.3.1. Airflow through the corridor inlet grilles..... | 62 |
| 4.3.2. Airflow through the floor grilles | 68 |
| 4.5. Energy performance of the building during the cooling season..... | 69 |
| 4.5.1. Energy savings in the building..... | 69 |
| 4.5.2. Estimation of cooling load reduction..... | 69 |
| 4.6. Cooling load in the atrium | 73 |
| 4.7. Summary..... | 75 |
| 5. NIGHT VENTILATION COOLING POTENTIAL – EXPERIMENTAL AND SIMULATION RESULTS | 78 |
| 5.1. Night time ventilation..... | 78 |
| 5.1.1. Night ventilation hours | 78 |
| 5.1.2. Night ventilation cooling potential | 80 |
| 5.2. Night time airflow and floor slab surface temperature measurements | 85 |
| 5.2.1. Slab surface temperature and airflow through the corridor inlet grilles on floor 6 | 87 |
| 5.2.3. Airflow rate measurements at corridor inlet grilles on floors 4 – 16..... | 89 |
| 5.3. Mathematical model for slab surface temperature change and heat removal prediction..... | 92 |
| 5.3.2. Surface temperature of the floor slab at different distances from the SE side inlet grilles..... | 102 |
| 5.3.3. Heat removed from the floor slab..... | 104 |
| 5.4. Summary..... | 107 |
| 6. CONCLUSIONS AND RECOMMENDATIONS | 109 |
| 6.1. Summary and conclusions | 109 |
| 6.2. Design and future work recommendations | 112 |
| REFERENCES | 113 |
| APPENDIX I: Instrumentation..... | 120 |
| APPENDIX II: Indoor and outdoor conditions | 129 |
| APPENDIX III: Mathcad calculation sheet..... | 154 |

LIST OF FIGURES

| | |
|---|----|
| Figure 2.1. Predicted ACH rate as a function of external wind speed, for all wind directions and the two vent model (DV). (Horan and Finn, 2008) | 11 |
| Figure 2.2. Predicted ACH rate plotted against wind direction for the double ventmodel (DV). (Horan and Finn, 2008)..... | 12 |
| Figure 2.3. Proposed adaptive comfort standard (ACS) for ASHRAE Standard 55, applicable for naturally ventilated building (De Dear et al., 2002)..... | 23 |
| Figure 2.4. Hourly measured air and surface slab-temperature variations over 24 h in an open-plan office with and without natural night-ventilation.. It shows that night ventilation reduces air and slab temperatures, and delays the peak internal temperature to later in the day (Kolokotroni, 1998) | 24 |
| Figure 2.5. Detailed stack airflow rate response for the Enschede Tax Office building to Los Angeles’ summer conditions operated in a natural night cooling mode. Results plotted for two assumed combined solar and internal gains—20 W/m ² and 30 W/m ² (Axley et al. 2002)..... | 25 |
| Figure 2.6. Comparison of the library’s annual energy consumption during 2004 with ECON19 benchmark values for typical and good practice offices (Krausse et al., 2007) 28 | 28 |
| Figure 3.1. Outside view of Concordia EV building and the 15-storey atrium on the SW façade (left), inside view of the top atrium (right) | 32 |
| Figure 3.2. Natural ventilation concept (design phase) | 33 |
| Figure 3.3. Corridor inlet grilles (left), atria connecting floor grilles (right)..... | 34 |
| Figure 3.4. Atrium air supply unit (left), outlet grilles to exhaust the air (right)..... | 34 |
| Figure 3.5. Hybrid ventilation in the atrium | 35 |
| Figure 3.6. Air exchange between 5-connecting atria and adjacent corridors during natural ventilation | 36 |
| Figure 3.7. Indicated by markers, thermocouples mounted near the façade (top), close to the east, west atrium walls and staircase (bottom left), at the back of the atrium space (bottom right) | 39 |
| Figure 3.8 Atrium schematic with thermocouples on the façade, the east and west atrium walls..... | 39 |
| Figure 3.9. Side view of thermocouples mounted near the façade..... | 39 |
| Figure 3.10. Velocity sensor mounted at the corridor grilles..... | 42 |
| Figure 3.11. Area of slab surface temperature measurements (indicated by circle) near the corridor inlet grilles | 43 |
| Figure 3.12. Movable lift used to attach thermocouples | 44 |

| | |
|--|----|
| Figure 4.1. Natural ventilation hours over total period hours per month for 2007 and 2008 cooling seasons..... | 47 |
| Figure 4.2. Atrium average temperatures under hybrid ventilation for different outdoor conditions..... | 51 |
| Figure 4.3. Air temperature variation throughout the day at six different heights near the façade..... | 53 |
| Figure 4.4. Air temperature variation throughout the day at three different heights in the atrium space | 53 |
| Figure 4.5. Air temperature profile a) near the façade (middle section), b) near the façade (all sections), c) in the atrium space; data based on peak temperature values | 54 |
| Figure 4.6. Air temperature variation throughout the day at six different heights near the façade..... | 55 |
| Figure 4.7. Air temperature variation throughout the day at three different heights in the atrium space | 56 |
| Figure 4.8. Air temperature profile a) near the façade (middle section), b) near the façade (all sections), c) in the atrium space; data based on peak temperature values | 56 |
| Figure 4.9. Air temperature variation throughout the day at six different heights near the façade..... | 58 |
| Figure 4.10. Air temperature variation throughout the day at three different heights in the atrium space | 58 |
| Figure 4.11. Air temperature profile a) near the façade (middle section), b) near the façade (all sections),c) in the atrium space; data based on peak temperature values | 59 |
| Figure 4.12. Air temperature variation throughout the day at six different heights near the façade..... | 61 |
| Figure 4.13. Air temperature variation throughout the day at three different heights in the atrium space | 61 |
| Figure 4.14. Air temperature profile a) near the façade (middle section), b) near the façade (all sections), c) in the atrium space; data based on peak temperature values | 62 |
| Figure 4.15. Airflow rate and pressure difference across the SE side inlet grilles | 64 |
| Figure 4.16. Airflow rate and pressure difference across the NW side inlet grilles | 64 |
| Figure 4.17. Airflow rate and pressure difference across SE side inlet grilles | 65 |
| Figure 4.18. Airflow rate and pressure difference across NW side inlet grilles | 66 |
| Figure 4.19. Airflow rate and pressure difference across SE side inlet grilles | 67 |
| Figure 4.20. Airflow rate and pressure difference across NW side inlet grilles | 67 |

| | |
|---|-------------------------------------|
| Figure 4.21. Airflow rate at top atrium floor grilles as a function of $\Delta T_{\text{indoor-outdoor}}$ | 68 |
| Figure 5.1. Calculated night ventilation time for three night ventilation schedules (based on 2007 weather data)..... | 79 |
| Figure 5.2. Calculated night ventilation time for three night ventilation schedules (based on 2008 weather data)..... | 79 |
| Figure 5.3. Internal heat gain that can be offset under different night ventilation schedules (based on 2007 weather data)..... | 83 |
| Figure 5.4. Internal heat gain that can be offset under different night ventilation schedules (based on 2008 weather data)..... | 83 |
| Figure 5.5. Corridor inlet grilles manually kept open a) on floor 6 (left), b) on all floors (right)..... | 86 |
| Figure 5.6. Slab surface temperature near the inlet grilles on floors 5 and 6..... | 88 |
| Figure 5.7. Airflow rates at corridor inlet grilles at different building heights..... | 90 |
| Figure 5.8. Measured and calculated airflow rates through the corridor inlet grilles at different building heights..... | 91 |
| Figure 5.9. Schematic of the modeled slab..... | 92 |
| Figure 5.10. Corridor divided in control volumes..... | 93 |
| Figure 5.11. Measured and calculated slab surface temperature near the SE and NW inlet grilles on floor 6..... | 101 |
| Figure 5.12. Measured slab surface temperature at different distances from the SE inlet grilles on floor 6..... | 103 |
| Figure 5.13. Calculated slab surface temperature at different distances from the SE inlet grilles on floor 6..... | Error! Bookmark not defined. |
| Figure 5.14. Calculated heat removal from the 30 m long slab for a 10 hour period under different outdoor temperature ranges..... | 105 |

LIST OF TABLES

| | |
|--|-----|
| Table 3.1. Areas and dimensions in the top atrium (floors 14-16)..... | 32 |
| Table 3.2. Air temperature – Number of thermocouples mounted in the atrium space | 40 |
| Table 3.3. Air and surface temperatures – Number of thermocouples mounted on the atrium façade | 40 |
| Table 4.1. Mean monthly outdoor temperature and RH% for years 2007, 2008 (Source: Environment Canada, Montréal-Trudeau Int'l Airport weather data station) | 47 |
| Table 4.2. Hourly and daily NV operating rates as a % of total period hours and days ... | 49 |
| Table 4.3. Wind, ΔT and airflow data for three different cases | 63 |
| Table 4.4. Estimated ‘free cooling’ rates from natural ventilation - first approach | 72 |
| Table 4.5. Estimated ‘free cooling’ rates from natural ventilation - second approach | 72 |
| Table 4.6. Estimated free cooling from natural ventilation (based on a 6-hour workday time period) | 72 |
| Table 4.7. Enthalpy of the air at different inlet/ outlet sources and transmitted solar radiation | 75 |
| Table 4.8. Thermal monitoring in the atrium..... | 76 |
| Table 4.9. Airflow monitoring at the corridor inlet grilles | 77 |
| Table 5.1. Average internal gains that can be offset (based on a 10-hour workday) and % cooling rate increase (2007)..... | 84 |
| Table 5.2. Average internal gains that can be offset (based on a 10-hour workday) and % cooling rate increase (2008)..... | 84 |
| Table 5.3. Outdoor temperature and airflow rates at corridor inlet grilles of floor 6..... | 87 |
| Table 5.4. Building height and airflow rates on floors 4 – 10 | 90 |
| Table 5.5. Values used to calculate the stack induced airflow through the inlet grilles.... | 91 |
| Table 5.6. Floor slab and air properties | 100 |
| Table 5.7. Calculated and measured slab surface total temperature drop on floor 6 | 102 |
| Table 5.8. Measured and predicted slab surface maximum temperature difference at different distances from the SE corridor inlet grilles on floor 6 | 103 |
| Table 5.9. Calculated heat flow rate and heat removed from the slab over a 10-hour period | 104 |
| Table 5.10. Heat removed from a 864 m ² slab area and cooling time needed under different outdoor temperatures | 106 |

NOMENCLATURE

| | |
|---------------------|--|
| A | cross sectional area of opening, m ² |
| A _{gr} | inlet grilles opening area, m ² |
| A _{slab} | floor slab area per control volume, m ² |
| A _w | area of the massive wall, m ² |
| c | specific heat capacity of the massive layer, J/kg·°C |
| C _d | discharge coefficient |
| C _p | specific heat capacity, J/ kg·°C |
| d | penetration depth, cm |
| g | gravitational acceleration, m/s ² |
| h | convective heat transfer coefficient, W/m ² ·°C |
| h _i | convective heat transfer coefficient at control volume i, W/m ² ·°C |
| H | building height at neutral pressure level, m |
| H _d | height from midpoint of lower opening to neutral pressure level, m |
| i | √-1 |
| k | thermal conductivity of the massive layer, W/m·°C |
| k _s | thermal conductivity of the floor slab, W/m·°C |
| k _f | thermal conductivity of the air, W/m·°C |
| L _w | thickness of the massive layer, m |
| L | characteristic length (distance from leading edge), m |
| M | mass flow rate, kg/sec |
| Nu | Nusselt number |
| P | period, s |
| Pr | Prandtl number |
| q | free cooling rate, W |
| \bar{q}_{cool} | average internal gain that can be offset, W |
| q _{night} | heat transfer rate for energy removed at night, W |
| q _{Sk,i-1} | convective heat flow to floor at time k and control volume i-1, W/m ² ·°C |
| Q _s | volumetric flow rate (m ³ /sec) |
| Re | Reynolds number |
| s | Laplace transform variable, j·ω for admittance calculations |
| t | time, hr |

| | |
|-----------------------|---|
| T_{exhaust} | temperature at the exhaust, °C |
| T_{e-i} | outdoor temperature – temperature of the air stream at time (i-1), °C |
| T_i | indoor temperature, °C or K |
| $T_{i\text{-csp}}$ | cooling set-point temperature, °C |
| T_{ij} | floor slab temperature at time i and depth j, °C |
| $T_{i-1,j}$ | floor slab temperature at time i-1 and depth j, °C |
| T_o | outdoor temperature, °C or K |
| $T_{o_{k,i-1}}$ | temperature of the air stream at time k and control volume i-1, °C |
| $T_{o_{k-1,i}}$ | temperature of the air stream at time (k-1) and control volume i, °C |
| $T_{S_{k,i}}$ | floor surface temperature at time k and control volume i, °C |
| $T_{S_{k-1,i}}$ | surface floor temperature at time k-1 and control volume i, °C |
| T_{∞} | temperature of the fluid, °C |
| $T(0,t)$ | solid temperature at $x=0$ and time t (surface temperature), °C |
| u | conductance behind the massive layer, $\text{W}/\text{m}^2\cdot\text{°C}$ |
| U | velocity of the air stream, m/sec |
| Y_{S_x} | self-admittance of massive wall of thickness x, $\text{W}/\text{°C}$ |
| $Y_{S_{\infty}}$ | self-admittance of very thick massive wall, $\text{W}/\text{°C}$ |
| x | medium (solid) depth, m |
| x_j | floor slab depth, m |
| α | thermal diffusivity of the wall/ floor slab, m^2/sec |
| α_{air} | thermal diffusivity of the air, m^2/sec |
| γ | $(s/\alpha)^{1/2}$ |
| Δt | workday time period, hours |
| ν | kinematic viscosity of the air, m^2/sec |
| ρ | density of the massive layer, kg/m^3 |
| ρ_{air} | density of the air, kg/m^3 |
| ω | frequency, s^{-1} |

1. INTRODUCTION

1.1. Background and context

Buildings account for about 30% of Canada's energy consumption, 50% of its electricity consumption and roughly 28% of its greenhouse gas (GHG) emissions (NRCan, 2006). In the context of sustainable development and with growing worldwide concern about building energy efficiency and climate change, there is a renewed interest in natural ventilation, a process that has been used in buildings for many centuries in the form of wind catchers/towers. The same basic principles of natural ventilation are used in modern design, integrating natural ventilation systems in buildings and using advanced technology to maximize energy savings. Climate characteristics (weather conditions, location) can restrict the potential of natural ventilation. While temperate climates allow for a building to be naturally ventilated throughout most part of the year, cold or hot/humid climates are more challenging and require careful design.

Mixed mode or hybrid ventilation is often adopted in sustainable buildings in most climates. Hybrid ventilation systems can be described as two-mode systems using features of both passive and active systems at different times of the day or season (Heiselberg, 2002). They combine natural ventilation, fan-driven ventilation, and mechanical air conditioning and can reduce energy operating costs and CO₂ emissions. Ventilation systems should be properly controlled to ensure that gains are removed and not added to the building; for example, not introduce outside air when that air is at a temperature greater than that in the building (other than the amount required to maintain air quality).

Bourgeois et al. (2002) performed a feasibility study on hybrid ventilation in office buildings in Canada and concluded that there are both barriers and opportunities related to its applicability. The largest barriers are related to climate and building regulations, yet solutions are available in most cases. Opportunities, such as integrating hybrid ventilation systems with solar technologies (e.g. atria or double façades), can lead to additional energy savings. For example, atria, as opposed to office zones, can act as a thermal buffer zone where comfort conditions do not need to be strictly controlled. The open space concept of atria, with high ceilings, also enhances buoyancy-driven flows.

An additional element of mixed mode cooling of buildings, applicable in many climates, is night ventilation. This technique utilizes the thermal mass of the building for cooling storage at night (Spindler and Norford, 2009). In general, for buildings with high thermal mass, efficient ventilation strategies can reduce the cooling load. During the day, ventilation is used to either remove the heat gains directly or transfer them to the building's mass. At night, heat gains are much lower or even negative and colder outdoor air can be used to remove heat from the surfaces. The magnitude of convective heat transfer between air and surfaces is important in these passive-cooling strategies, determining the efficiency of the night cooling system (Carrilho da Graça, 2003).

The motivation for research arises from the need for improved design in order to meet increasingly demanding energy and thermal comfort criteria. In the design of naturally/mixed mode ventilated buildings, several issues are addressed, i.e. sufficient ventilation rates, optimal orientation of the building and atria façades, prevailing climatic conditions, thermal comfort and energy consumption. Integrating atria as part of a building's natural ventilation system poses an additional challenge in the design as large tall glazed spaces,

although they enhance natural ventilation, are susceptible to glare and overheating problems. The use of simulation programs and the practical assessment of ventilation systems and indoor conditions can facilitate several design aspects of such buildings.

1.2. Objectives and scope

During the early design stages of the Engineering building of Concordia University, several design options for the façade and building envelope were proposed (Tzempelikos et al., 2007). The purpose of the simulation study was to design a high performance building with reduced energy consumption for cooling, heating and lighting while maintaining comfortable indoor conditions. In order for the design to produce an energy efficient building, innovative technologies such as natural ventilation and daylighting were employed. Recommendations were made on the selection of the natural ventilation strategies, glazings, shading devices and lighting controls.

The present thesis is the first stage of a long-term project that has the objective of developing simulation strategies (e.g. coupled thermal-airflow and CFD models) for hybrid ventilation systems integrated with atria, as well as design guidelines and control strategies for the shading system (Park et al., 2008), the inlet openings and the HVAC system suitable for Canadian climatic conditions. The main objective of the present study is to evaluate the performance of the natural ventilation system during the operation phase of the building, under real conditions. The building's passive design features (i.e. stack and wind-driven natural ventilation, high level of exposed thermal mass, large glazed façades oriented west of South and receiving high amounts of solar radiation –

thus enhancing natural ventilation – and motorized roller shades) create a space ideal for the experimental investigation of a natural ventilation system and the assessment of its cooling potential.

Long-term monitoring and manual measurements were employed to evaluate the indoor conditions in the atrium and determine the ventilation flow rates. The atrium has already been used as a case study and monitoring results (Mouriki et al., 2008) have been used to validate CFD simulation programs (Cable et al. 2007, Basarir et al, 2009).

The study also originally aimed at estimating the energy consumption in the building for cases when the building is in mechanical or hybrid ventilation. Unfortunately such data from the building energy management system (BEMS) are not available therefore a simplified approach to estimate the energy savings was undertaken. A simple mathematical model was developed to quantify the energy savings attributed to the night cooling. The study considered the existing natural ventilation schedule and modified schedules in order to investigate whether night cooling strategies (i.e. night ventilation at lower outdoor temperatures) that were originally suggested but not adopted in the design of the building, could have resulted in improved performance.

1.3. Thesis layout

A review of existing research on natural/ hybrid ventilation is performed in the first part of the thesis, Chapter 2. Predicting airflow and temperature patterns, examining parameters such as wind and buoyancy forces, improving temperature and airflow predictions by coupling methods and investigating thermal comfort and system

performance issues in naturally ventilated buildings are among the topics of the studies conducted in the papers reviewed.

Chapter 3 describes the Concordia University Engineering building and the natural ventilation system used. The experimental set-up is also presented, along with the instrumentation used.

Results for the ventilation system performance are presented in Chapter 4, including the airflow rates through the motorized grilles, the indoor environmental conditions in the atrium, as well as the energy savings.

Theoretical and experimental results for the night cooling potential to reduce the building's cooling load are presented in Chapter 5. Experimental values are combined with a simple mathematical model to estimate the cooling storage capacity of the concrete slab.

The main conclusions drawn from this research are summarized in Chapter 6, together with design guidelines and recommendations for future work.

2. LITERATURE REVIEW

Introduction

Natural/hybrid ventilation systems integrated with atria are increasingly used in commercial buildings to reduce energy consumption for cooling and ventilation while promoting indoor air quality and comfort. Atria are being incorporated for aesthetic reasons as well as to facilitate passive building design, e.g. by providing daylight and solar heat gains in the winter and enhancing buoyancy-driven flows during the summer.

The need for improved design on natural ventilation and atria has been the motivation for numerous studies. Atria's large space and extended glazing surface give way to complex airflow and temperature distribution patterns. These phenomena are less significant in conventional rooms, thus rendering simulation programs inadequate for atria spaces.

Through simulation programs and experiments, there has been an attempt to identify flow characteristics and the parameters that affect them, as well as to predict temperature and airflow patterns in ventilated enclosures. Wind and buoyancy forces are among the most common parameters considered in studies while combined enclosures and vents configurations have also been examined. A considerable number of studies, identifying certain limitations that exist in simulation programs, are oriented towards improving temperature and airflow predictions by modifying or coupling simulation methods. Finally, much research has been done in monitoring the thermal performance of passively designed buildings, addressing issues such as energy consumption, thermal comfort, and control strategies, while simulations have been used as a practical way to evaluate the performance of these buildings under different conditions.

2.1. Design parameters - flow characteristics, temperature and airflow predictions

2.1.1. Thermal and airflow studies in natural (wind/ buoyancy forces) or mechanical ventilation

A preliminary assessment of natural ventilation in buildings is done by Joubert and Mathews (1989) who developed a simplified thermal network simulation model aiming at predicting indoor conditions in a building with open windows. They point out how a comprehensive simulation program to predict the indoor environment of a future building is sometimes not practical or economical since input data is not available and the building configuration is not fully defined. Their model is based on theoretical considerations while also having empirical constants. Four buildings are used to validate the method for a range of designs. A good agreement between predicted and measured values is observed. They conclude that the simplified model proves to be reliable in predicting the thermal performance of a ventilated building and therefore it is a useful tool for any designer who wishes to economically assess their different design options. Interaction between airflows and indoor air temperatures is not considered in this study.

Rousseau and Mathews (1996) enhanced the thermal network model by adding it to a flow network model to predict both ventilation flow rates and indoor temperatures in naturally ventilated buildings. Empirical data is used as input in the model and its applicability is tested through a case study, a factory building in South Africa. They consider both wind and buoyancy forces when developing the model – making the assumption that the “effective” pressures of these forces can be added (Sinden, 1978) –

but a windless summer design day is examined. It is found that the combination of roof insulation and roof ventilators would result in the most reduced indoor temperatures. They conclude that insulation is necessary – as it will also aid in controlling heat losses in the winter – and that there is a maximum number of roof ventilators (expressed as % of floor area) above which the resulting indoor temperatures will not be much lower. The study suggests the model is a useful tool to optimize passive building design. However, there is a lack in experimental measurements that would validate/ calibrate the model and while it is addressing the important issue of both thermal and airflow predictions, the simplicity of the building and the absence of internal loads may affect its applicability to other more complex buildings.

Hunt and Linden (1999) use a simple mathematical model to predict temperatures and thermal stratification in a space. The enclosure studied is subject to wind and buoyancy driven ventilation and research is focused on the transient draining flows of combined forces. Small scale measurements (emptying box) are compared to the modeling results. Unlike previously assumed by Rousseau and Mathews (1996), the authors point out that airflows coming from buoyancy and wind effects cannot be obtained by adding the results of the two processes in isolation as they are non-linear. Using the emptying box approach, they find that combined forces result in less emptying time than just buoyancy-driven ventilation; the rate increases as the inlet-outlet pressure drop increases and as the density difference between the interior and exterior environment increases. The rate of descent of the interface is well predicted and the majority of theoretical predictions were within 10% of the observed values, with the theoretical model giving overestimated values. It was also shown that wind can enhance or hinder ventilation, depending on

speed, direction, and indoor-outdoor temperature difference. A quadratic relationship is drawn for buoyancy and wind and buoyancy/ wind driven velocities in isolation.

A fully-mixed model and an emptying water-filling box model previously used in other studies is re-examined in a case of a thermally stratified simple one-zone building under buoyancy-driven natural ventilation studied by Li (2000). The objective is to produce airflow and thermal stratification solutions. Buoyancy and thermal radiation between surfaces are considered. Four parameters are predicted, ventilation airflow rate, indoor air temperature profile, neutral level and clear zone height. By comparing different models, a new model is developed to help balance the over-predicted or under-predicted ventilation parameters found in the other models. It is shown that the old models are particular cases of a more general emptying air-filling box model. The author suggests that thermal stratification should be considered in multi-zone models for naturally ventilated buildings with large openings.

The complexity of natural ventilation even for simple systems is then studied by Li et al. (2001). Wind and buoyancy forces can be opposing each other or assisting each other. The authors show that under certain conditions, multiple solutions for the flow rate exist in a natural ventilation system which is induced by the interaction of buoyancy and wind forces. Even though the calculations assume fully-mixed air in the space, the existence of multiple solutions was confirmed in small-scale laboratory tests where stratification was observed with buoyancy-dominated flows. In every case examined, flow rate exhibited hysteresis.

An experimental study of airflow distribution is performed by Reardon et al. (2002) using the tracer gas technique in a mechanically ventilated atrium. For the particular facility (a three-storey atrium in Ottawa, also studied by Laouadi and Atif, 1999), it is found that air follows upward movement mixing well with the respective perimeter zones. Air supplied at ground floor is transported upward and distributed to the upper floors and perimeter walkway areas. Air supplied on the 2nd/ 3rd floor mixes well with perimeter areas and any floor levels above but never reaches the ground floor. When doors are closed, only a small amount of air supplied at the core of the building (atrium) finds its way to the adjacent zones. Overall, the tracer gas technique applied is found to be successful in helping understand the air distribution patterns created by the building's HVAC system in the atrium. However, the study is limited in respect to ventilation sources as the building is only mechanically ventilated. Moreover, tests were run after normal office hours, therefore some parameters – such as users' disturbances and solar radiation – that would most likely affect the airflow distribution were not taken into account.

The performance of a natural ventilation system in a building is directly linked to the building configuration and the outdoor conditions. Even though natural ventilation is a simple concept, detailed design can be challenging because of the building form and its surroundings. Karava et al. (2007) study important parameters in the natural ventilation design of a building. In the case of wind-induced ventilation, wind flow around the building is essential for the placement of the openings in order to fully benefit from the cross ventilation potential. The study yields results on the opening area, discharge coefficients, airflow and pressure drop that are very important for the natural ventilation design.

Wind speed and wind direction effects on the ventilation rates are examined extensively through CFD simulations in a two-storey atrium by Horan and Finn (2008). Results of this study show an almost linear relationship between wind speed and ACH, an approximately linear relationship between wind direction and ACH for 0°-90° angles and a non-linear relationship for 90°-135° angles (Figure 2.1, Figure 2.2).

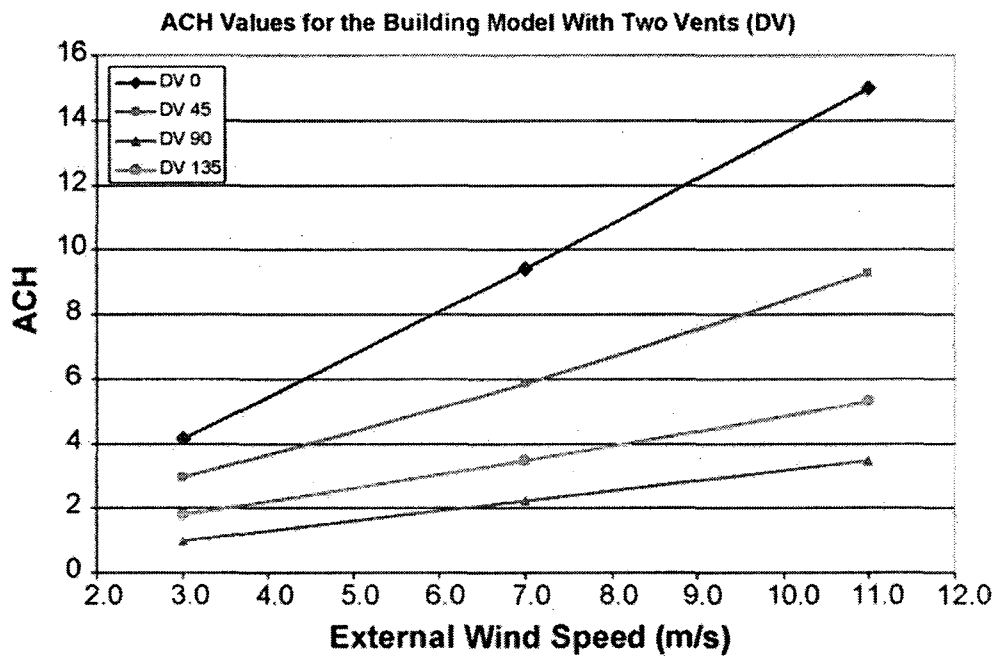


Figure 2.1. Predicted ACH rate as a function of external wind speed, for all wind directions and the two vent model (DV) (Horan and Finn, 2008)

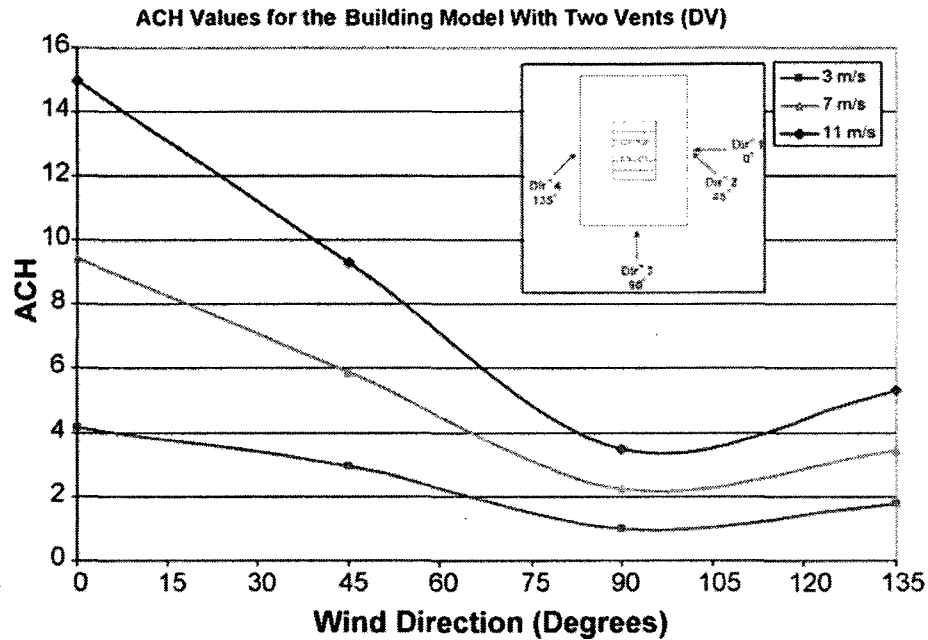


Figure 2.2. Predicted ACH rate plotted against wind direction for the double ventmodel (DV) (Horan and Finn, 2008)

They also conclude that external wind direction has little effect on the extent of the change in the ACH rate caused by an increase in external wind speed. As shown, non-design wind conditions should be considered in the design of a natural ventilation building. This study presents interesting results regarding the wind effect on ventilation rates and is very useful at the design stage of a naturally ventilated building. Wind forces occur in a random manner and are often not taken in consideration. A more complete quantitative approach on the ventilation rates would have been a case where buoyancy forces are also considered along with some airflow measurements in a representative building.

2.1.2. Flow enhancement in an atrium – single storey configuration

Atria are typically part of or adjacent to other building zones. The effect of ventilated and unventilated atria connected to single-storey spaces on the flow characteristics (thermal stratification, airflow rates, height of interface) is investigated using analytical/experimental techniques by Holford and Hunt (2003). Flow enhancement that can be achieved by an atrium is examined. A theoretical model is used to predict the steady stack-driven displacement flow and thermal stratification in the building caused by heat gains in the storey and solar gains in the atrium. It is compared with the results of laboratory experiments. It is found that air reaching the atrium is further warmed by direct solar heating and the deep warm layer enhances the flow. Solar heating of the unventilated atrium will shift the steady interface of the storey upwards, increasing the flow rate. Temperature in upper storey decreases while temperature in upper atrium increases. Storey conditions are improved but in order to avoid unpleasant conditions in atrium a) lower regions have to be shielded b) ambient air at low level through displacement ventilation has to be supplied. It was also shown that tall atria do not always enhance the flow and opening areas should be considered to ensure that increased ventilation rates will be achieved. The authors note that the model was simplified and that work is in progress to also consider heat exchange between surfaces.

The same type of adjoined enclosures (atrium connected to single storey room) is looked at by Ji et al. (2007). The capability of CFD for modeling natural displacement ventilation in this type of combined enclosures was tested. CFD key issues such as boundary conditions and solution controls were investigated. Results were compared to analytical model predictions and small-scale experiments (by Holford and Hunt, 2003).

Several topics were addressed, e.g. natural displacement ventilation flows, non-dimensional flow rates and reduced gravities, interface height (stratification level), constant pressure boundary condition, enhancement of ventilation flow. The existence of qualitative and quantitative discrepancies on some of these topics is discussed. In general, airflow patterns, temperature distribution and ventilation flow rates predicted by CFD are in good agreement with the analytical models and the experiments and the study demonstrates the capability of CFD in predicting buoyancy-driven displacement natural ventilation flows in simple connected spaces.

2.1.3. Opening configurations

The opening area and position of the air vents has an impact on the resulting flow characteristics. Two interconnected rooms subject to hybrid ventilation is the topic of a study by Tovar et al. (2007). Using laboratory experiments, they examine the effect of the supply and return vent positions on the flow patterns, the thermal stratification and the cooling efficiency. They point out how the use of a vertical barrier at the ceiling to shield an upper vent from cool air can reduce cooling loss rate and make night cooling a practical option in building cooling with increased efficiency.

Vent configurations along with buoyancy and inertia forces are investigated by Awad et al. (2008). In this experimental study, ways in which flow operation parameters lead to stratification within ventilated rooms are examined. More particularly, the focus is on the effect of inlet/outlet locations and flow rates on the temperature profiles in order to evaluate the characteristics of stratified flow, the interface height and thickness and the

stability of stratified layers. It is found that the location where flow becomes stratified is influenced by ventilation parameters relative to the geometry, size and shape of the enclosure as well as the power of the heat sources. It is also found that relative influence of inertia and buoyancy forces determines the stratified flow characteristics. Moreover, they verify what was previously documented, that the height of the exhaust vent is proportionally linked to the point where the flow becomes stratified. It is found however that this point is not changed when momentum forces dominate the flow. They conclude that stratified layers and ventilation flow rates are two important parameters in the natural ventilation system design, affecting energy requirements of the building and that the results of this study can be used to test the effectiveness of a ventilation system at the design stage.

2.2. Simulation programs – limitations, coupling methods, modifications and testing applicability

In the early design stage, what is typically examined is the energy demand of the building to be constructed. For such cases, simple building simulation tools can apply such as the “MIT Design Advisor” (B.J. Urban, 2007). This building energy simulation tool offers quick modeling and rapid comparisons, allowing the user to easily decide upon those building components that will result in less energy consumption and optimal indoor conditions. Further ahead in the design stage of sustainable buildings, more detailed simulation programs are needed to predict complex airflow and thermal patterns that develop in naturally/mechanically ventilated spaces. These simulation programs

encounter certain limitations, especially in the case of atria spaces. In cases where high resolution is required, microscopic scale (CFD) models deem appropriate, whereas when dealing with entire building zones, macroscopic scale models apply better. However, macroscopic models assume well mixed air and this is rarely the case in large atria or buildings.

Part of the International Energy Agency Task 12 (Building Energy Analysis and Design Tools for Solar applications) was the Atria Model Development, Aiulfi (1994). The project marks out certain limitations that exist in the building simulation programs. Issues such as natural ventilation, temperature stratification, solar gain distribution in the atria (wide glazed surfaces) and thermal comfort (radiation, air velocities, temperature stratification) are not dealt with by tools used at the time. The project focuses on natural ventilation and velocity distribution, using the Flovent CFD program to balance the lack of measurement data. A winter case and summer case are investigated, comparing temperature fields measured in a real atrium with Flovent calculations. It is found that Flovent calculations correspond well to the measured values. Thermal stratification over a height of 16 meters reaches 6 °C in the winter (at night, heating provided) and 16 °C in the summer (midday, clear sky). Stratification and average temperature level both decrease when vents are open. Solar radiation and its effects on CFD calculation are also studied. Overall, use of Flovent is successful and it addressed issues to be further examined.

Even in the absence of natural ventilation, atria building zones are difficult to accurately simulate. The accuracy of an energy simulation program in predicting thermal parameters in an atrium (ESP-r was the simulation tool considered) is tested by Laouadi and Atif

(1999). CFD needed yet to be validated for atria and energy simulation software packages for conventional office buildings did not apply to atria buildings since atria involve complicated airflow patterns, significant thermal phenomena and complex types of fenestration (affecting solar radiation distribution in the space). Their specific objective is to compare predicted values and field measurements in relation to thermal parameters in an atrium space. A 3-storey atrium in Ottawa with a pyramidal skylight is monitored in a summer and winter month to consider extreme conditions of the outdoor climate. Solar radiation and indoor air temperature simulation results using ESP-r are compared to measured values. Solar radiation results are in good agreement with the measured values while predicted indoor temperatures were ± 2 °C of the measured in the winter time and 2-3 °C higher in the summer. Temperature stratification is more significant in the summer than the winter, with its presence mainly due to electrical lighting (internal heat gains) and solar radiation. The study concludes that more validation studies for atria should be conducted in order to establish atria design guidelines, that energy prediction methods should be properly validated to assist the energy efficient buildings design and that energy computer programs need to be enhanced in order to deal with the thermal aspects in the atrium.

The issue of enhancing energy simulation programs to deal with atria thermal aspects was approached by Laouadi and Atif (1999), however the study was restricted in an unventilated, unoccupied atrium and airflow patterns were not addressed. Voeltzel et al. (2001), driven by the inadequacy of simulation programs in cases of large highly-glazed spaces, develop a new model aiming at improving the prediction of thermal behaviour in such spaces. The model, called AIRGLAZE, is based on the coupling of a zonal airflow

module (to predict air motion in the room) with an envelope module (to calculate conductive and radiative heat transfer in the building envelope) to accurately model the sun patch and the internal distribution of shortwave and longwave radiation in the building. The objectives are to predict thermal and ventilation behaviour of large glazed spaces in transient conditions, compare simulation results with field data and evaluate the added value of modeling airflows within the space through a zonal approach. AIRGLAZE results are compared with measurement data from two experimental test cells, IEA Annex 26 experimental atrium and a test cell at ENTPE. Experimental and numerical data are in good agreement while measurement data (boundary conditions) simplified calculations. Among other findings, the zonal approach is proved to be beneficial when predicting the air temperatures.

The zonal approach is also followed by Axley et al. (2002) who use a multi-zone coupled thermal/ airflow macroscopic tool. A representative naturally ventilated atrium building in Enschede, the Netherlands, is used to calibrate their tool (i.e. validate the application through comparison of measured and predicted results, calibrate building models used for subsequent analytical studies). Following the analysis, it was evident that coupled thermal/airflow analysis can provide detailed dynamic response results that can be used to evaluate both general system performance and detailed air distribution and temperature response. Overall, the macroscopic tool used (CONTAM97R) provides important spatial and temporal details that can help improve design related to both whole-building and inter-room air distribution and thermal performance.

In the case of pollutants dispersion, accuracy in predicting temperature and airflow variations in the room is needed. Ren and Stewart (2003) – dealing with source emission

rates, local concentrations and pollutants dispersion – modify a program used to model air flows inside buildings (“COMIS”) in order to divide individual rooms into smaller zones. Difficulties and lack of information on airflow and pollutant concentration variations often encountered using microscopic or macroscopic scale models are described, justifying the use of the modified version of “COMIS”. The new version is evaluated by comparing findings with experimental data (from a test chamber and an experimental atrium) and other CFD model predictions. Findings indicate that enhancing the COMIS program with the sub-zonal model can yield reasonably accurate airflow and temperature predictions for a number of different cases. The study also points out the advantages of the modified COMIS version over other models, namely no convergence problems and shorter calculation time.

Tan and Glicksman (2005) refer to the lack of accurate and efficient design tools capable to predict the performance of natural ventilation. To improve the predictions, they integrate a multi-zone model with computational fluid dynamics. Multi-zone models of large openings and atria configurations, commonly used to enhance natural ventilation, integrated with CFD simulations are examined. Both buoyancy and wind-buoyancy forces are investigated in this study. The authors conclude that the tool is useful when the ventilated building is properly divided into zones. Large openings and atria should be carefully considered when predicting the performance of natural ventilation. Using the results from the multi-zone model calculations, CFD can provide accurate predictions for a zone of interest. Regarding the boundary conditions, attention should be given to the data transferring surface. Recommendations are made concerning velocity and pressure

coupling methods as well as zone division of large openings and atria. This integrated method is overall considered successful and will be validated with small-scale modeling.

Djunaedy (2005) in his PhD thesis examines the advantages of using coupled simulation methods (internal or external, e.g. CFD coupled with BES) instead of uncoupled ones (e.g. ESP-r alone). It is shown that coupling methods offer flexibility when limitations are faced and they can capture the dynamics of airflow patterns, as opposed to other simulation methods. When predicting air temperature, it is found that external coupling has some benefits over internal coupling.

Walker and Glicksman (2006) later on broached the subject of accurate predictions in a different manner. They support that at the design stage, full-scale modeling is not practical. An alternative way is to use small scale modeling, gather data in a more manageable way and scale it back to full-scale. A reduced-scale model is built, using a scale factor to simulate a prototype building, and boundary conditions provided by the experiments are input in their CFD model. The results are then compared to experimental data from the prototype building. It is found that the small-scale model generally follows the same trend as the prototype building. Some temperature differences are observed and are attributed to open windows and wind fluctuations while solar heat gains seem to be causing discrepancies. The study makes reference to several techniques – such as analytical, numerical, and physical – and each technique's limitations, strengths and weaknesses. It is shown that validation of data with full-scale measurements and numerical simulations provides an additional tool for the prediction of airflow and temperature distribution in naturally ventilated buildings. The research appears as a different option to coupling methods or the zonal approach. Similitude factor, required

when scalability is used, is carefully addressed to ensure similar phenomena take place in reduced and full scale models. A limitation of the proposed approach is that solar radiation is not considered therefore the tool is perhaps better applied to naturally ventilated buildings with low solar gains.

High accuracy is not always needed therefore modeling and boundary conditions details may vary according to the case. Jayaraman et al. (2006) test four different types of CFD models for a case of mixed convection conditions in an experimental atrium. The goal was to investigate how the level of detail in the temperature boundary conditions and choice of turbulence model affects the accuracy of the pollutant transport predictions. The results are compared to field tracer gas measurements taken in a mechanically ventilated atrium with dimensions 7 m x 9 m x 11 m high. The four simulation versions rely on different boundary conditions and turbulence models. When more detailed boundary conditions are assigned, the results are in good agreement with the experimental data. On the contrary, standard and isothermal models do not perform well, since buoyancy and thermal stratification cannot be ignored in large spaces. Attention was mostly given to the transport of pollutants within the space. The authors mention that they also have to examine cases of unstable stratified flow and improve the predictions. In this study, the conditions leading to natural convection are unclear as the surface temperatures are relatively close, the atrium is only mechanically ventilated and no solar radiation or some other heat source is specified. Another point that is not clear is the experimental atrium; in the reference given for its description (Fischer et al., 2001) the enclosure is referred to as a test chamber with no mention of glazings.

2.3. Performance evaluation of mixed mode buildings

2.3.1. Thermal comfort in naturally ventilated environments

De Dear et al. (2002) study the revisions to ASHRAE Standard 55 on the thermal comfort in naturally ventilated buildings. Earlier versions of ASHRAE Standard 55 had limited flexibility, interior thermal conditions falling into a very narrow range. Meeting this narrow definition of thermal comfort has been very difficult without any mechanical assistance. The study points out that ASHRAE Standard 55 heat balance model ignores the psychological dimension of adaptation, namely peoples' expectations depending on their interactions with the environment or diverse thermal experiences. They propose an Adaptive Comfort Standard (ACS) (Figure 2.3) which is presented in ASHRAE Standard 55 as "Section 5.3 – optional method for determining acceptable thermal conditions in naturally conditioned spaces". The authors describe the ways in which the ACS can be used during the design stage or to operate and evaluate an existing building. Their research strongly suggests that user control and air movement can have an impact on the acceptable indoor temperature ranges and consequently on the cooling energy savings.

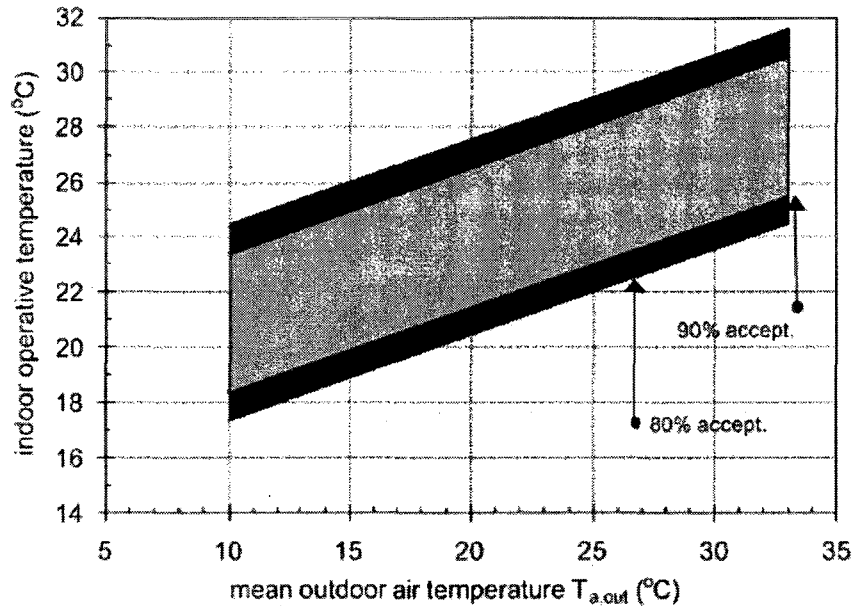


Figure 2.3. Proposed Adaptive Comfort Standard (ACS) for ASHRAE Standard 55, applicable for naturally ventilated building (De Dear et al., 2002)

2.3.2. Thermal performance –impact of climatic conditions and user behaviour

A naturally ventilated educational building in UK is subject to monitoring and modeling by Kolokotroni et al. (2001). Monitoring results and building performance are discussed while modeling is employed to produce some performance optimization guidelines. Monitoring consisted of measurements of ventilation rates, indoor air and slab temperatures and relative humidity and external air temperature, relative humidity, wind speed and wind direction. Examining hot, typical and cold summer days, the study presents the resulting indoor conditions on the first and third floor of the building. For hot summer weather, first floor (featuring thermal mass and shading) responds well while the third floor exhibits uncomfortable conditions. For typical summer weather, first floor again responds well while the third floor appears to follow external conditions and thermal comfort in the space is strongly linked to the presence/ absence of solar gains. On

the occasion of a cold summer spell, thermal mass and night ventilation result in low indoor air and slab temperatures while the third floor seems to benefit from the solar gains in this case thus providing comfortable conditions. Analyzing the monitoring results and modeling scenarios on different external temperatures, ventilation rates and % shading, the authors verify the cooling effectiveness of exposed thermal mass and night ventilation (Figure 2.4, as previously found by Kolokotroni, 1998) and point out the need to quantify the effect of external weather conditions and the need for a model-based control relating to daytime/night-time ventilation and shading that would also consider occupancy disturbances and user interactions.

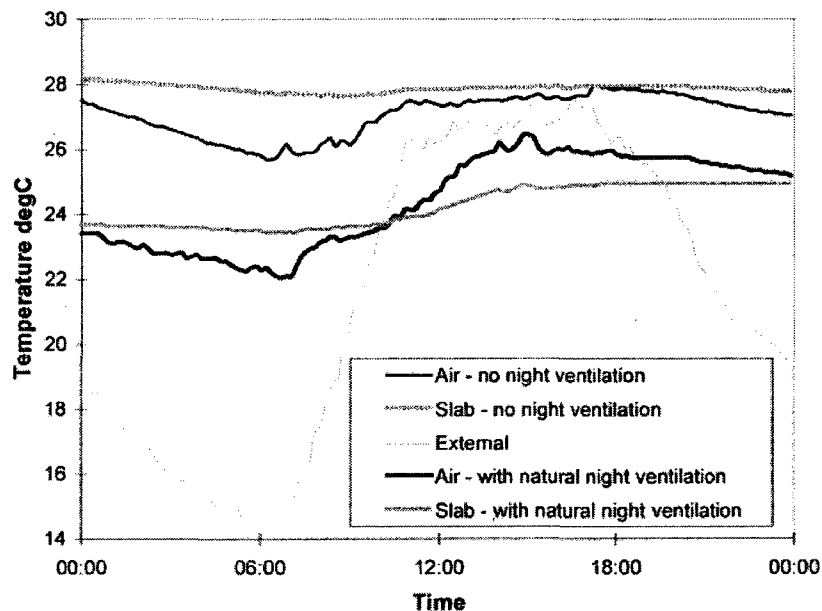


Figure 2.4. Hourly measured air and surface slab-temperature variations over 24 h in an open-plan office with and without natural night-ventilation. It shows that night ventilation reduces air and slab temperatures, and delays the peak internal temperature to later in the day (Kolokotroni, 1998)

The second objective of Axley et al. (2002) in their research is to test the night cooling potential of a naturally ventilated atrium building in Enschede, the Netherlands, in different climates. The building's natural ventilation system is based on operable

windows, self-regulating trickle ventilators, a central slot atrium with passive stacks and mechanical-assist fans. System can be used in direct or indirect (night cooling) mode. Air flows in through inlet vents (driven by buoyancy and wind forces) in the offices, flows out towards the atrium, and is then exhausted through the atrium roof. If natural forces are insufficient, fans assist the exhausting of the air. It was found that in order to optimize the cooling system's performance, inlet vents should be controlled using "night cooling" strategies throughout the day during warm periods. The building performed well in Los Angeles weather. For all combinations of thermal (solar and internal) gains considered, the number of overheating hours, according to the cooling season comfort criteria (Equ. 3.3 in Axley et al., 2001), was not exceeded. The authors offer a more thorough look at the building's ventilation system and its response in different area zones. As an example, stack-driven flows are given in Figure 2.5.

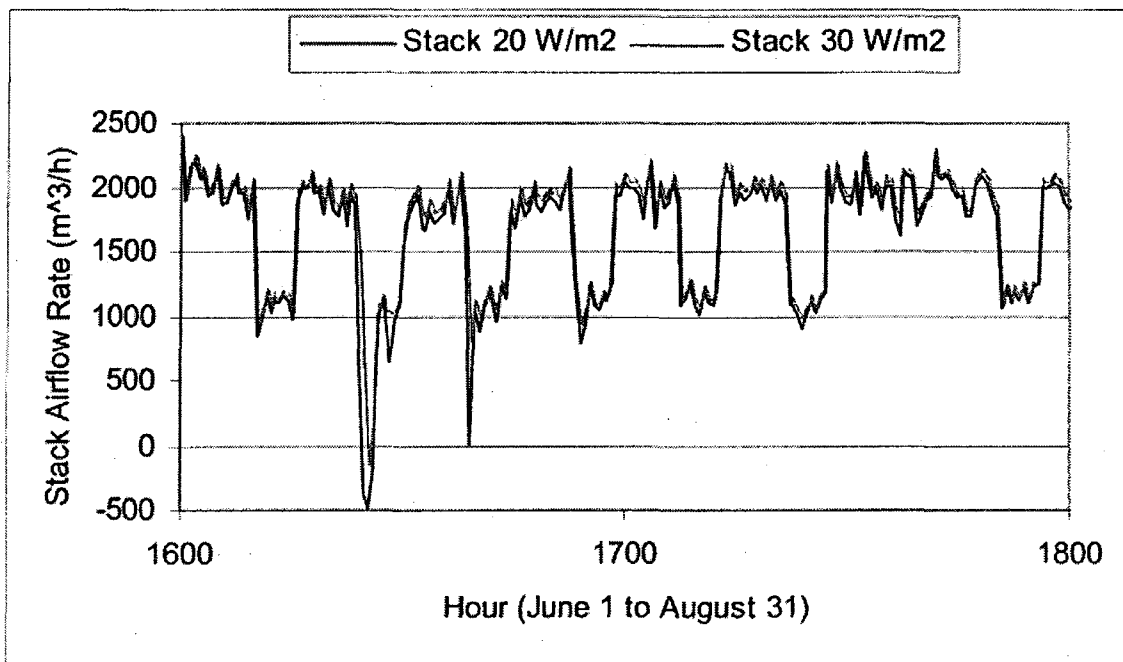


Figure 2.5. Detailed stack airflow rate response for the Enschede Tax Office building to Los Angeles' summer conditions operated in a natural night cooling mode. Results plotted for two assumed combined solar and internal gains— 20 W/m^2 and 30 W/m^2 (Axley et al. 2002)

A large naturally ventilated building is the focus of the research by Da Graca et al., (2003). The design for the new Federal Building in San Francisco included an office tower that would be naturally ventilated. Each floor is designed to be cross ventilated through upper windows that are controlled by the building management system (BMS) and user controlled lower windows. Building performance and control strategies are examined with a modified version of EnergyPlus. The control strategy has ten window opening modes. The effects of these modes are simulated and different forms of user behaviour were assessed. Simulations show that low energy indoor climate control system is expected to have excellent performance. The use of night ventilation and chilled slabs is a suitable approach in order to manage warm periods. Results demonstrate how user behaviour can significantly affect the performance of the building. However, simulations of different control strategies showed that the operation of the BMS always improves indoor conditions, even when occupants' behaviour is unfavourable to thermal comfort.

The challenge of designing a sustainable low-energy building without compromising the thermal comfort is the subject of a study by Holmes and Hacker (2007). In addition to investigating the performance of naturally/mixed mode ventilated buildings, they run simulations to take account of the climate change in the future years. For their simulation study a design summer year is used rather than a test reference year. Features of the buildings tested are high mass, high level of insulation, natural or mixed mode ventilation, adiabatic cooling, night cooling and advanced control systems. Thermal comfort standards used in the study are according to ASHRAE's Adaptive Comfort

Standard, which the authors further use to predict the upper comfort limits that would apply in the future years. They demonstrate how a mixed mode ventilated building can be an excellent way to reduce energy consumption while still providing a comfortable building environment. In the design stage it is important to consider present and future climate conditions, how the building is going to be used and the ability of people to adapt in their environment. Different buildings are compared on the basis of indoor temperatures, their performance in present and future climates and their carbon dioxide emissions. Based on the results of the study, the authors suggest as general guidelines the shading and controlling of internal gains, the distribution of the gains to reduce the peak, the use of an appropriate ventilation strategy (e.g. night cooling) and the use of mechanical cooling when it is necessary.

The performance of a naturally ventilated city centre library in UK was examined by Krause et al. (2007) and then evaluated in other locations (similar to Axley et al., 2002). The careful design of the building makes it energy efficient with a less than 50% energy consumption compared to a standard air-conditioned building (Figure 2.6). The overheating criterion is met in most cases of hot summer days, even in the top floors that are the most susceptible to overheating problems in stack ventilated buildings. The building also proves to be able to maintain thermal comfort standards in most UK locations. The authors acknowledge the importance of what is largely adopted in low energy building design (e.g. exposed thermal mass and night cooling, solar shading, high level of insulation, maximizing daylight, high quality glazing) and recommend further actions to be taken in order to improve the performance of a naturally ventilated building.

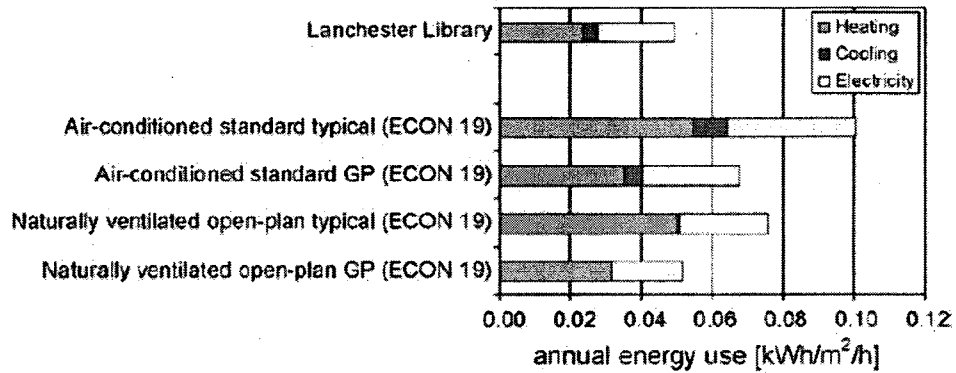


Figure 2.6. Comparison of the library's annual energy consumption during 2004 with ECON19 benchmark values for typical and good practice offices (Krausse et al., 2007)

2.3.3. Thermal performance of naturally ventilated atrium buildings – simulation and monitoring studies

EnergyPlus and FLUENT were used to assess the thermal performance of a prototype atrium building in Istanbul by Gocer et al. (2006). These simulation tools are combined to calculate the heating, cooling and lighting energy consumption and air temperature stratification in the three-storey building (data from EnergyPlus serve as input to FLUENT). In the summer, the stack-driven flows help maintain comfortable conditions in the atrium. The study indicates that an atrium should be considered as part of the energy strategy of a building and should be designed as a thermal buffer zone rather than a full comfort conditioned space that would cause high energy consumption. The results in the study are lacking information with regards to the outdoor conditions and the indoor-outdoor temperature difference assumed resulting in the stack-driven flows. Presenting more detailed air temperature results in areas running a risk of overheating (i.e. top part of the atrium and adjacent spaces) would also be of interest.

Abdullah et al. (2008) monitor the indoor thermal environment of an atrium in a tropical climate. They investigate the effect of two methods – water spray, shading – to help control the overheating problems occurring all year long. Naturally, lower level is easier to condition and control unlike the top atrium levels and the floors adjacent to it. Maintaining acceptable indoor conditions in a partially conditioned three-level atrium in a hot humid climate poses a great challenge and discomfort to occupants is often inevitable. The study concludes that atria are more beneficial in high latitudes (daylight and useful solar heat gains in the winter).

Finally, a naturally ventilated building located in Sheffield, England, featuring high thermal mass – used to promote the use of night cooling – and a southerly oriented active façade to provide daylight, is the focus of the study by Altan et al. (2009). Indoor environment of the building is chosen for investigation due to its passive design strategies. The study concludes that there are obvious advantages in having a glazed façade that introduces daylight and high level of illuminance while also enhances the natural ventilation. However, a shading system should always be in effect to avoid glare problems and the ventilation rates should be better controlled to prevent overheating during warm sunny days. They highlight the fact that a passive design, as is the case of this building, can lead to a high quality working environment, provided that optimization techniques account both for daylight and natural ventilation.

2.4. Summary

Airflow and temperature prediction as well as energy performance evaluation of mixed mode ventilated buildings have been some of the topics addressed in numerous studies. Parameters such as climatic conditions and user behaviour significantly affect the performance of the building while high-rise naturally ventilated buildings are more liable to varying ventilation rates and temperature patterns.

Presently there is a need for case studies of hybrid ventilated buildings with the aim of developing design guidelines and control strategies suitable for Canadian climatic conditions. In this context, the thesis aims at providing long-term monitoring data for an institutional building (Concordia Engineering Building) located in Montreal. This data is combined with a simple mathematical model to evaluate the performance and the cooling potential of a hybrid ventilation system, and provide design guidelines.

3. EXPERIMENTAL SETUP

Introduction

This chapter presents the experimental setup at the Concordia University Engineering building. A description of the building and its natural ventilation system is given followed by the measurements employed and the instrumentation that was used. The installation of the monitoring sensors is briefly described at the end of the chapter.

3.1. Building description

The 17-storey-high building is located in downtown Montreal (45.5°N, 74°W). It has two main large façades facing approximately southwest and southeast. The total floor area is about 53,000 m² while the floor area covered by perimeter spaces is 5000 m². The perimeter spaces include offices (4 x 4 x 4.25 m high), labs (8 m x 8 m x 3.5 m high) and an atrium on the southwest façade of the building extending from the second to the sixteenth floor. The atrium is subdivided into five 3-storey atria separated with a floor slab so as to reduce the size of fire/smoke control zones (floor grilles are fire-proof and close in the event of a fire). The atrium presents several advantages; it can provide passive solar gains, view to the outside, diffuse daylight into the room and adjacent spaces and a pleasant environment to occupants. Moreover, it serves as a solar chimney that enhances the air movement when the building is in mixed ventilation mode. The atrium receives high amounts of solar radiation and daylight during the year, therefore, shading is necessary in order to avoid glare and overheating problems in the spaces

(Tzempelikos et al, 2007). Each of the five 3-storey atria has a 35° west of South orientation, is equipped with motorized roller shades and has dimensions of 9 m x 12 m x 12 m high, a total volume of ~1300m³. The façade glass and blind areas are 97 m² and 82 m² respectively. The top atrium (floors 14 – 16) was used as the test facility for this project. An outside view of the atrium building and an inside view of the atrium are shown in Figure 3.1 while important areas and dimensions are summarized in Table 3.1.

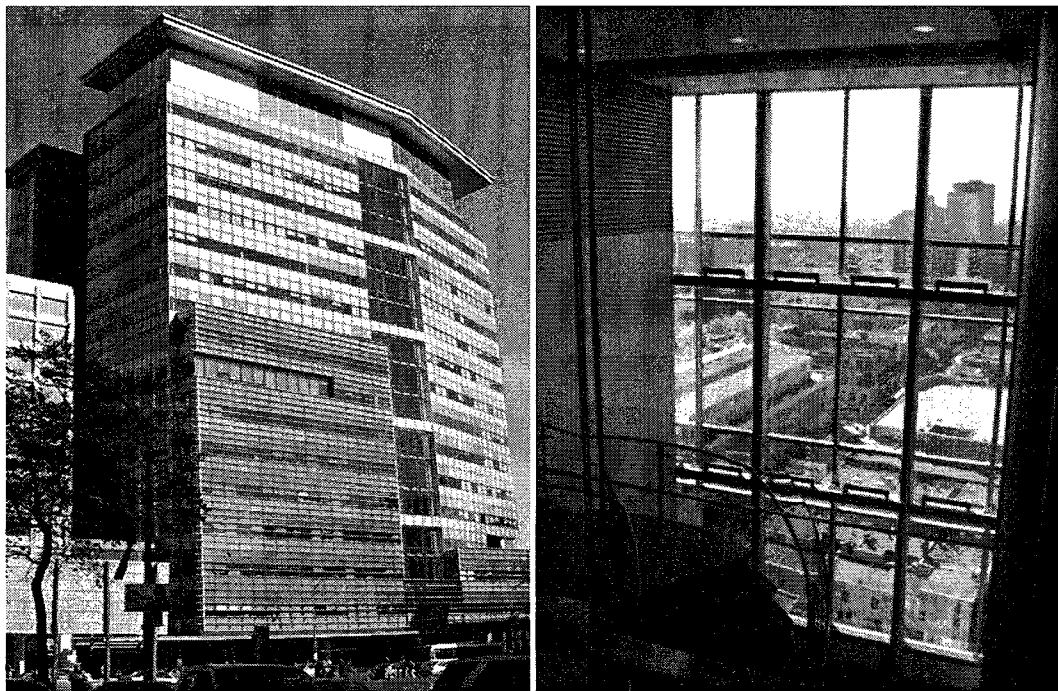


Figure 3.1. Outside view of Concordia EV building and the 15-storey atrium on the SW façade (left), inside view of the top atrium (right)

Table 3.1. Areas and dimensions in the top atrium (floors 14-16)

| | |
|---|------|
| Atrium height (m) | 11.6 |
| Atrium width (m) | 9.0 |
| Atrium depth (m) | 12.0 |
| Façade glass area (m ²) | 97 |
| Façade blind area (m ²) | 82 |
| Air supply (net) area (m ²) | 0.40 |
| Air return (net) area (m ²) | 7.44 |
| Floor grilles (net) area (m ²) | 1.97 |
| Corridor grilles (net) area (m ²) | 1.40 |
| Air exhaust (net) area (m ²) | 5.40 |

3.2. Hybrid ventilation system

At the design stage, the initial natural ventilation concept included one large chimney (a duct) exhausting air from floors 2 – 14, inlet openings at the corridor ends (two on each floor to increase the potential for cross-ventilation), and trickle ventilators in the offices of the perimeter zone (Tzempelikos *et al*, 2007). The chimney would operate with a variable speed fan-assist to ensure a total air flow of 30,000 l/sec (including stack effect). The concept is illustrated in Figure 3.2.

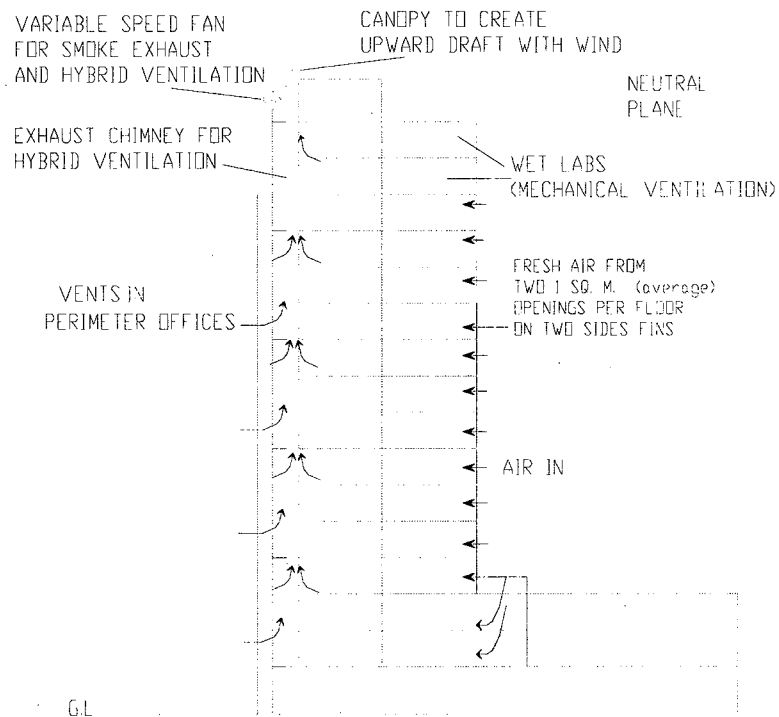


Figure 3.2. Hybrid ventilation concept (design phase)

The proposed perimeter vents and variable speed fan were not adopted in the final design in order to reduce costs. The current natural ventilation concept of the building involves:

- inlet grilles with motorized dampers (opening area about 1.4 m²) located at the end of the corridors in the southeast and northwest façade of each floor (Figure 3.3, left), and
- five 3-storey atria that are separated with a floor slab and connected with grilles of a

varying area of 1.3 – 4 m² (Figure 3.3, right); grilles have motorized dampers to achieve buoyancy driven flow.

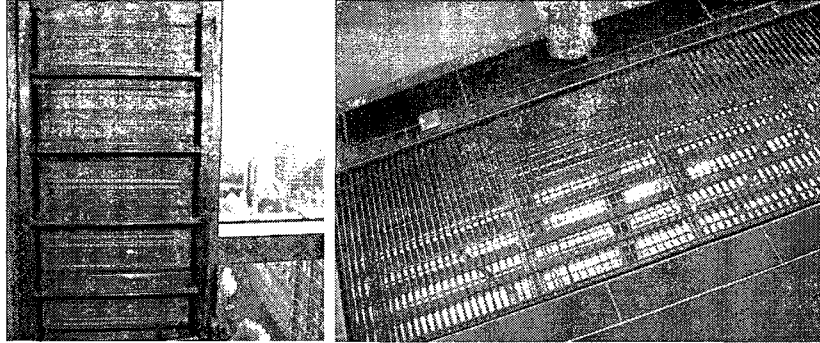


Figure 3.3. Corridor inlet grilles (left), atria connecting floor grilles (right)

The natural ventilation system operates when the outdoor temperature is between 15 °C and 25 °C and the relative humidity is less than 70%. The inlet grilles on the façade and the grilles connecting the atria are controlled by the building automation system and, based on weather monitoring data, they open or close simultaneously. More specifically, when the building is in hybrid ventilation mode: a) the corridor inlet grilles at the southeast and northwest façade of the building and the grilles connecting the atria open, b) the mechanical supply airflow rate in the atria (Figure 3.4, left) is reduced to a minimum value, c) the exhaust vent in the atrium (Figure 3.4, right) opens and d) the air supply units located at the corridors close.

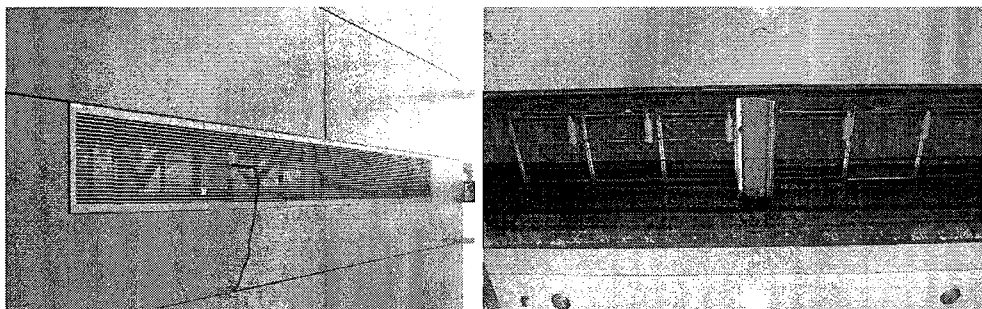


Figure 3.4. Atrium air supply unit (left), outlet grilles to exhaust the air (right)

In the atria spaces, air is mechanically/ naturally supplied and directed to other zones through the return or exhausted through the outlet vent in the top atrium. A schematic representation of the hybrid ventilation concept in the top atrium is shown in Figure 3.5. The air exchange within the five building atria and adjacent corridors is illustrated in Figure 3.6. Air entering the building through the corridor inlet grilles will heat up, move upwards through the atria-connecting grilles and be exhausted at the top.

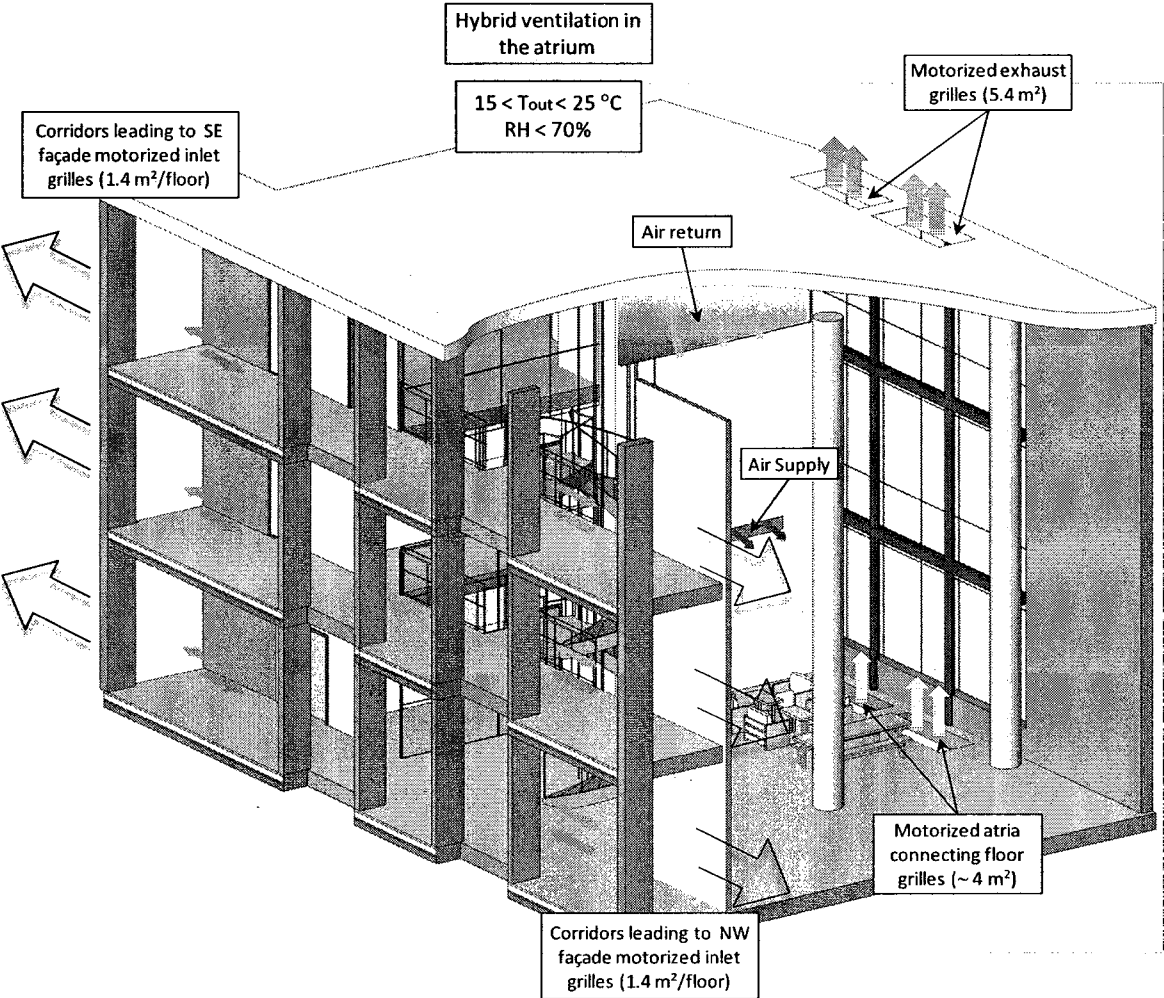


Figure 3.5. Hybrid ventilation in the atrium

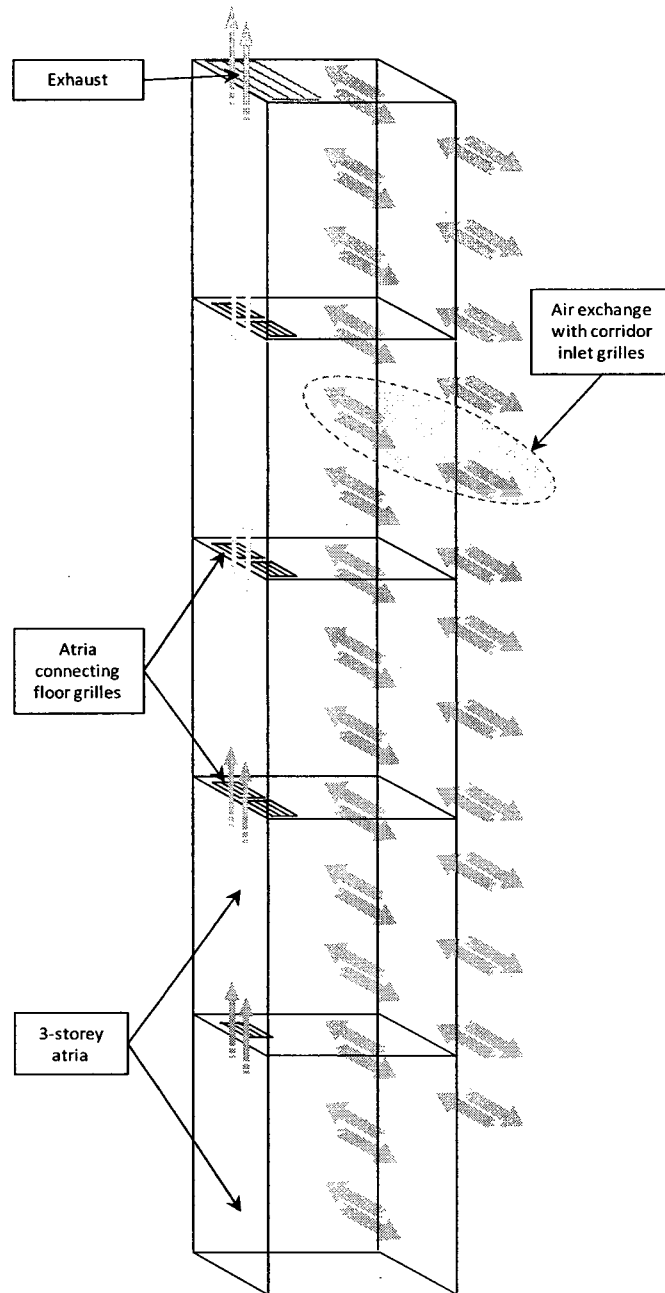


Figure 3.6. Air exchange between 5-connecting atria and adjacent corridors during natural ventilation

3.3. Natural ventilation system performance

The assessment of the natural ventilation system performance required a) measurements for the evaluation of the indoor conditions in the top atrium, and b) measurements for the

estimation of energy savings attributed to natural ventilation. Manual short-term measurements were employed at the initial stage to investigate the airflow patterns and thermal stratification in the atrium and assist in the design of monitoring set-up. In some cases, manual measurements were performed to complete continuous monitoring data (e.g. long-term air velocity measurements at the atria-connecting floor grilles) while in other cases they were the primary source of experimental data.

3.3.1. Initial short-term measurements

Atrium air temperature was measured at different days and times throughout a three-month period, using the HHM290 Supermeter and a K-type thermocouple (accuracy of 2% of reading or 2°C; Appendix I). Temperature was taken on all three atrium levels on both clear and overcast days and at several locations near the façade, the middle and the back of the room space. The purpose of these measurements was to observe the temperature stratification and subsequently determine the location and number of thermocouples that would be required for the thermal monitoring of the atrium.

Blind surface temperature was measured using the FLIR SYSTEMS thermaCAM PM595 infrared camera (accuracy of +/-2% of readings or 2 °C; Appendix I). The advantage of the infrared camera was that it provided both point and area temperatures. Measurements were mostly performed on clear days in order to examine the temperature profile of the roller shades, which are interrupted by the metal frames. As the camera temperature readings are affected by solar radiation incident on the blinds, the temperature obtained with the infrared camera was corrected with the use of a thermocouple (covered in

aluminum foil on its one side) that was placed on the blind surface. The purpose of the measurements was to select the location and number of thermocouples required for the atrium monitoring phase.

Air velocity was measured at the atrium air inlet and outlet vents as well as the corridor inlet grilles using the KANOMAX velocity meter (velocity range of 0.10 – 30 m/s, accuracy of $\pm 3\%$ of readings or ± 0.015 m/s, whichever is greater; Appendix I). Since the velocity sensors that would be used to monitor the air velocity could only be mounted in one place, it was necessary to examine and pre-determine the optimum location to ensure the most representative data.

3.3.2. Thermal and airflow monitoring in the atrium

Monitoring the indoor conditions in the atrium consisted of temperature and air velocity measurements. Surface and air temperatures were measured at various locations in the top atrium (floors 14 – 16), for different positions of the roller shades (fully open/closed). 60 T-type thermocouples (with an accuracy of less than 0.5 °C) were mounted at different locations around the atrium space to measure glass, blind and air temperature. Thermocouples measuring air temperature were shielded with aluminum foil to avoid direct exposure to solar radiation that would affect the temperature readings. The position of thermocouples near the façade and around the atrium space is shown in Figure 3.7 and illustrated in Figure 3.8 and Figure 3.9. The number and location of the thermocouples is specified in Tables 3.2 and 3.3.

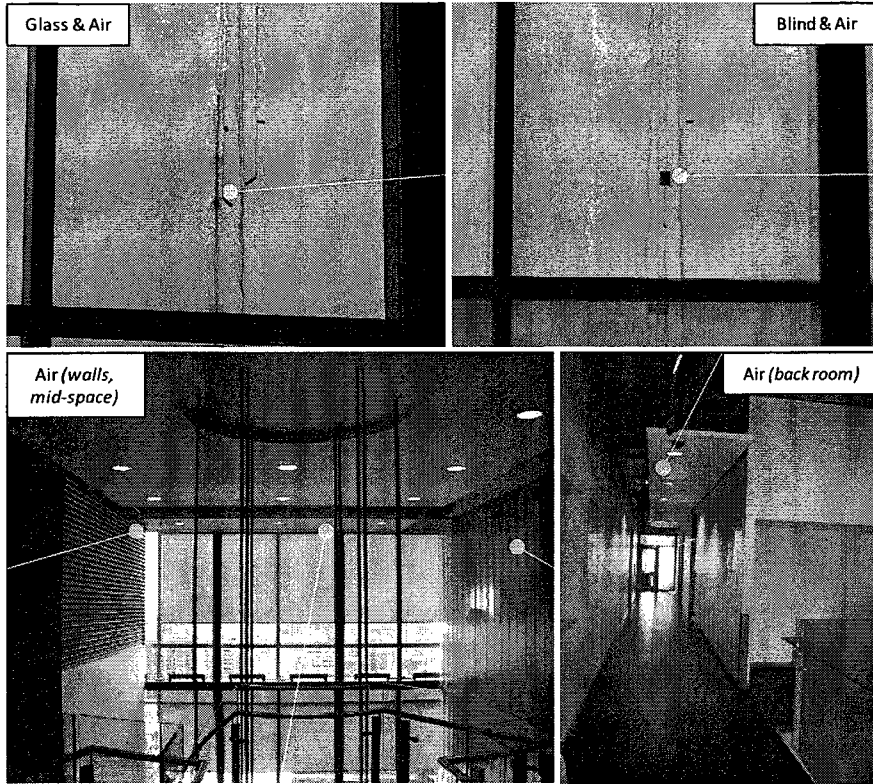


Figure 3.7. Indicated by markers, thermocouples mounted near the façade (top), close to the east, west atrium walls and staircase (bottom left), at the back of the atrium space (bottom right)

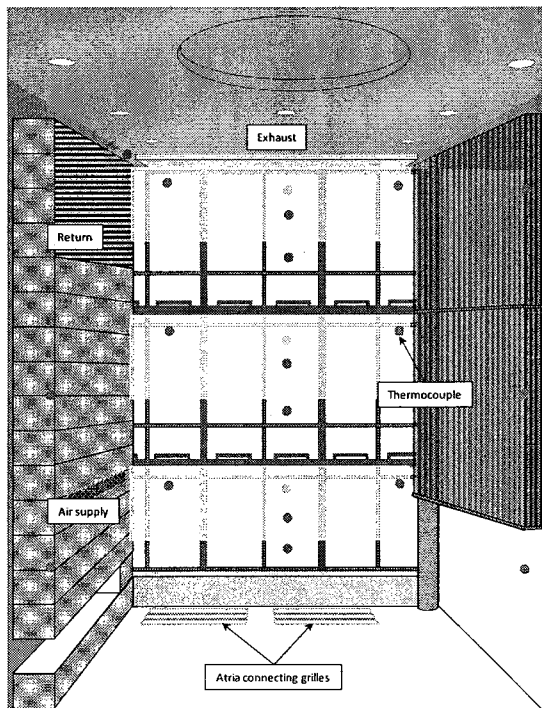


Figure 3.8 Atrium schematic with thermocouples on the façade, the east and west atrium walls

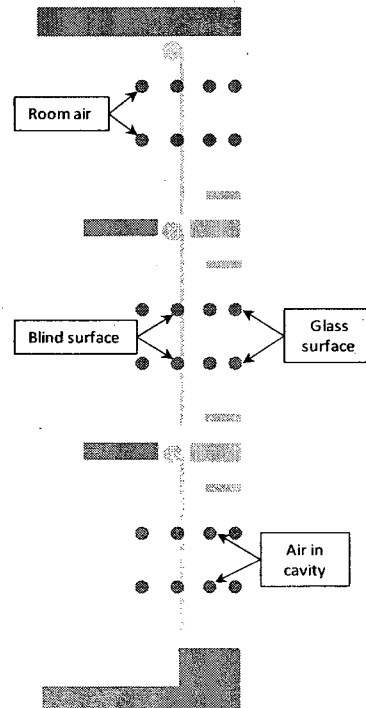


Figure 3.9. Side view of thermocouples mounted near the façade

Table 3.2. Air temperature – Number of thermocouples mounted in the atrium space

| Height (m) | East Wall | West Wall | East Corridors | West Corridors | Staircase | Air supply | Exhaust |
|------------|-----------|-----------|----------------|----------------|-----------|------------|---------|
| 10.3 | 1 | 1 | 1 | 1 | 1 | 1 | 1 |
| 6.2 | 1 | 1 | 1 | 1 | 1 | | |
| 2.1 | 1 | 1 | 1 | 1 | 1 | | |
| Total | 3 | 3 | 3 | 3 | 3 | 1 | 1 |

Table 3.3. Air and surface temperatures – Number of thermocouples mounted on the atrium façade

| Left Façade | | Middle Façade | | Right Façade | |
|-------------|----------------------------|---------------|------------------------------------|--------------|----------------------------|
| Height (m) | Number of t/c | Height (m) | Number of t/c | Height (m) | Number of t/c |
| 10.3 | 3 (glass, blind, room air) | 10.9 | 4 (glass, blind, cavity, room air) | 10.3 | 3 (glass, blind, room air) |
| | | 9.4 | 4 (glass, blind, cavity, room air) | | |
| 6.2 | 3 (glass, blind, room air) | 6.9 | 4 (glass, blind, cavity, room air) | 6.2 | 3 (glass, blind, room air) |
| | | 5.2 | 4 (glass, blind, cavity, room air) | | |
| 2.1 | 3 (glass, blind, room air) | 3.1 | 4 (glass, blind, cavity, room air) | 2.1 | 3 (glass, blind, room air) |
| | | 1.4 | 4 (glass, blind, cavity, room air) | | |
| Total | 9 | | 24 | | 9 |

Two ‘Sensor HT-400’ velocity sensors (velocity range of 0.05 – 5 m/s, repeatability ± 0.02 m/sec or $\pm 1\%$ of readings in the 0.05 – 1 m/sec range and $\pm 3\%$ of readings in the 1 – 5 m/sec range; Appendix I) were installed at the atrium air supply and exhaust vents. The solar radiation transmitted through the glass was measured with a Li-cor pyranometer (error of 5% under most conditions of natural daylight; Appendix I) mounted on the façade. All sensors were connected to a data acquisition system (Agilent 34970A Data Acquisition/ Switch Unit, Appendix I) to enable the continuous recording of temperature, air velocity and solar radiation over a period of six months (July 2007 – January 2008). Outdoor conditions, such as temperature and relative humidity, were also available through the weather data station located on the roof of the EV building of Concordia University.

Velocity of the air through the atria-connecting floor grilles was measured on floor 14 during a period of one month (September – October 2007) using the KANOMAX velocity meter. Velocity was taken at several points above the area of the grilles and an average value was used in the analysis of the results.

3.3.3. Airflow monitoring at the corridor grilles

Depending on the wind speed and direction and the stack effect, air can flow in or out through the corridor grilles at different velocities. For a period of two months and on days when the building was under mixed mode ventilation, air velocity and pressure difference were monitored on the southeast and northwest side of floor 15 using the Sensor HT-400 and Dwyer 607 pressure differential transmitter (range of 0 – 25 Pa, accuracy of $\pm 0.25\%$ or $\pm 0.5\%$; Appendix I) respectively. In Figure 3.10, the velocity sensor mounted at the corridor grilles is shown. Air velocity and pressure difference data were recorded every five seconds and then averaged over ten minute increments.

Wind speed and direction data were obtained from the Montreal International Airport weather station and were properly adjusted to meet the city height and building conditions. In the results analysis, North corresponds to a 0° wind angle while SE façade is at 125° and NW façade is at 305° . It should be noted that the pressure transmitter mounted on the NW façade grilles was limited to a positive pressure range. As a result of this, in the cases where air was flowing out of the building, the negative pressure difference reading output was zero.

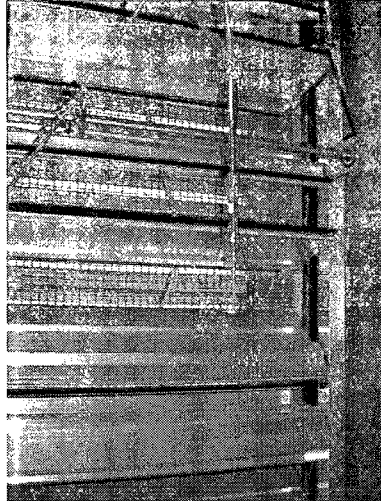


Figure 3.10. Velocity sensor mounted at the corridor grilles

3.3.4 Investigation of night cooling potential - floor slab temperature and corridor inlet grilles airflow measurements

Using the infrared camera, surface temperature of the slab located near the corridor inlet grilles (Figure 3.11) and at different distances from the grilles was measured. A first set of measurements aimed at confirming the temperature decrease caused by the air flowing in through the inlet grilles and passing over the floor. These measurements, performed during daytime and under different outdoor conditions, were done on floor 15 and were limited in number. A more extensive set of measurements was done during night time. To select days suitable for night measurements, all of the three requirements described below had to be met:

- Presence of sunny skies for a significant part of the day preceding the night of measurements so that solar heat gains could be absorbed by the building thermal mass and cause a rise in the temperature of the floor slab.

- Temperature expected to drop below 15 °C at night so as to a) ensure that the cooling effect of the incoming air stream is significant enough to be detected in surface temperature measurements, b) examine the cooling effect in the case where a night ventilation schedule (making use of lower outdoor temperatures) is adopted.
- Winds expected to be low at night so that temperature difference would be the sole driving force in the incoming air through the grilles.



Figure 3.11. Area of slab surface temperature measurements (indicated by circle) near the corridor inlet grilles

Measurements of slab surface temperature were done on floors 5 and 6 of the building – where inflow of the air is mostly due to the stack effect –, starting late afternoon of one day and lasting until early morning of the following day. Infrared pictures were analyzed to get the temperature of the floor slab. Due to reflections, temperature acquired with the infrared camera is consistently overestimated; measuring the surface temperature with a thermocouple, the two values were compared and a correction factor was then repeatedly applied in the analysis to obtain the actual temperature of the floor slab.

Along with the slab surface temperature, air velocity at the corridor grilles was taken during daytime and night time measurements (KANOMAX velocity meter, Appendix I). Air velocity was measured at different heights along the inlet grilles area and an average value was drawn to be used in the results analysis.

3.4. Installation

A detailed plan for the number and location of sensors was prepared before the installation. The atrium is an open space frequently used by the public therefore attention was given to discretion and simplicity when choosing the monitoring locations. A movable lift (Figure 3.12) was used to reach points located in the top part of the atrium (12 meters from the ground).



Figure 3.12. Movable lift used to attach thermocouples

Welding of the thermocouples was done prior to installation and all sensors were labelled and checked before mounting while most of them (42) were mounted near the façade area. Due to the large number of wires, an incised hose was used to facilitate moving them along the façade in batches. The thermocouples, connected to the data acquisition

system, were transported in the atrium and mounted on the assigned locations (glass, blind and air or cavity). Velocity and solar radiation sensors were installed in a similar way. Each sensor was tested after installation to ensure its compatibility with the data acquisition reading output. The same procedure was applied for the velocity sensors and pressure transmitters that were installed at the inlet corridor grilles of floor 15.

4. HYBRID VENTILATION SYSTEM PERFORMANCE

Introduction

This chapter presents results for the performance of the natural ventilation system of the Engineering Building of Concordia University. Monitoring data for the natural ventilation system operation hours are presented and compared with theoretical calculations based on the weather conditions for the city of Montreal during the cooling season. A large number of data on the atrium indoor conditions, monitoring of which took place from July 2007 until January 2008, was analyzed and results are presented for the following cases: a) peak air temperatures in the atrium when the building is naturally ventilated, b) air temperature patterns and profiles for four clear days and c) stack and wind-driven ventilation rates under different outdoor conditions. Using experimental data, simplified calculations for the energy performance of the building are presented.

4.1. Natural ventilation system operation hours

The natural ventilation system of Concordia University Engineering Building is in its operational mode when the outdoor temperature is between 15 and 25 °C and the relative humidity below 70%. Table 4.1 presents the mean monthly temperature and relative humidity during the cooling seasons of years 2007 and 2008. Although local weather conditions were monitored by using a weather station located on the roof of the building, a significant number of data was lost or unavailable. Therefore, to avoid inconsistency in calculations, weather data from the Montreal International Airport (Environment Canada) weather station were used instead.

Table 4.1. Mean monthly outdoor temperature and RH% for years 2007, 2008 (Source: Environment Canada, Montréal-Trudeau Int'l Airport weather data station)

| Year | 2007 | | 2008 | |
|-----------|-------------------------------|------------------------------------|-------------------------------|------------------------------------|
| | Mean monthly temperature (°C) | Mean monthly relative humidity (%) | Mean monthly temperature (°C) | Mean monthly relative humidity (%) |
| April | 5.9 | 68 | 8.2 | 58 |
| May | 14.1 | 56 | 12.8 | 57 |
| June | 20.0 | 65 | 19.7 | 72 |
| July | 20.6 | 74 | 21.6 | 70 |
| August | 20.5 | 70 | 19.7 | 72 |
| September | 17.1 | 71 | 16.9 | 72 |
| October | 11.6 | 78 | 8.6 | 70 |

The building was in mixed ventilation mode from April to October and in mechanical ventilation mode during the remaining of the time. Monitored and calculated (based on data from the Montréal-Trudeau Int'l Airport weather station) natural ventilation total time of operation (ON/OFF) is shown in Figure 4.1.

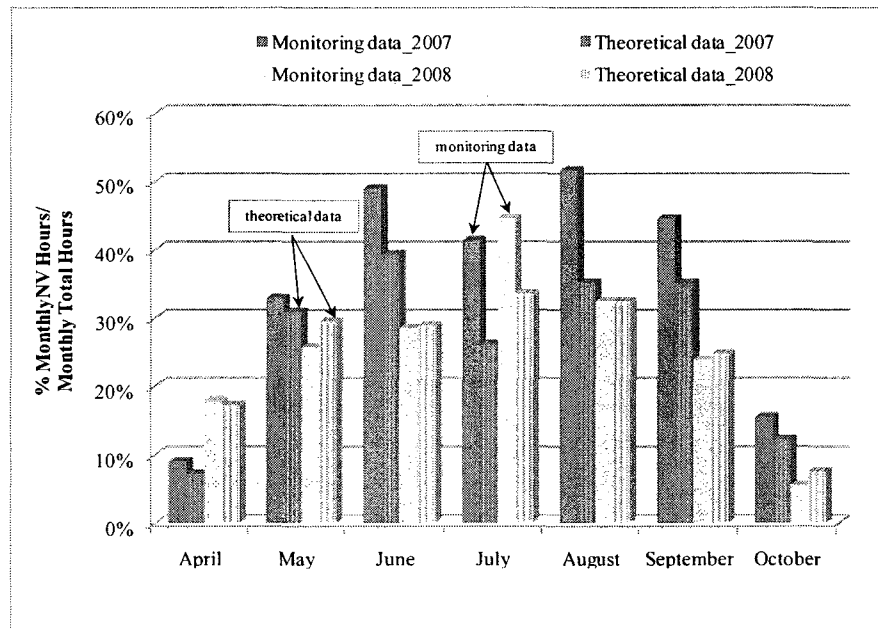


Figure 4.1. Natural ventilation hours over total period hours per month for 2007 and 2008 cooling seasons

For year 2007, the natural ventilation system was operational 49%, 52%, and 45% of the time during the months of June, August, and September respectively. The system was active 35% of the time over a period of 7 months, operating on a total of 146 days (with minimum operation of one hour) that corresponds to a rate of 68%.

For the same period of time in year 2008, natural ventilation was operating 26% of the time, approximately 10% less time than 2007. June, July and August have the highest rates of operation, 28%, 45% and 32% respectively. If the days when the natural ventilation system was active for at least one hour are considered, the rate is 65%.

Taking into account both weather requirements ($15^{\circ}\text{C} < T_{\text{out}} < 25^{\circ}\text{C}$ and $\text{RH} < 70\%$), operation rates were calculated for the two cooling seasons. The expected natural ventilation time appears to be consistently underestimated in 2007 and slightly underestimated or overestimated in 2008. These discrepancies can be attributed to one or more of the following reasons:

- Weather data used to calculate the system's operation time are obtained from the Montreal International Airport weather station. However, in reality, natural ventilation system is controlled based on data collected from the weather station located on the roof of the building. Ideally, the natural ventilation weather requirements would be adjusted to account for the – sometimes considerable – differences in temperature and relative humidity levels observed between the two stations but this is practically difficult (differences are not consistent).

- Relative humidity levels recorded at the airport are usually higher than local values. This results in under-estimated natural ventilation system operation rates, especially during the months where humidity was higher than 70% (June, July and August).
- Conditions upon which the natural ventilation system will start or stop operating are slightly different. More specifically, for the system to begin operating the temperature has to either rise above 15 °C or drop below 25 °C, while the relative humidity remains below 60%. On the other hand, the condition for the system to cease operating (while in its active mode), is the temperature to either fall under 14 °C or exceed 26 °C, or the relative humidity to surpass 70%.

Number of hours/days of natural ventilation and the corresponding operation rates for years 2007 and 2008 are summarized in Table 4.2. These rates indicate that natural ventilation presents a significant potential to reduce energy consumption for cooling and ventilation.

Table 4.2. Hourly and daily NV operating rates as a % of total period hours and days

| Year | 2007 | | 2008 | |
|-----------------------------|------|-----------|------|-----------|
| Total period days | 214 | | 214 | |
| Total NV days | 146 | NV/period | 138 | NV/period |
| | | 68.2% | | 64.5% |
| Total period hours | 5136 | | 5136 | |
| Total NV hours (recorded) | 1788 | NV/period | 1310 | NV/period |
| | | 34.8% | | 25.5% |
| Total NV hours (calculated) | 1362 | NV/period | 1285 | NV/period |
| | | 26.5% | | 25.0% |

4.2. Temperature Measurements

Investigation of the natural ventilation system performance requires monitoring of the indoor conditions, especially in a space such as an atrium, bound to receive a great amount of solar heat gains.

First, indoor temperature data is presented for days that the atrium was naturally ventilated. Temperature profiles are then examined for two cases when the natural ventilation system is operational and two cases when it is not in operation (for comparison purposes). Three types of graphs are presented for each case, 1) temperature variation near the façade, where temperature data corresponds to different elevation points “T_(h)” near the middle section of the façade (e.g. T_11 denotes the temperature at 11 meters from the ground), 2) air temperature variation in the atrium space, averaged over the atrium area at three different levels; average temperature on every level is derived using nine temperature locations (including locations near the façade), 3) air temperature profiles (façade and atrium space) based on peak measured values.

4.2.1. Natural ventilation system in operation

Atrium air temperatures under hybrid ventilation are shown in Figure 4.2. Each temperature in the graph is based on the peak value occurring on a clear day and it represents the average temperature of 27 measuring locations. Among these locations, highest temperatures are typically observed close to the façade and at the top part of the atrium while the lowest temperatures are usually measured near the corridors, at the back of the atrium space. Data was collected during a period of four months (July – October

2007) when outdoor temperature at peak times was between 15 °C and 26 °C, maximum daily solar radiation transmitted through the glass ranged from 165 – 295 W/m² and mechanical cooling was supplied at varying rates of 0.2 – 0.4 m³/sec. Results indicate that overheating was prevented even on warm days or days with high solar radiation levels, remaining – most of the time – under 27 °C. Temperatures in the atrium for two different days are presented in more detail Figure 4.2.

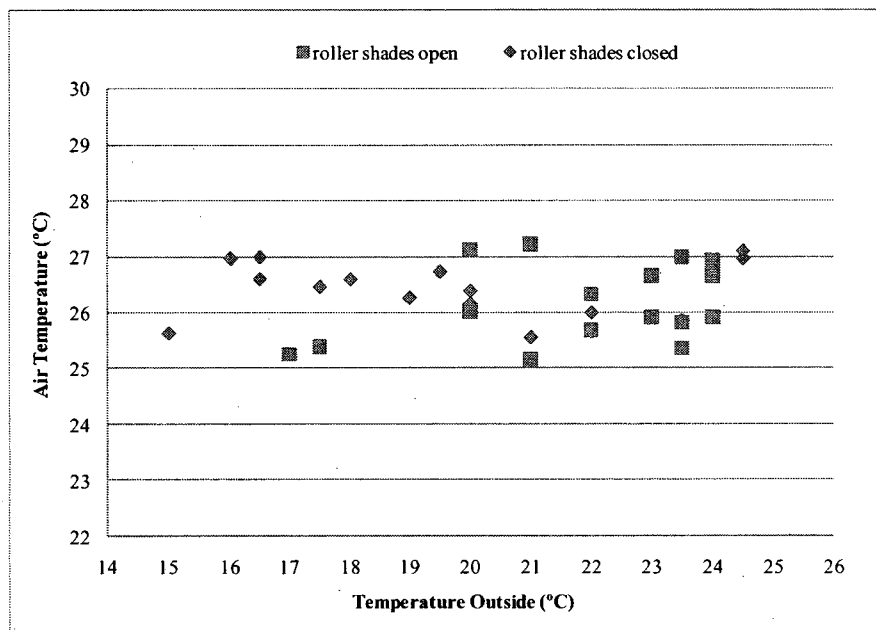


Figure 4.2. Atrium average temperatures under hybrid ventilation for different outdoor conditions

The variation of air temperature near the façade for a warm sunny day (September 1, 2007) is shown in Figure 4.3 and the variation of air temperature in the atrium space is shown in Figure 4.4. Outdoor temperature fluctuated between 12.5 and 20 °C while transmitted solar radiation reached a maximum of 220 W/m². Roller shades were kept open throughout the day and indoor space was mainly cooled by natural ventilation. There was low use of mechanical ventilation, supplying air at a rate of 0.12 m³/sec and a

temperature of 17 °C. Plotted data of indoor and outdoor conditions can be found in Appendix II.

As the day is progressing, thermal stratification reaches its maximum at about 16:00 (Figure 4.3). The lowest temperatures would have been expected at the lowest measuring location, T_1.5, however, because of the location of the thermocouple, temperature at that point is possibly affected a) by the warm air entering the space through the floor grilles, b) by the short-wave radiation reflected in the window frame, c) the long-wave radiative heat exchange with the window frame.

Considering the entire atrium space, maximum temperatures range between 25.5 – 27.5 °C (Figure 4.4). At the top part of the atrium, near the office located further back on the east atrium wall, some discomfort may be experienced. Overall, the temperature in the atrium space is within acceptable limits, especially on floor 14 where occupants often sit in the lobby area.

Air temperature profiles around maximum stratification time (daily peak temperature values) are plotted in Figure 4.5. The highest temperature difference near the middle section of the façade and over a height of 8 meters is approximately 4 °C, while over the entire façade area the temperature difference is 2.5 °C. Regarding the atrium space, averaging the temperatures on each of the three levels yields a temperature difference of 2 °C between the top and low level.

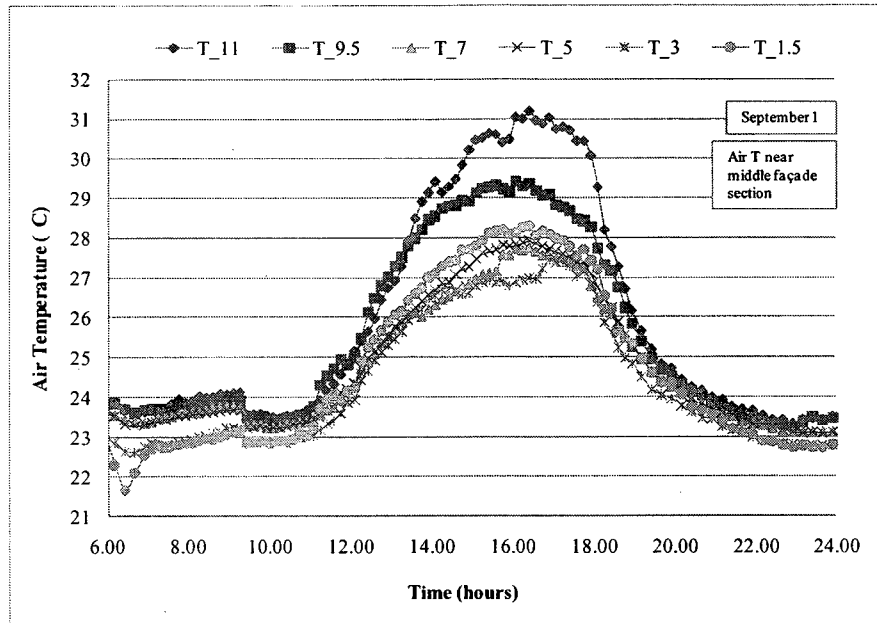


Figure 4.3. Air temperature variation throughout the day at six different heights near the façade

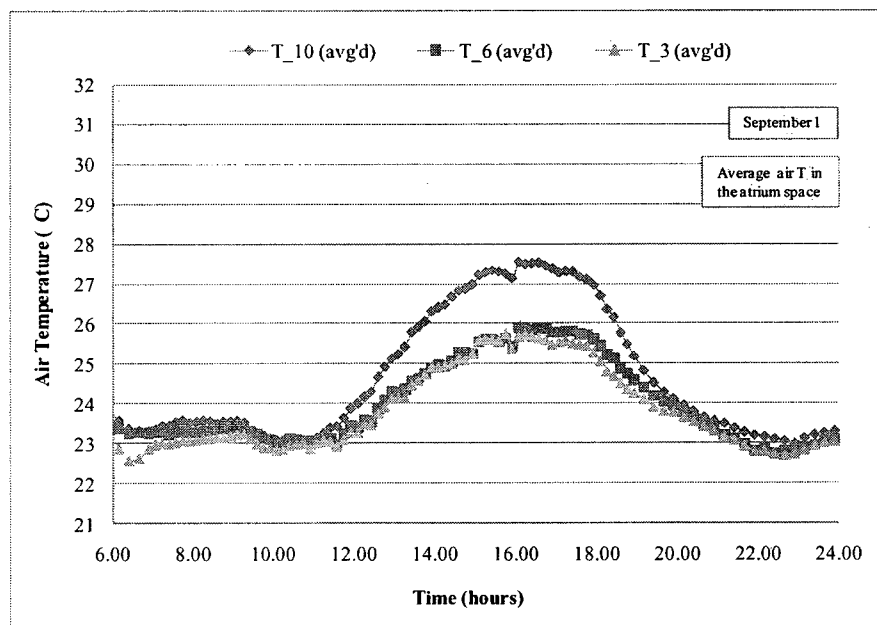


Figure 4.4. Air temperature variation throughout the day at three different heights in the atrium space

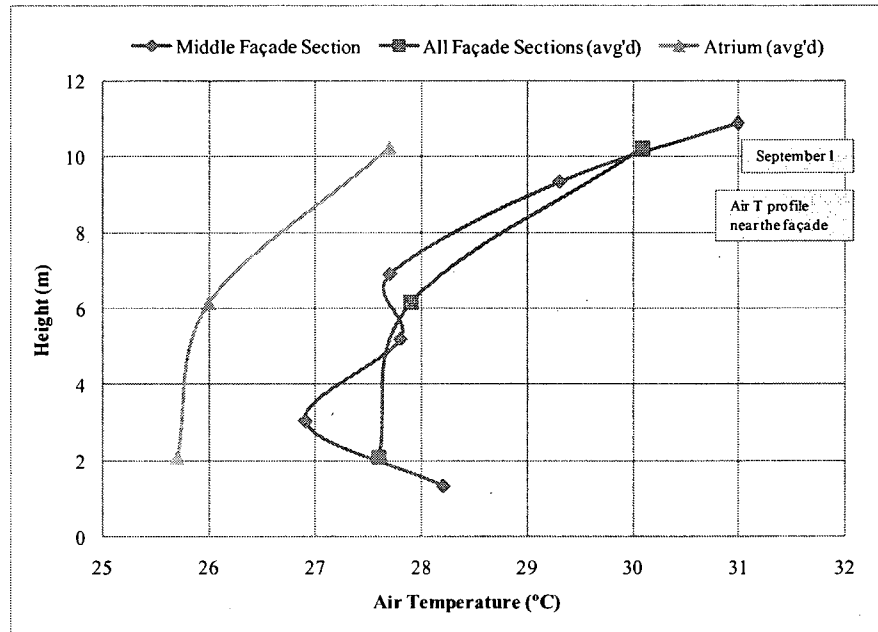


Figure 4.5. Air temperature profile a) near the façade (middle section), b) near the façade (all sections), c) in the atrium space; data based on peak temperature values

The variation of air temperature near the façade and in the atrium space for a day with conditions similar to the case previously presented but with the roller shades closed is shown in Figure 4.6 and Figure 4.7 (September 23, 2007). On that day, outdoor temperature reached a low of 12.5 and a high of 21 °C while maximum measured solar radiation transmitted through the glass was 260 W/m². Indoor space was cooled by natural and mechanical ventilation; low to moderate use of mechanical ventilation was maintained throughout the day supplying air at a rate of 0.2 m³/sec and at a 17 °C temperature. Data for the indoor and outdoor conditions can be found in Appendix II.

As shown in Figure 4.6, air near the façade is stratified reaching a maximum temperature difference around 16:00. Lowest temperature is detected at measuring point T₃, only slightly lower than T_{1.5}. Unlike the previous case, the temperature difference between points T₃ and T_{1.5} is not as pronounced; this could be attributed to the significantly less amount of solar radiation (transmitted through the roller shade) reflected by the

window frame. In the atrium space, temperatures in the room range from 25.5 °C at the lobby area to 28.5 °C at the top of the atrium (Figure 4.7). Even though there was no occupancy in the building on that day, the same conditions on a workday could cause some discomfort for a period of two or three hours, mostly in the offices adjacent to the top atrium level.

Figure 4.8 illustrates the air temperature profile based on the peak temperature values occurring in mid-afternoon of that day. Near the middle section of the façade, the temperature profile resembles the profile shown in the previous case (September 1, 2007). Maximum temperature difference for that section is almost 3 °C. The same temperature difference is observed in the case of the entire façade area and the atrium, based on the average façade and atrium space air temperatures on each level.

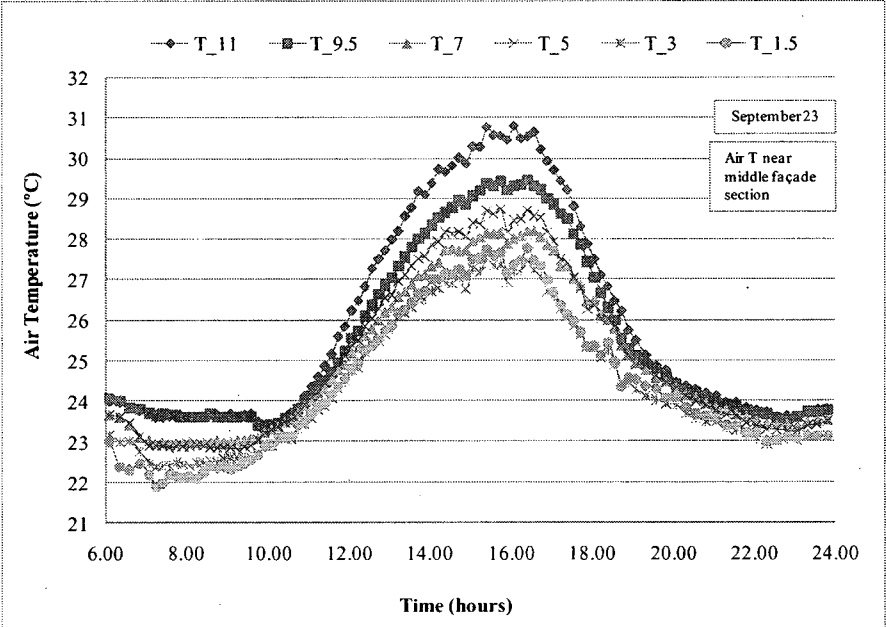


Figure 4.6. Air temperature variation throughout the day at six different heights near the façade

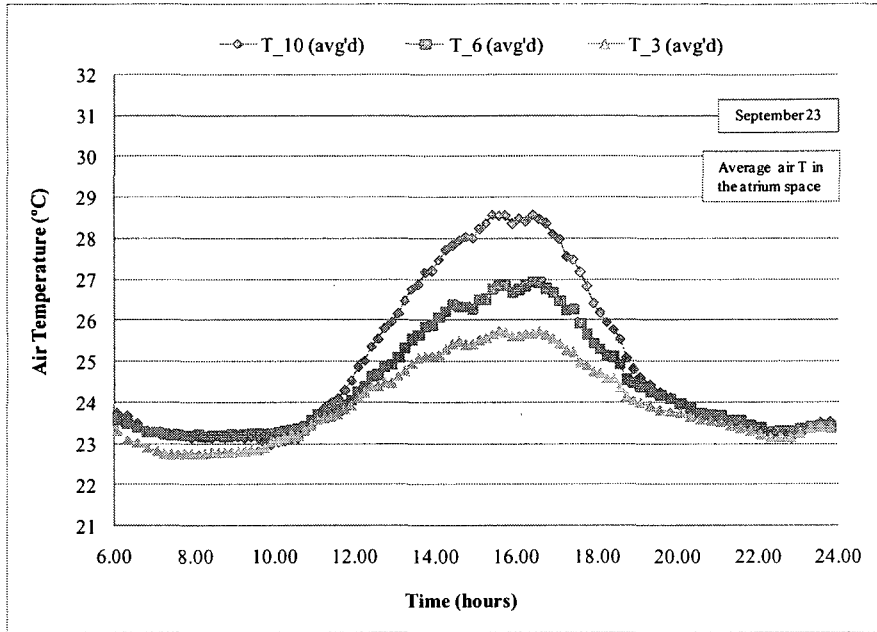


Figure 4.7. Air temperature variation throughout the day at three different heights in the atrium space

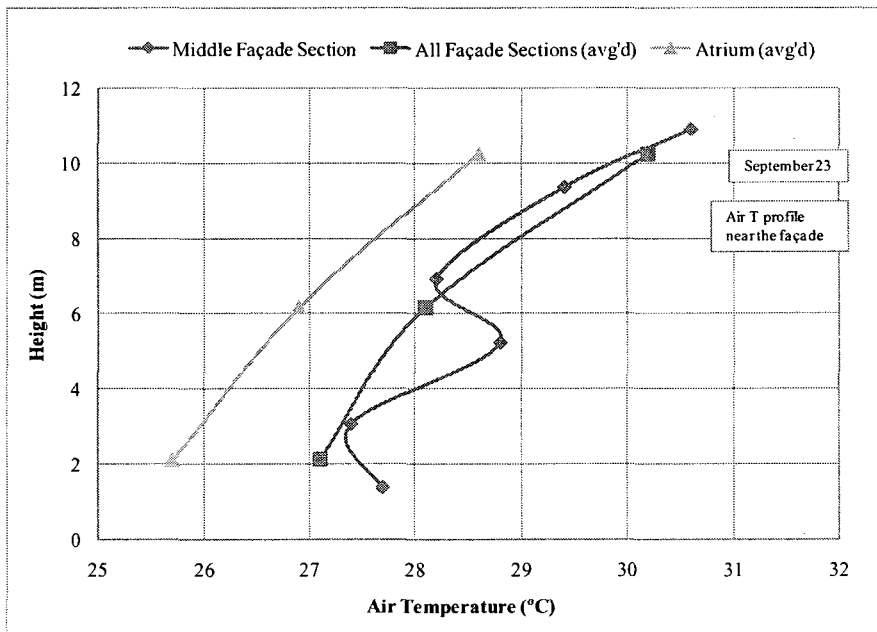


Figure 4.8. Air temperature profile a) near the façade (middle section), b) near the façade (all sections), c) in the atrium space; data based on peak temperature values

4.2.2. Natural ventilation system not in operation

For comparison purposes, a cold and a warm day when the atrium was only mechanically ventilated, were examined and are described below. Air temperature change over time near the façade and in the atrium space is shown in Figure 4.9 and Figure 4.10 for a clear day with the outdoor temperature ranging from -1 to 7 °C (November 2, 2007). Maximum measured solar radiation transmitted through the glass was 290 W/ m². Roller shades were open during the day and the indoor space was conditioned with air supplied at a 1.1 m³/sec rate and a temperature of 16 °C. Indoor and outdoor conditions can be found in Appendix II.

Lowest and highest temperature is observed at points T_1.5 and T_11 respectively (Figure 4.9). Air stratification under the conditions maintained in the atrium is displaying a typical pattern. High solar radiation levels justify the high temperatures near the façade.

Regarding the temperatures in the room (Figure 4.10), around peak time, the temperature is 24 °C in the lobby space and about 26 °C at the top of the atrium.

Air temperature profiles for the air near the façade and in the atrium are shown in Figure 4.11. Near the façade, in the absence of natural convection, air is not as mixed as before resulting in the temperature profile seen in the graph. Temperature stratification at peak time is 4.5 °C in the middle section of the façade and approximately 2.5 °C for the entire façade area. When the whole atrium space is considered, temperature difference between the top and low levels is a little over 2 °C. It can also be noticed that temperatures near the façade and the rest of the space are not as apart as in the two previous cases, suggesting that air on each level is more uniformly distributed across the room.

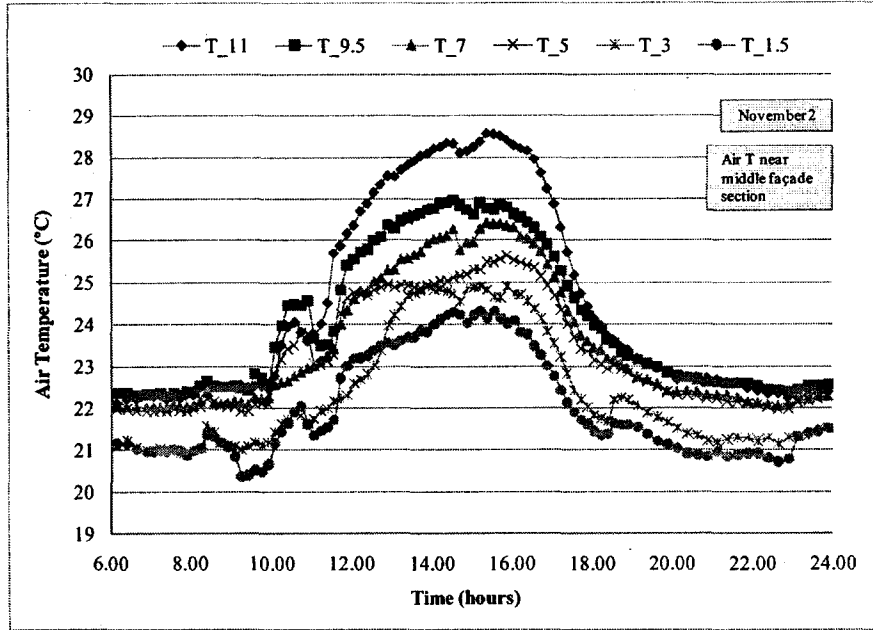


Figure 4.9. Air temperature variation throughout the day at six different heights near the façade

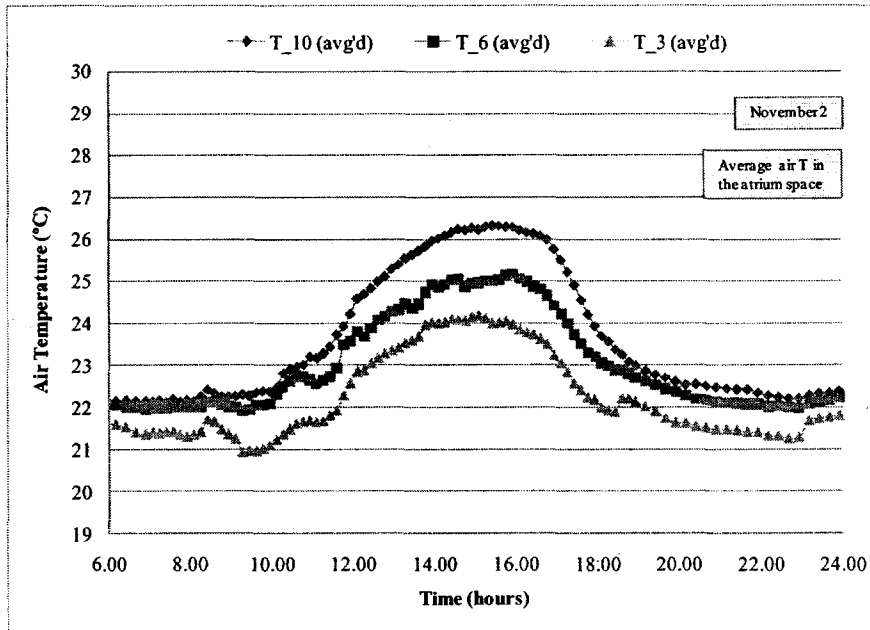


Figure 4.10. Air temperature variation throughout the day at three different heights in the atrium space

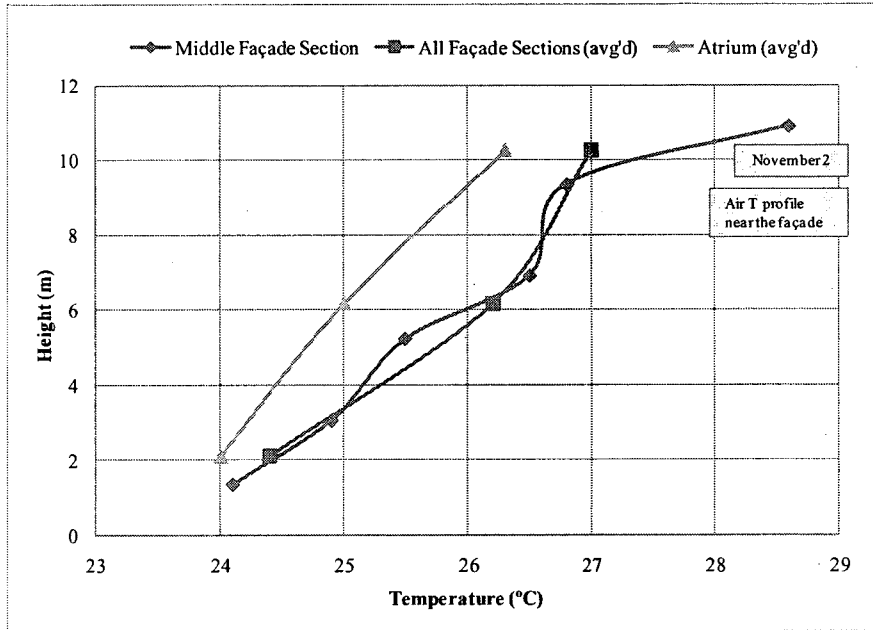


Figure 4.11. Air temperature profile a) near the façade (middle section), b) near the façade (all sections), c) in the atrium space; data based on peak temperature values

Air temperature variation with time near the façade and in the atrium space is shown in Figure 4.12 and Figure 4.13 for a hot sunny day with an outdoor temperature between 22.5 – 32 °C (August 2, 2007). The maximum solar radiation transmitted through the glass was 160 W/ m². Indoor air was naturally and mechanically ventilated until 11:00 and from then on air was only mechanically supplied at a flow rate of 1.2 m³/sec and a temperature of 15 °C. Roller shades were kept open until late afternoon. Indoor and outdoor conditions on that day can be found in Appendix II.

Air is stratified with the lowest temperature met at T_{1.5} and the highest one at T₁₁. Thermal stratification reaches its maximum around 16:00 in the afternoon. Comparing August 2 to November 2 (comparing a hot day to a cold day – Figure 4.9 and Figure 4.12), it is noticed that air temperatures along the middle section of the façade in these two cases are very close, a clear indication that solar radiation is a dominant factor in the air temperature forming in the atrium. Upon closing the roller shades, there is an almost

immediate temperature decrease at the measuring points T_1.5 and T_5 of about 1 °C. This is likely caused by the considerable reduction of the solar radiation transmitted through the room that is directly or through reflections affecting the temperature sensor. At 18:30, the shift in temperature at T_1.5 and T_3 is due to the change in cooling rate (going from 1.2 m³/sec down to 0.6 m³/sec).

Temperatures on each atrium level are given in Figure 4.13. Switching from mixed mode to mechanical ventilation around 10:00 in the morning is causing the temperature drop occurring on floor 14 (T_3). From 13:00 – 17:00, temperature in the lobby is around 24 – 25 °C, only slightly lower than the temperature range formed on September 1 and September 23 when the atrium was mostly naturally ventilated for the same period of time.

Peak daily temperatures are portrayed in Figure 4.14. Their profiles are comparable to the ones on November 2. Temperature difference from bottom to top is 4.5 °C near the middle section of the façade and a little over 3 °C when the entire façade area is considered. In the room, averaging air temperatures on each level yields a temperature difference of about 3 °C. Similar to November 2 and unlike September 1 and September 23, air is more evenly distributed across each room level.

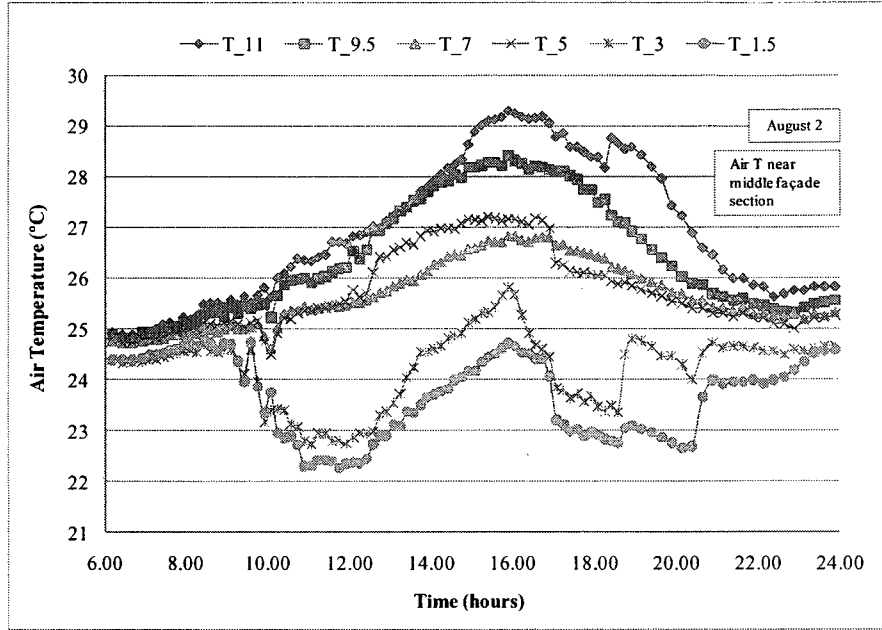


Figure 4.12. Air temperature variation throughout the day at six different heights near the façade

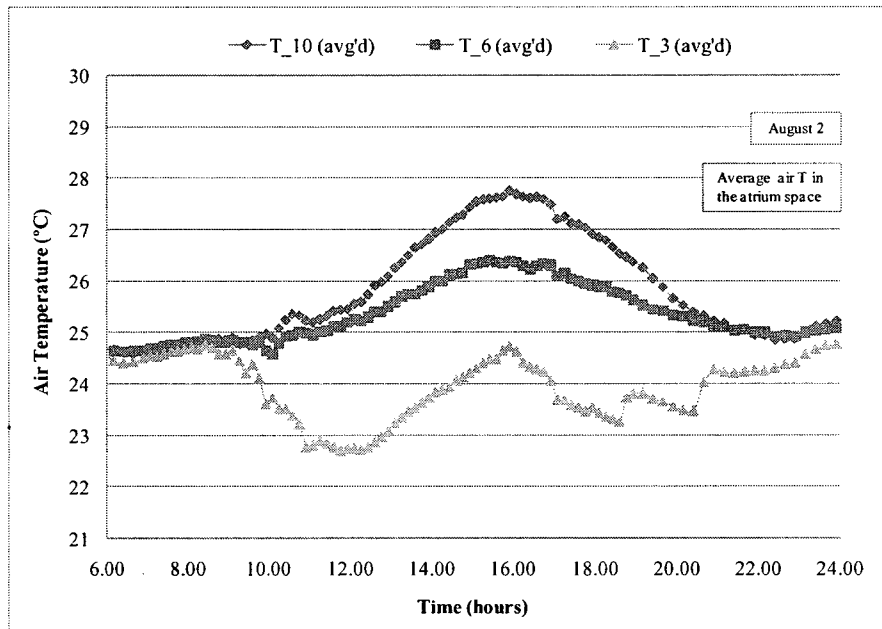


Figure 4.13. Air temperature variation throughout the day at three different heights in the atrium space

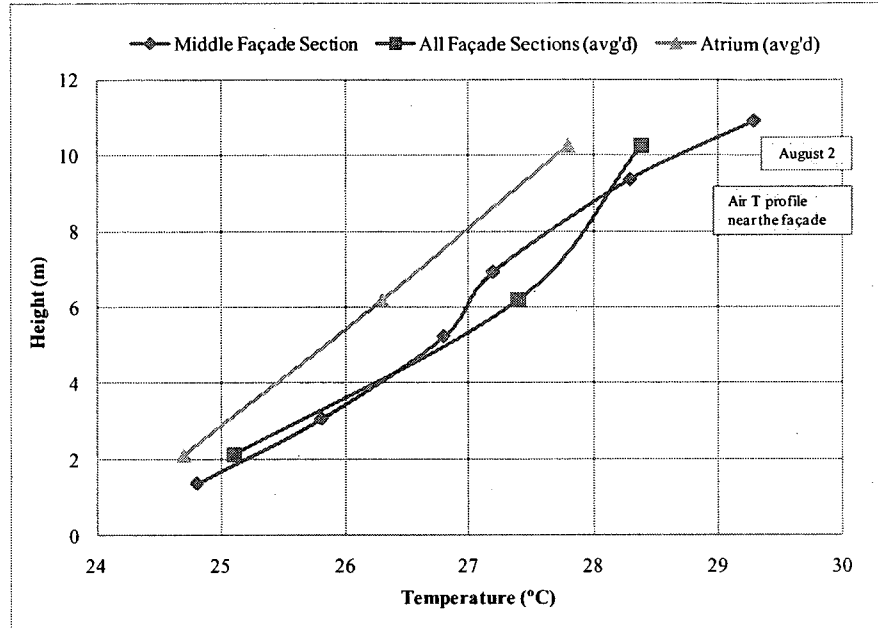


Figure 4.14. Air temperature profile a) near the façade (middle section), b) near the façade (all sections), c) in the atrium space; data based on peak temperature values

4.3. Airflow measurements

When the building is under mixed ventilation mode, a) corridor inlet grilles are open to let outdoor air enter the building and b) atria-connecting floor grilles are open to allow air moving upwards from the lower floors be exhausted through the top. Air velocity and pressure difference across the corridor inlet grilles on floor 15 was continuously monitored while air velocity at the floor grilles of floor 14 was manually measured.

4.3.1. Airflow through the corridor inlet grilles

Ventilation rates and airflow direction at the inlet grilles depends on the wind speed, wind direction and the indoor-outdoor temperature difference. Three cases for three

different days are presented while their respective indoor and outdoor conditions are summarized in Table 4.3. Detailed wind and outdoor temperature data can be found in Appendix II.

Table 4.3. Wind, ΔT and airflow data for three different cases

| Date | September 23, 2007 | | September 30, 2007 | October 5, 2007 |
|--|--------------------|-------------|--------------------|-----------------|
| Time period | 11:00-18:00 | 18:00-20:00 | 15:00-20:00 | 14:00-20:00 |
| Wind speed (km/hr) (W.D.) | 25 | 12 | 5 – 7 | 6 – 13 |
| Wind direction (degrees) (W.D.) | 270 | 270 | 145 | 220 |
| ΔT_{in-out} (°C) (M, W.D.) | 7 – 8.5 | 5 | 10 – 11 | 4 – 6 |
| Airflow at floor grilles (m ³ /sec) (M) | 2.6 | 0.8 | 4.7 | 1.6* |
| Airflow at exhaust (m ³ /sec) (M) | 2 – 3 | 2 – 3 | 5.4 | 1.6 – 3.2 |

(W.D.): Weather Data (Source: Environment Canada), (M): measured, *theoretically calculated

Figure 4.15 and Figure 4.16 illustrate the airflow and the pressure drop across the corridor grilles at the SE and NW façade on floor 15 of the building on September 23, 2007. Both wind and stack effects are significant during that day (Table 4.3, wind speed and ΔT_{in-out}). Air is coming in through the inlet grilles on the NW side and going out through the SE side (as indicated by the inverted airflow values in Figure 4.15). Inflow (Q_{in}) is about 600 l/sec and almost equal to the outflow (Q_{out}) until around 16:00. Then, as the day progresses (16:00 – 18:00), Q_{in} becomes higher than Q_{out} due to the decreasing stack effect. This difference is more pronounced as a result of the strong wind.

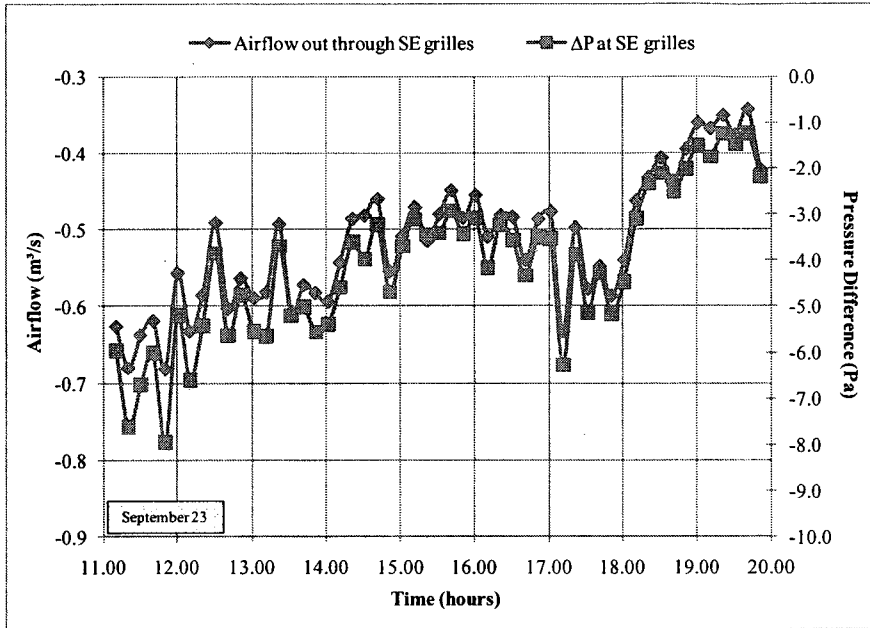


Figure 4.15. Airflow rate and pressure difference across the SE side inlet grilles

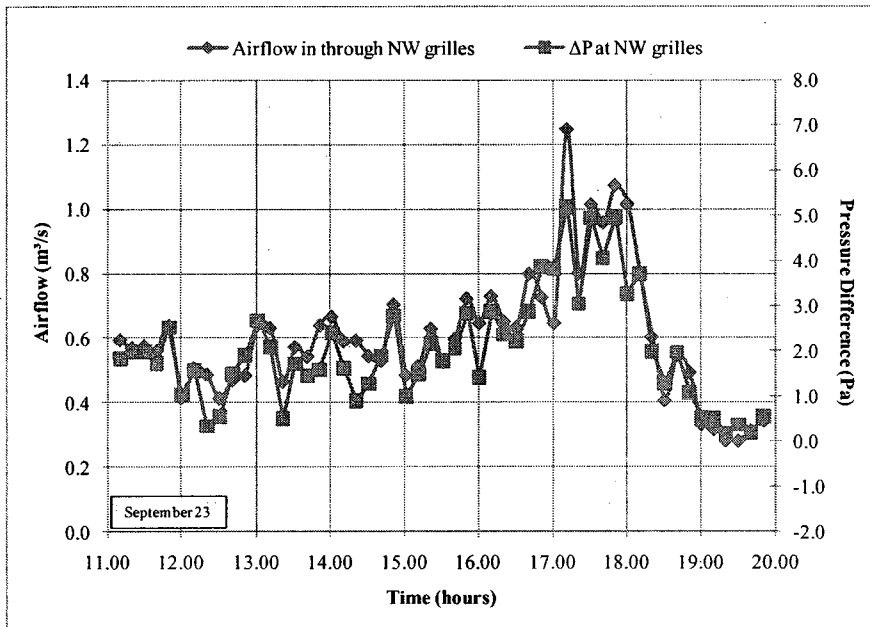


Figure 4.16. Airflow rate and pressure difference across the NW side inlet grilles

In a similar way, pressure difference (ΔP) across the grilles is 1.7 Pa until 16:00 then increases to 4 Pa. Change in wind speed (going from 25 km/hr down to 12 km/hr) causes both flows and ΔP to considerably decrease after 18:00. As expected, strong stack effect will create an inflow through the corridor inlet grilles on the lower levels (below NPL)

and an outflow on the top floors (14 – 16), while inflow on higher floors is wind driven. In this case, the strong wind speed coupled with a wind direction at 270° favours an inflow on the NW side while negative pressures caused by the wind and the stack effect result in an outflow on the SE side.

Airflow and pressure difference across the inlet grilles on a day with strong stack effect (September 30, 2007) are presented in Figure 4.17 and Figure 4.18. As previously mentioned in Chapter 3 (section 3.2.3), “0” value for the pressure difference at the NW façade indicates negative ΔP . Even though wind is almost incident to the SE façade, this alone does not create an inflow through the grilles; wind speed is very low and strong stack effect causes negative pressures to prevail. Consequently, an outflow (indicated by the negative airflow rate values) through both sides of the building’s upper floors is generally observed.

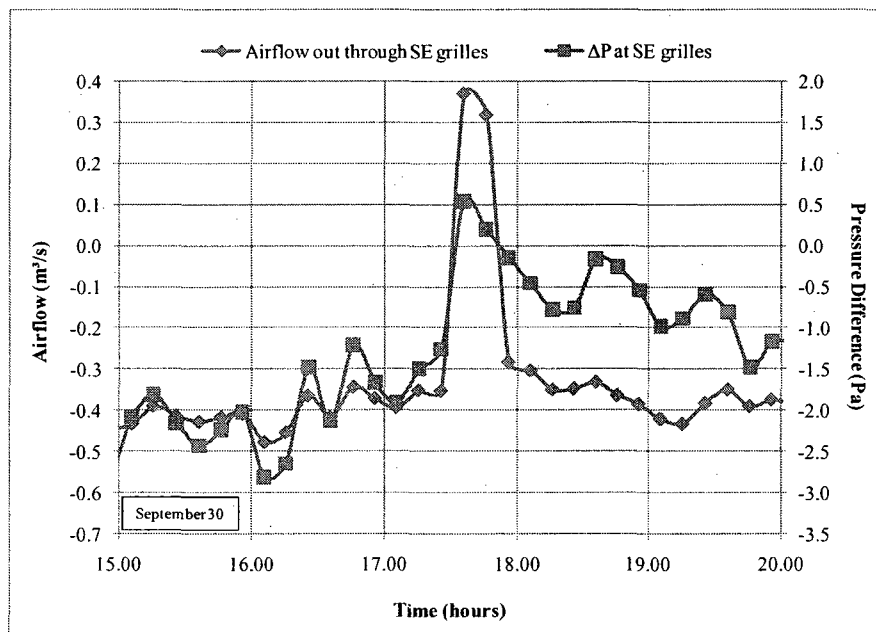


Figure 4.17. Airflow rate and pressure difference across SE side inlet grilles

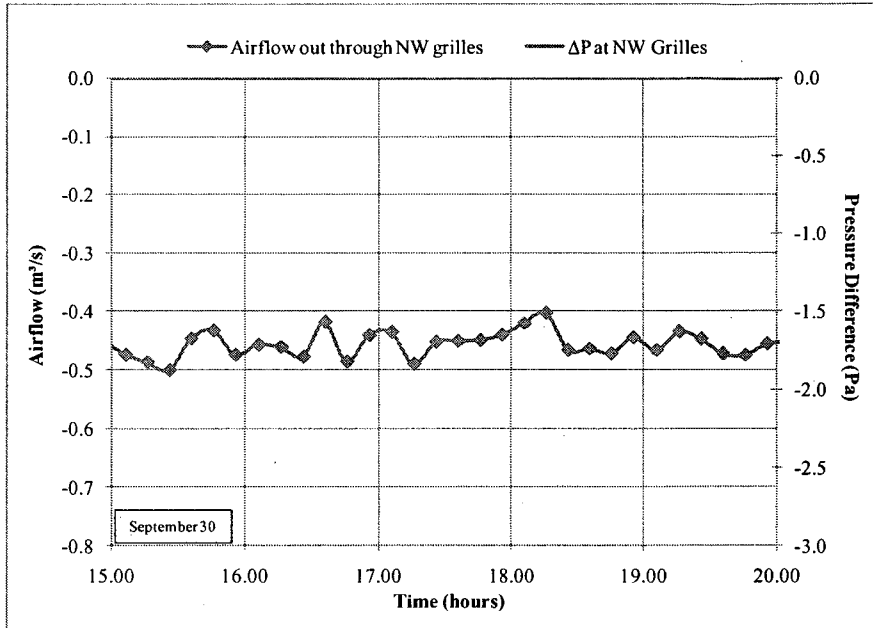


Figure 4.18. Airflow rate and pressure difference across NW side inlet grilles

Figure 4.19 and Figure 4.20 show the pressure drop and airflow rate through the SE and NW corridor grilles on, a day with low stack and low wind effect (October 5, 2007). Wind is directed at an angle that generates positive pressures on both façades which in turn, in the absence of strong stack effect, causes air to flow in through both sides. The total inflow rate is up to 700 l/sec while pressure difference is about 1.2 Pa and 0.7 Pa across the SE and NW side inlet grilles respectively.

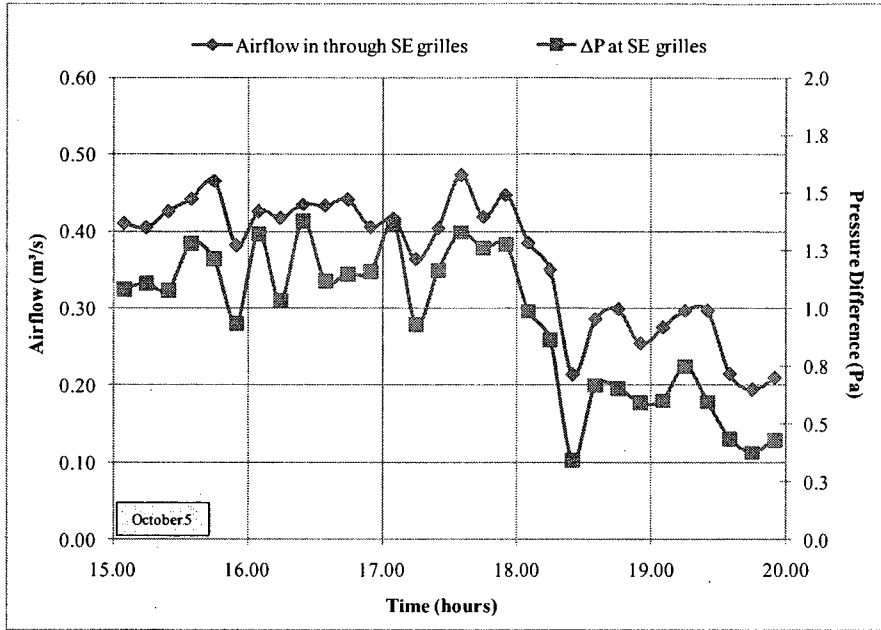


Figure 4.19. Airflow rate and pressure difference across SE side inlet grilles

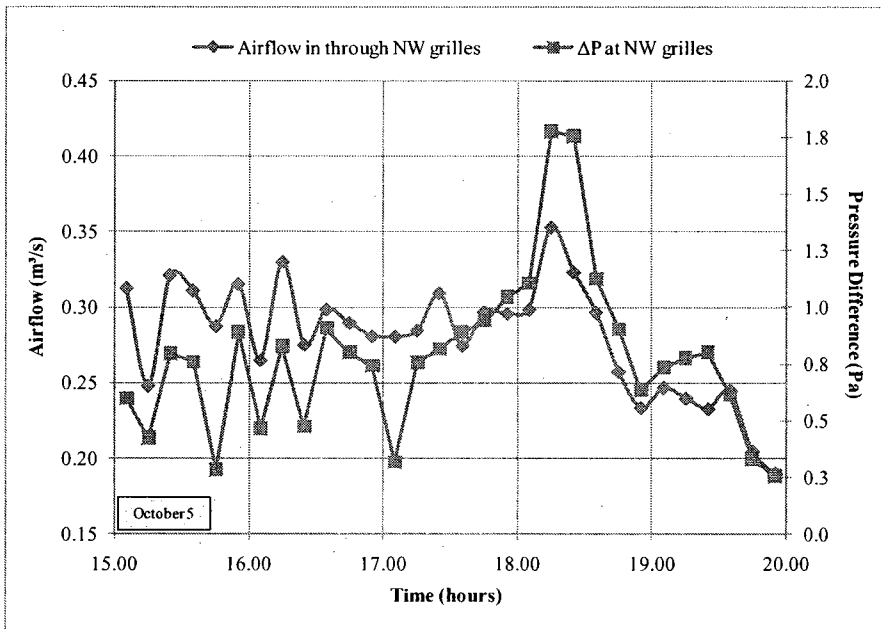


Figure 4.20. Airflow rate and pressure difference across NW side inlet grilles

4.3.2. Airflow through the floor grilles

Velocity of the air entering the top atrium through the atria connecting floor grilles was regularly measured during a period of one month. Figure 4.21 shows the variation of the airflow rate through the atria connecting floor grilles (on floor 14) with the indoor-outdoor temperature difference. Increasing temperature difference results in higher airflow rates. A linear correlation (correlation coefficient of 0.82) between the airflow through the floor grilles that connect the atria (due to buoyancy-driven flow) and the square root of the indoor-outdoor temperature difference is observed, as expected based on the following theoretical equation for the airflow induced by stack effect:

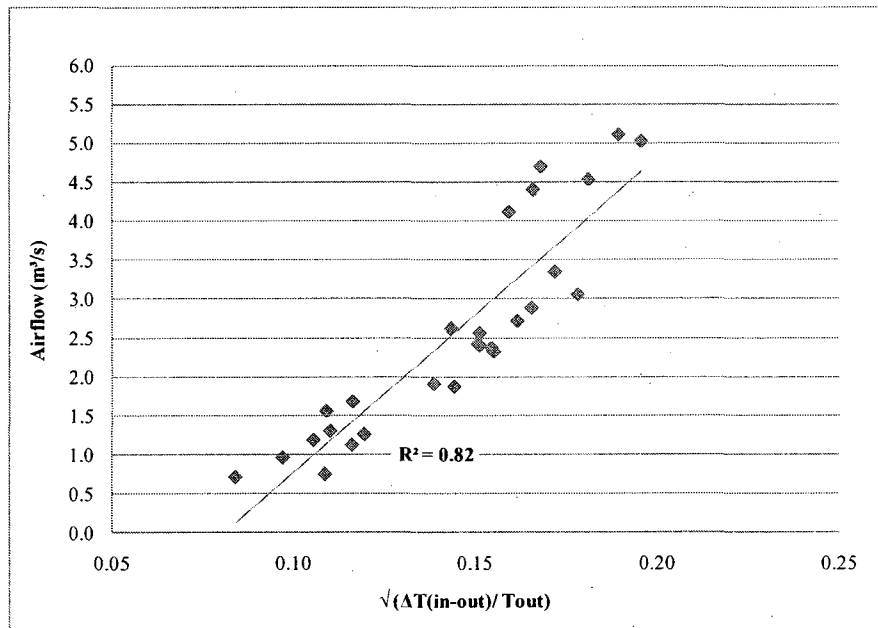


Figure 4.21. Airflow rate at top atrium floor grilles as a function of $\Delta T_{in\text{-}out}$

$$Q_s = C_d \cdot A \cdot \sqrt{2 \cdot g \cdot H_d \cdot \frac{T_i - T_o}{T_i}} \quad (\text{Equation 4.1})$$

where:

$$Q_s = \text{airflow rate (m}^3\text{/sec)}$$

A = cross-sectional area of opening (m^2)

C_d = discharge coefficient

g = gravitational acceleration (m/s^2)

H_d = height from midpoint of lower opening to neutral pressure level (m)

T_i = average indoor temperature between inlet and outlet (K)

T_o = outdoor temperature (K)

4.5. Energy performance of the building during the cooling season

4.5.1. Energy savings in the building

As described in Chapter 3, when the building is in mixed ventilation mode, the air supply units in the corridors shut down. This alone accounts for a significant amount of energy. A typical example to demonstrate this would have been to compare two similar days where one parameter (e.g. high relative humidity) prevents the natural ventilation system from operating. It can be reasonably expected that the load for the chillers would be less in the case where the building is under hybrid ventilation. However, only part of the monitoring data for the chillers' load is available, therefore the building energy consumption in cooling could not be properly estimated in this way.

4.5.2. Estimation of cooling load reduction

The reduction in cooling load is estimated assuming that the free cooling gained from natural ventilation would normally have been provided through mechanical cooling and

ventilation. Two simple approaches for this estimation are followed using monitoring, manual measurements and weather station data.

The first approach is based on the amount of air that is exhausted at the top of the building. A workday time period from 12:00-18:00 (time of high transmitted solar radiation levels in the atrium) was considered for the calculations. Air is flowing in through the corridor inlet grilles and is being exhausted from the ceiling of the top atrium. However, as previously seen in section 4.3, under wind and stack effects, air can also flow out through the corridor grilles or returned to other zones of the building and exhausted through local vents. Consequently, the amount of air measured at the exhaust is only part of the total incoming fresh air. The return unit on each atrium is typically running at a higher airflow rate than the air supply unit, therefore the mechanical air supply in the atria is not considered to cause erroneous (over-predicted) flow rates for the incoming outdoor air.

The second approach is based on the stack-driven inflow at levels below the neutral pressure level of the building (floors 2-10). Similar to the first approach, a workday time period from 12:00-18:00 was considered for the calculations. The total amount of air entering the building is likely to be exceeding the inflow induced only from stack effect. Compared to the previous case, this approach is probably more appropriate when trying to estimate the free cooling obtained from natural ventilation but it is, on the other hand, based on more assumptions. Exhaust temperature for the air coming in through floor levels 2-10 was assumed to be 24 °C (relative temperature value according to the temperature of the exhaust on floor 16) while a representative air velocity for the inlet grilles at levels 2-10 was used (based on experimental data).

In summary, the data used are:

- Average outdoor temperature for time periods of interest
- Average air temperature at the exhaust for time periods of interest
- Average air velocity at the exhaust for time periods of interest
- Average air velocity at the inlet grilles as a function of outdoor temperature (theoretically calculated)
- Opening areas of exhaust and inlet grilles

In both cases, the following equation was used to calculate the free cooling rate q :

$$q = M \cdot C_p \cdot (T_{\text{exhaust}} - T_o) \quad (\text{Equation 4.2})$$

where:

M = mass flow rate of incoming air, kg/sec

C_p = specific heat capacity of air, kJ/ kg ·°C

T_{exhaust} = temperature at the exhaust, °C

T_o = outdoor temperature, °C

Calculations were made for the months of August, September and October. The free cooling rate (or heat removal) rate obtained by natural ventilation as well as the values used in calculations are presented in Tables 4.4 and 4.5. The number of days considered for each month is different, depending on the operation of the natural ventilation system.

Table 4.4. Estimated 'free cooling' rates from natural ventilation - first approach

| Month | August | September | October |
|---|--------|-----------|---------|
| $q_{cooling1}$, kW | 30.5 | 29.9 | 31.9 |
| Average T_{out} , °C | 21.3 | 20.5 | 18.7 |
| Average $T_{exhaust}$, °C | 24.9 | 25.6 | 25.7 |
| Average $V_{exhaust}$, m/sec | 1.3 | 0.9 | 0.7 |
| Exhaust opening area, m ² | 5.4 | 5.4 | 5.4 |
| Average $Q_{exhaust}$, m ³ /sec | 7.0 | 4.9 | 3.8 |
| Days considered for data | 18 | 22 | 10 |

Table 4.5. Estimated 'free cooling' rates from natural ventilation - second approach

| Month | August | September | October |
|--|--------|-----------|---------|
| $q_{cooling2}$, kW | 18.4 | 30.8 | 70.3 |
| Average T_{out} , °C | 21.3 | 20.5 | 18.7 |
| Average $T_{exhaust}$, °C | 24 | 24 | 24 |
| Average $V_{inletgrilles}$, m/sec | 0.26 | 0.35 | 0.54 |
| Grilles opening area, m ² | 22.4 | 22.4 | 22.4 |
| Average $Q_{inletgrilles}$, m ³ /sec | 5.8 | 7.8 | 12.1 |
| Days considered for data | 18 | 22 | 10 |

Applying these cooling rates on a workday time period of six hours (12:00 – 18:00), the amount of energy that is gained by natural ventilation was calculated, taking into account the natural ventilation system operation time for each month (section 4.1, Figure 4.1). The results are shown in Table 4.6.

Table 4.6. Estimated free cooling from natural ventilation (based on a 6-hour workday time period)

| Month | August | September | October |
|-----------------------------|--------|-----------|---------|
| Free cooling (1), kWh | 2925 | 2448 | 914 |
| Free cooling (2), kWh | 1821 | 2681 | 2213 |
| Days | 31 | 30 | 31 |
| Workday time period (hours) | 6 | 6 | 6 |
| NV system operation rate | 51.6% | 45.5% | 15.4% |

The total free cooling obtained during a period of three months is found to be 6287 kWh with the first approach and 6715 kWh with the second approach, an average of 6500 kWh. The heat removal in the top atrium for the same period of time was found to be

2800 kWh (as indicated by the monitoring data for the mechanical air supply in the atrium). Even though the demand for cooling is probably higher in the top atrium (susceptible to overheating), it can be assumed that the same amount of heat was removed in all five building atria, thus a total of 14,000 kWh. This heat removed by the mechanical system does not really represent the building's demand in cooling since part of it is already covered for by natural ventilation. If the free cooling from natural ventilation is considered as additional load, the total heat removal demand for the atrium and corridors would have been approximately 20,500 kWh. From this it can be concluded that the existing natural ventilation schedule can only provide for part (about 30%) of the cooling requirements in these zones. Introducing some modifications in the system's operation (e.g. night cooling at lower than 15 °C outdoor temperatures) could help reduce the cooling load.

4.6. Cooling load in the atrium

Measured temperature and air velocities in the atrium were utilized to estimate the heat removed in the space for a three-month period during the cooling season. Taking into consideration additional parameters such as the position of the roller shades, the weather conditions and the presence or absence of natural ventilation, the following observations can be made for the months of August – October:

- No shading or inappropriate use of shading on a sunny day will increase the cooling load of the subsequent day.

- When the building is not naturally ventilated for consecutive days, this is likely to result in increased cooling requirements.
- Repeated absence of natural ventilation at night time appears to have an impact on the cooling demand in the daytime.
- Roller shade control and natural ventilation for prolonged periods of time help reduce the energy consumption.
- The effect of night time ventilation is noticeable at lower outdoor temperatures.

A steady state energy balance was performed for floors 14 – 16 on a clear day with low occupancy, using manual measurements and monitoring data at a certain time in the afternoon. The control volume for the energy balance consists of the atrium and the corridors. The inlet and outlet sources in these spaces are:

- Mechanical air supply in the atrium
- Air return in the atrium
- Exhaust vents in the atrium
- Floor grilles in the atrium
- Exhaust vents in the washrooms
- Corridor inlet grilles on the SE and NW side of each floor

The complexity of multiple air inlet and outlet sources at different temperatures and airflow rates was overcome with the use of enthalpies. The psychrometric chart in equation form was used (Athienitis, 1999) to calculate the enthalpy of incoming/outgoing air at the sources considered within the control volume. The enthalpy of the air

in each location and the energy from the solar radiation transmitted in the space are shown in Table 4.7.

Table 4.7. Enthalpy of the air at different inlet/ outlet sources and transmitted solar radiation

| Air sources | Inlet source | | | Outlet sources | | | |
|--|---------------------|---------------|------------------------|----------------|---------------|------------------|------------------------|
| | Atrium air supply | Floor grilles | Inlet grilles, NW side | Atrium exhaust | Atrium return | Washroom exhaust | Inlet grilles, SE side |
| Temperature, °C (M) | 16.5 | 27.0 | 20.7 | 26.7 | 26.8 | 23.0 | 25.2 |
| % RH (A) | 0.55 | 40 | 40 | 40 | 40 | 40 | 40 |
| Airflow rate (m ³ /sec) (M) | 0.17 | 2.9 | 1.9 | 1.1 | 2.0 | 0.6 | 1.6 |
| Mass rate (kg/sec) (C) | 0.2 | 3.3 | 2.3 | 1.3 | 2.3 | 0.7 | 1.9 |
| Enthalpy h (kJ/kg) (C) | 32.7 | 49.7 | 36.1 | 48.9 | 49.2 | 40.7 | 45.4 |
| Enthalpy* H (kW) (C) | 6.5 | 164.0 | 83.0 | 63.6 | 113.2 | 28.5 | 86.3 |
| Solar radiation transmitted in the space, kW (M) | 6.5 | | | | | | |
| Inlet + Solar – Outlet, kW | 260 – 291.6 = -31.6 | | | | | | |
| Error | 12% | | | | | | |

* $H=h \cdot (\text{mass rate})$, (C): calculated value, (M): measured value, (A): assumed value

The energy balance in the control volume requires that the energy of the incoming air and the energy from the transmitted solar radiation should be equivalent to the energy of the air leaving the space. The error produced for the energy balance in this case is within reasonable limits, considering the data input are based on measurements under transient conditions.

4.7. Summary

The natural ventilation system operated on average 35% of the time in year 2007 and 26% of the time in year 2008 during the cooling season (April – October), contributing to energy savings in the building cooling. Detailed energy calculations were not possible due to limited BEMS data. Two simplified approaches undertaken to estimate the free cooling obtained by natural ventilation indicate that the existing natural ventilation

schedule accounts for approximately 30% of the hybrid cooling in the atrium and adjacent corridors. The potential of the system can be improved by including some control strategies and introducing a night time operation schedule at lower outdoor temperatures. Utilization of a variable speed fan at the top of the atrium to raise the neutral plane to the roof level as recommended in the design (but not adopted) would have resulted in improved performance.

Regarding the indoor conditions, temperatures in the top atrium of the building were examined; on clear days and under mixed mode ventilation (with low rate mechanical air supply), maximum air temperature in the space was found to be within acceptable ranges, 25 – 27 °C. Thermal and airflow monitoring was implemented in the top atrium (floors 14 – 16) and the corridor inlet grilles of floor 15. Temperature profiles and airflow rates were studied on days with different indoor and outdoor conditions. The results are summarized in Tables 4.8 and 4.9.

Table 4.8. Thermal monitoring in the atrium

| Date | September 1 | September 23 | November 2 | August 2 |
|---|---|--|---|--|
| T_{outdoor} | 12.5-20 °C | 12.5-21 °C | -1-7 °C | 22.5-32 °C |
| NV system | ON | ON | OFF | OFF |
| Cooling supplied | 0.12 m ³ /s 17 °C 1.3 kW | 0.2 m ³ /s 17 °C 1.9 kW | 1.1 m ³ /s 16 °C 12.7 kW | 1.3m ³ /s 15 °C 17.9 kW |
| Roller shades | open | closed | open | open |
| $T_{\text{atrium,max}}$ (at peak time) | 25.5-27.5 °C | 25.5-28.5 °C | 24-26 °C | 25-28 °C |
| ΔT_{max} atrium space (avg'ed) | 2 °C | 3 °C | 2 °C | 3 °C |
| ΔT_{max} façade (avg'ed) | 2.5 °C | 3 °C | 2.5 °C | 3 °C |
| ΔT_{max} middle façade | 4 °C | 3 °C | 4.5 °C | 4.5 °C |

Table 4.9. Airflow monitoring at the corridor inlet grilles

| Date | September 23 | September 30 | October 5 |
|----------------|--|--|---|
| Driving force | <ul style="list-style-type: none"> • Strong wind effect • Stack effect | <ul style="list-style-type: none"> • Strong stack effect • Low wind effect | <ul style="list-style-type: none"> • Low wind effect • Low stack effect |
| Wind direction | 30° East of NW façade | 20° West of SE façade | 80° East of NW façade 95° West of SE façade |
| Airflow | 0.5 m ³ /sec (SE façade) 0.6 m ³ /sec (NW façade) | 0.4 m ³ /sec (SE façade) 0.5 m ³ /sec (NW façade) | 0.4 m ³ /sec (SE façade) 0.3 m ³ /sec (NW façade) |
| Flow direction | IN (SE façade) OUT (NW façade) | OUT (SE façade) OUT (NW façade) | IN (SE façade) IN (NW façade) |

5. NIGHT VENTILATION COOLING POTENTIAL – EXPERIMENTAL AND SIMULATION RESULTS

Introduction

This chapter focuses on the night ventilation cooling potential of the building. First, the system's existing temperature range condition for operation during night time is modified and the additional night ventilation hours are theoretically calculated. Next, a qualitative approach towards energy savings from night cooling is undertaken. Results for the airflow and slab surface temperature measurements from two relatively cool nights are presented. Experimental data are used as input values in a simplified analytical model that was developed to predict the surface temperature decrease for areas of the slab located near and at a distance from the inlet grilles. Simulation results are compared to experimental results and the model is used to quantify the cooling storage in the slab that can be achieved with different night ventilation strategies.

5.1. Night time ventilation

5.1.1. Night ventilation hours

The building is ventilated at night at a minimum allowable outdoor temperature of 15 °C (under the standard natural ventilation system operation currently in use). Night ventilation hours were calculated for three temperature ranges, 15 – 25 °C (standard night schedule), 12 – 25 °C (night schedule #1), and 8 – 25 °C (night schedule #2), for a relative humidity below 70%. All temperature ranges were imposed at night time, from

19:00-7:00. Figure 5.1 and Figure 5.2 show the night ventilation hours obtained with each of the three night ventilation schedules. Calculations are based on monitored weather data for the 2007 and 2008 cooling seasons.

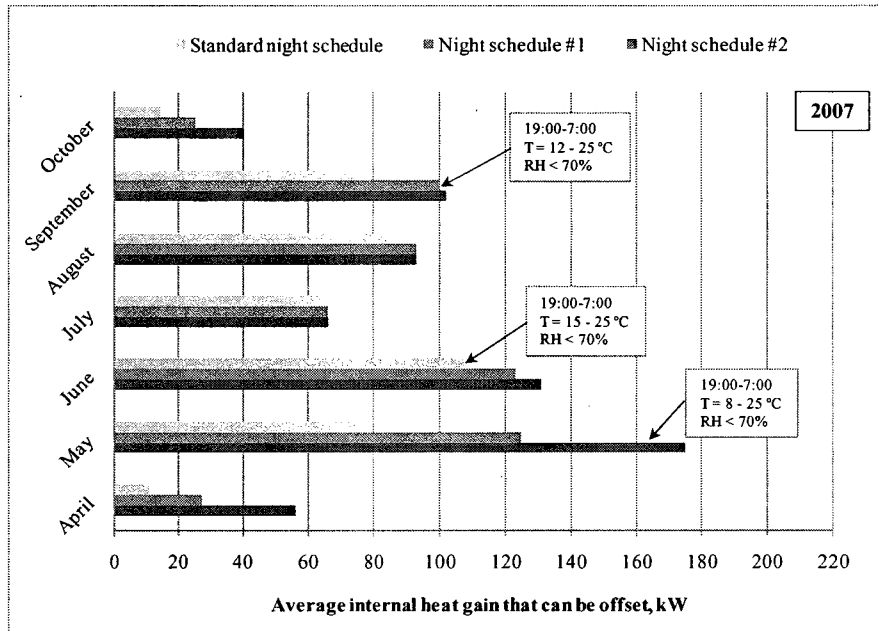


Figure 5.1. Calculated night ventilation time for three night ventilation schedules (based on 2007 weather data)

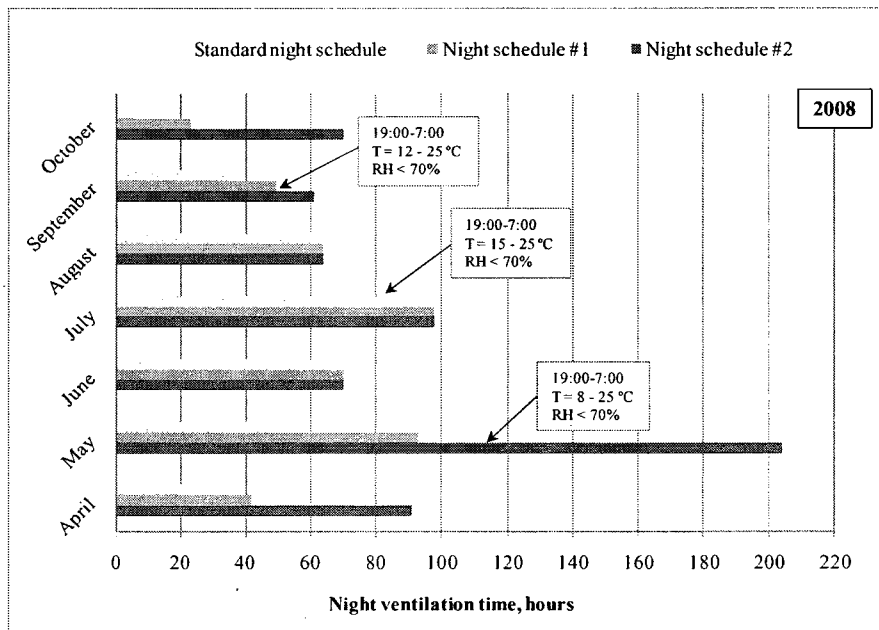


Figure 5.2. Calculated night ventilation time for three night ventilation schedules (based on 2008 weather data)

For the 2007 cooling season, a total of 431 hours of night ventilation were obtained under the standard ventilation schedule. Had the system been allowed to operate at lower outdoor temperatures, 559 and 663 hours of night ventilation time would have been obtained with night schedules #1 and #2 respectively, an increase of 30% and 54% compared to the standard night schedule.

During the 2008 cooling season, the standard schedule provided a total night ventilation time of 338 hours while schedule #1 and schedule #2 provide 440 and 658 hours respectively, an increase of 30% and 95 % compared to the standard schedule.

The increase in night ventilation time for both cooling seasons can be mainly accredited to the months of April, May, September and October.

Night ventilation hours account for 7 – 8% of the entire cooling season time (5136 hours for seven months) in the case of the standard night schedule, and 9 – 11%, 13% if schedules #1, #2 respectively are in effect. Although the number of hours is considerable, night ventilation has a different function than daytime ventilation; taking advantage of the absence of occupants and added internal and solar heat gains, the main purpose of night ventilation is to cool down the building mass and thus to reduce the cooling load of the following day.

5.1.2. Night ventilation cooling potential

A methodology proposed by Axley and Emmerich (2002) was adopted in order to qualitatively estimate the energy savings attributed to night cooling. When the outdoor

temperature drops below the cooling set-point temperature during the night, night cooling can be used to remove energy from the building mass. The heat transfer rate for this energy removal, in the limit of a very massive building, approaches:

$$q_{night} \approx M \cdot C_p \cdot (T_{i-csp} - T_o) \quad (\text{Equation 5.1})$$

where:

M = mass flow rate of incoming air, kg/sec

C_p = specific heat capacity of air, kJ/ kg·°C

T_{i-csp} = cooling set-point temperature, °C

T_o = outdoor temperature, °C

The total energy removed from the building's thermal mass during the evening may then be used to offset internal gains on the subsequent workday. The average internal gain that may be offset is equal to the integral of the night removal rate divided by the workday time period:

$$\bar{q}_{cool} = \frac{\int_{nighttime} q_{night}}{\Delta t} \quad (\text{Equation 5.2})$$

where:

q_{night} = heat transfer rate, W

Δt = workday time period, hours

Equation 5.1 and Equation 5.2 were used for estimating the potential energy savings due to night cooling. Weather data, such as mean monthly outdoor temperature, mean monthly temperature fluctuation (monthly average of daily T_{max} - T_{min}) and relative humidity, were considered in the calculations. For the mass flow rate calculation, stack-

driven flow was assumed through the corridor inlet grilles on both façades of floors 2 – 10 (total opening area of $\sim 22 \text{ m}^2$) with an air velocity of 0.5 – 1.7 m/sec (dependent on the mean monthly outdoor temperature). The cooling set-point temperature was assumed equal to 25 °C (to harmonize with the upper temperature set for the night ventilation schedules) and the workday time period was 10 hours. Calculations correspond to a night cooling period starting at 19:00 and ending at 7:00, applied on the previously examined three night ventilation temperature ranges:

- Standard night schedule; $T_{\text{out}} = 15 - 25 \text{ °C}$, RH <70%
- Night schedule #1; $T_{\text{out}} = 12 - 25 \text{ °C}$, RH <70%
- Night schedule #2; $T_{\text{out}} = 8 - 25 \text{ °C}$, RH <70%

For each night ventilation schedule, results on the average internal gains that can be offset the following day are shown in Figures 5.3 and 5.4. The months of April, May, September and October present the greatest potential for energy savings from night cooling if cooler outdoor temperature ranges are applied. As expected, schedules #1 and #2 appear to have little or no additional effect on the summer months.

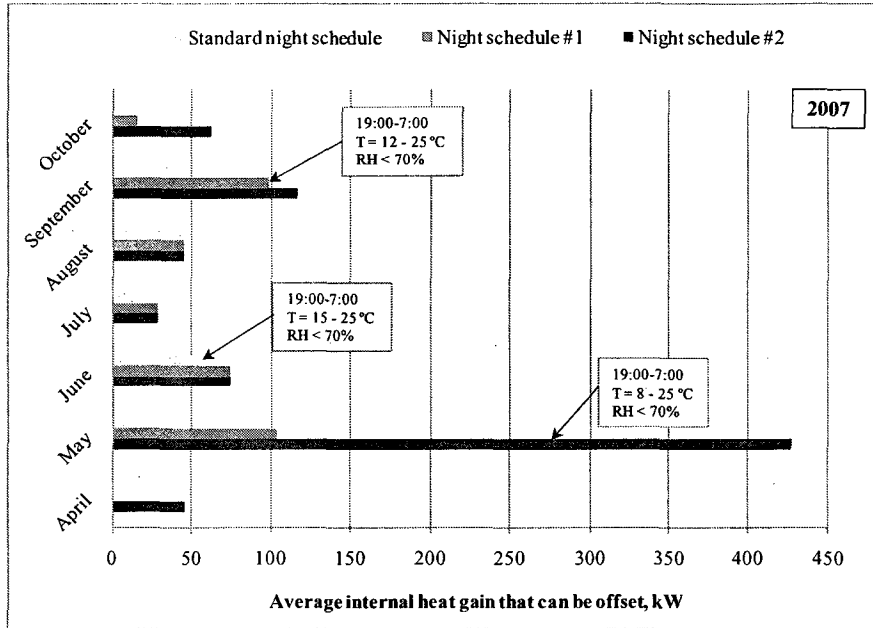


Figure 5.3. Internal heat gain that can be offset under different night ventilation schedules (based on 2007 weather data)

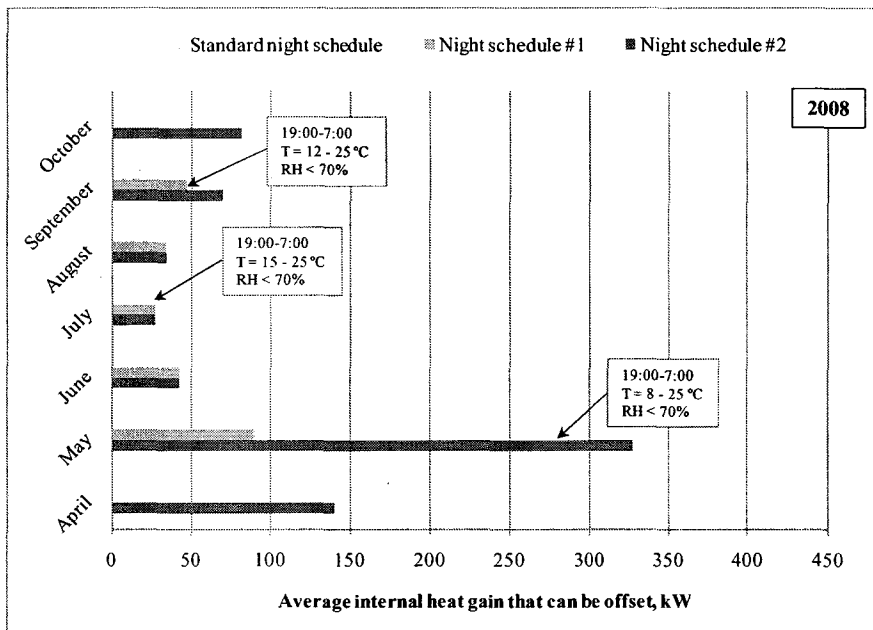


Figure 5.4. Internal heat gain that can be offset under different night ventilation schedules (based on 2008 weather data)

Tables 5.1 and 5.2 summarize the average internal gains that can be offset and include the increase in cooling rate for night ventilation at lower outdoor temperatures. Due to outdoor temperature restrictions, energy savings from night cooling in the months of

April and October would require the ventilation temperature range to extend to as low as 8 °C. A substantial difference is noticed in the months of May and September when the night schedule is modified to allow air in the building at 12 °C and 8 °C. Finally, an increase of 35 – 40% in the heat removal rate would have been possible in the summer months of June 2007 and August 2008 if night ventilation had operated at a 12 – 25 °C outdoor temperature range.

Table 5.1. Average internal gains that can be offset (based on a 10-hour workday) and % cooling rate increase (2007)

| Night ventilation schedule | 2007 | | | | |
|----------------------------|--------------------------|--------------------------|---|-------------------------|---|
| | Standard (15 – 25 °C) | Schedule #1 (12 – 25 °C) | | Schedule #2 (8 – 25 °C) | |
| | $q_{cool,standard}$, kW | $q_{cool,#1}$, kW | $\frac{q_{cool,#1} - q_{cool,standard}}{q_{cool,standard}}$ | $q_{cool,#2}$, kW | $\frac{q_{cool,#2} - q_{cool,standard}}{q_{cool,standard}}$ |
| April | 0 | 0 | - | 45.7 | - |
| May | 38.8 | 103.6 | >100 % | 426.9 | >>100% |
| June | 55.7 | 74.7 | 34 % | 74.7 | 34 % |
| July | 29.1 | 29.1 | 0 % | 29.1 | 0 % |
| August | 44.9 | 44.9 | 0 % | 44.9 | 0 % |
| September | 39.0 | 98.1 | >100 % | 116.5 | >100 % |
| October | 0 | 15.3 | - | 62.7 | - |

Table 5.2. Average internal gains that can be offset (based on a 10-hour workday) and % cooling rate increase (2008)

| Night ventilation schedule | 2008 | | | | |
|----------------------------|--------------------------|--------------------------|---|-------------------------|---|
| | Standard (15 – 25 °C) | Schedule #1 (12 – 25 °C) | | Schedule #2 (8 – 25 °C) | |
| | $q_{cool,standard}$, kW | $q_{cool,#1}$, kW | $\frac{q_{cool,#1} - q_{cool,standard}}{q_{cool,standard}}$ | $q_{cool,#2}$, kW | $\frac{q_{cool,#2} - q_{cool,standard}}{q_{cool,standard}}$ |
| April | 0 | 0 | - | 139.9 | - |
| May | 28.6 | 89.5 | >100 % | 326.9 | >>100 % |
| June | 42.5 | 42.5 | 0 % | 42.5 | 0 % |
| July | 26.8 | 26.8 | 0 % | 26.8 | 0 % |
| August | 24.4 | 34.3 | 40 % | 34.3 | 40 % |
| September | 16.9 | 46.8 | >100 % | 69.4 | >100 % |
| October | 0 | 0 | - | 81.3 | - |

5.2. Night time airflow and floor slab surface temperature measurements

Throughout a set of daytime measurements performed on floor 15, on a day that wind speed and direction favoured the inflow of air through the grilles located at the NW façade, it was found that over a period of 12 hours (11:00 – 23:00) the surface temperature of the slab dropped by almost 4 °C. During that period of time, the floor slab was subjected to an air stream of 0.2 – 0.6 m/sec at a 16 – 20 °C outdoor temperature. Even though measurements can only represent the temperature difference occurring on the surface of the slab, they indicate that under a constant air stream, cooling of the floor slab in greater depths can be achieved.

Night time measurements were employed to examine the effect of the cool air stream on the floor slab temperature in the absence of occupants and solar heat gains. Grilles are controlled by the Building Energy Management System (BEMS) and they will open or close depending on the outdoor conditions (temperature and relative humidity). The system was overridden on some particular nights so as to allow the grilles to remain open even though the outdoor temperature was expected to exceed the low threshold. Two cases, illustrated in Figure 5.5, have been examined:

- Corridor inlet grilles manually kept open on the SE and NW side of floor 6 and closed on every other floor. Atria connecting floor grilles were opened from the 7th floor upward (in four atria) to allow the air to be exhausted through the top.
- Corridor inlet grilles and atria connecting floor grilles manually kept open on all floors.

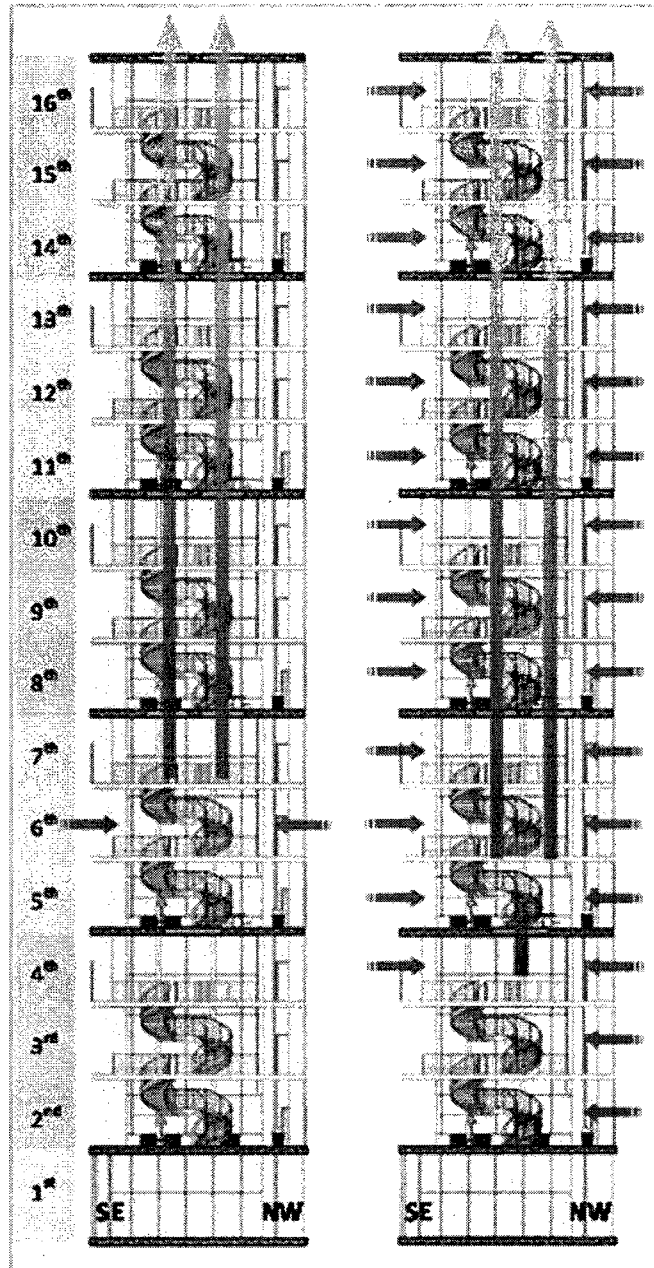


Figure 5.5. Corridor inlet grilles manually kept open a) on floor 6 (left), b) on all floors (right)

It is noted that although the air supply units at the corridors are programmed to shut down under natural ventilation mode, when the system is overridden (to manually keep the grilles open) they remain in operation. However, in the absence of occupants, the flow rates are expected to be low and not affecting the measurements.

5.2.1. Slab surface temperature and airflow through the corridor inlet grilles on floor 6

Slab surface temperature measurements were performed the night following a mainly clear day (September 10, 2008). On that day, the outdoor temperature ranged between 8 – 16 °C while winds during night time (September 10-11, 2008) were low. Data on the outdoor conditions can be found in Appendix II.

Surface temperature of the floor near the grilles (on floors 5 and 6) and velocity of the air coming in through the grilles (on floor 6) were measured every few hours, starting September 10 at 17:00. Due to the stack effect, an increase in airflow occurs as outdoor temperature decreases during the night. Table 5.3 gives the airflow rates and outdoor temperatures at different times.

Table 5.3. Outdoor temperature and airflow rates at corridor inlet grilles of floor 6

| Time | Outdoor Temperature, °C | SE façade Airflow (m ³ /s) | NW façade Airflow (m ³ /s) |
|-------|-------------------------|---------------------------------------|---------------------------------------|
| 17:00 | 16.3 | 0.8 | 1.1 |
| 20:00 | 14.7 | 1.1 | 1.0 |
| 00:00 | 13.1 | 1.8 | 1.8 |
| 03:00 | 11.7 | 1.8 | 1.8 |
| 06:00 | 9.7 | 2.1 | 2.1 |
| 09:00 | 11.9 | 2.2 | 1.8 |
| 12:00 | 16.4 | 1.3 | 1.0 |
| 15:00 | 17.7 | 1.3 | 1.1 |

Figure 5.6 shows the surface temperature variation from 17:00 September 10 until 15:00 September 11. Open data points correspond to open inlet grilles and bold data points to closed grilles. Natural ventilation system was in operation until shortly after 20:00 when the outdoor temperature dropped below 15 °C. Inlet grilles on floor 6 were however kept

open throughout the whole night and the effect of the cool air entering the building through both the SE and NW side can be seen in Figure 5.6.

During a period of 10 hours (20:00 – 6:00, hours 20 – 30 in the graph), slab surface temperature on floor 5 (grilles closed) remained almost constant (~20 °C) while on floor 6 (grilles open) it dropped by 4 °C on the SE side and almost 3 °C on the NW side. Minimum surface temperature was observed around 6:00 and from then on, rising outdoor temperature caused the surface temperature of the floor slab to increase. The temperature rise on the SE side (from 9:00 – 12:00, hours 33 – 36 in the graph) is greater than the one on the NW side due to solar heat gains.

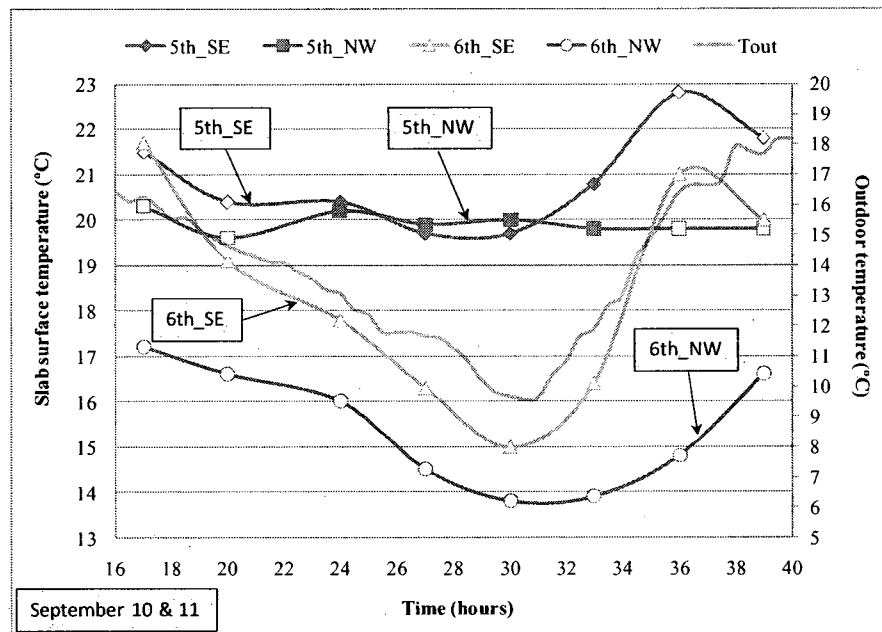


Figure 5.6. Slab surface temperature near the inlet grilles on floors 5 and 6

5.2.3. Airflow rate measurements at corridor inlet grilles on floors 4 – 16

Corridor inlet grilles were kept open on all floors during the night of September 25 and 26. This allowed for velocity measurements on every floor to help portray the stack effect in regards to the building height. Measurements began at 20:30 and ended at 8:00. During this time, winds were low to calm and outdoor temperature fluctuated between 12.5 and 20 °C. More details on the weather conditions can be found in Appendix II.

Velocity of the air flowing in through the corridor grilles was manually measured on floors 4 – 13 and monitored on floors 14 – 16. The measurements were targeted to be taken around times 21:00, 00:00, 3:00 and 7:30 and each set lasted about one hour. A total of four airflow values, one every time period, were used to derive the average airflow rate plotted in Figure 5.7. Data appearing in the graph correspond to floors 4 – 10 while data for floors 11 – 16 were omitted as approaching floor 11, the flow was no longer consistently directed in, indicating the level of neutral pressure (NPL; further measurements would be needed to verify the NPL). Their respective heights and airflow rates on each façade are summarized in Table 5.4.

As shown in Figure 5.7, airflow is decreasing with the building height (smaller H_d values). A linear correlation (correlation coefficient of ~0.9) between the airflow and the square root of H_d is observed, as expected by Equation 4.1.

Table 5.4. Building height and airflow rates on floors 4 – 10

| Floor | Height (m, distance of midpoint to ground level) | Average airflow rate (m ³ /s) | |
|-------|--|--|-----------|
| | | SE façade | NW façade |
| 4 | 18 | 1.3 | 1.0 |
| 5 | 22 | 1.0 | 1.0 |
| 6 | 26 | 0.8 | 0.8 |
| 7 | 30 | 0.7 | 0.5 |
| 8 | 34 | 0.8 | 0.7 |
| 9 | 38 | 0.5 | 0.4 |
| 10 | 42 | 0.2 | 0.2 |

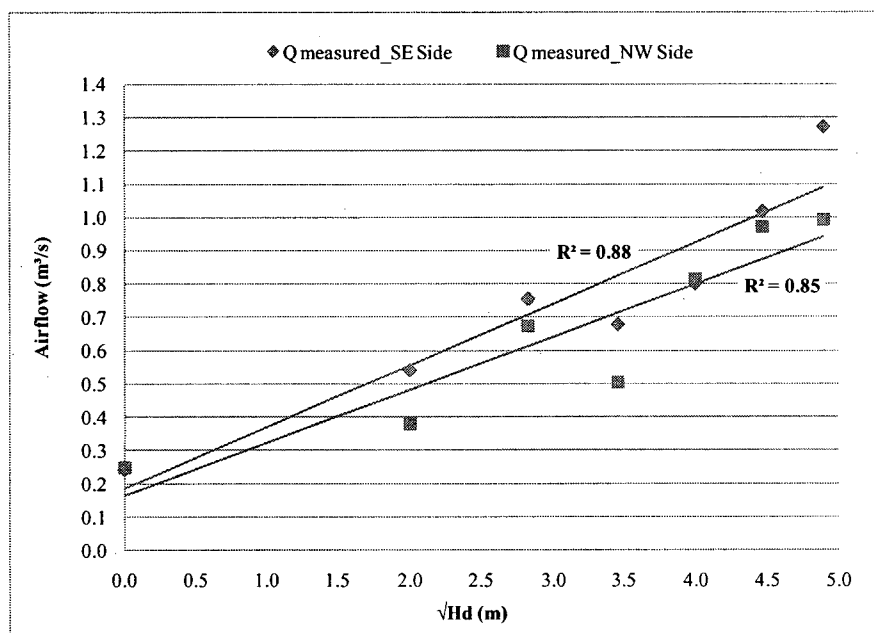


Figure 5.7. Airflow rates at corridor inlet grilles at different building heights (H_d = NPL height – height of opening at midpoint)

Using Equation 4.1, airflow at the corridor grilles at different building heights was theoretically calculated. A typical indoor temperature of 23 °C was assumed on all floors while the outdoor temperature used was the average temperature during the time of measurements. Values used in Equation 4.1 to estimate the airflow are shown in Table 5.5 while measured and calculated airflow rates are presented in Figure 5.8.

Table 5.5. Values used to calculate the stack induced airflow through the inlet grilles

| | |
|---|------------|
| Cross sectional area of opening A, m ² | 1.4 |
| Discharge coefficient C _d | 0.5 |
| NPL height H, m | 42 |
| Indoor temperature T _i , K (°C) | 296.5 (23) |
| Outdoor temperature T _o , K (°C) | 287 (13.5) |

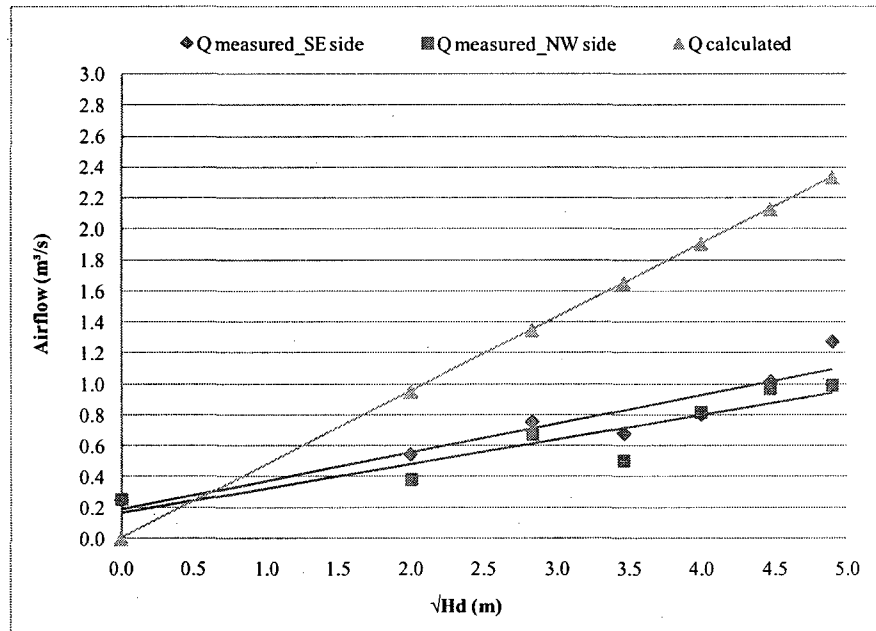


Figure 5.8. Measured and calculated airflow rates through the corridor inlet grilles at different building heights (H_d = NPL height – height of opening at midpoint)

As it can be seen in the graph above, discrepancies between calculated and measured values are more pronounced at lower levels (higher H_d values) and overall, the airflow rate is theoretically overestimated. This can be attributed to the following reasons:

- The assumption that the indoor temperature was uniform on every floor.
- The assumption that the stack effect was the only driving force for the airflow through the inlet grilles; possible outflow caused by local wind effects (due to negative pressures) was not considered.

5.3. Mathematical model for slab surface temperature change and heat removal prediction

A model developed in Mathcad (Athienitis, 1999) was modified to predict a) the surface temperature of the slab near the corridor inlet grilles on the SE and NW side of floor 6, b) the surface temperature of the slab at a distance from the inlet grilles on the SE side of floor 6 and, c) calculate the heat removal that can be attained under different outdoor conditions.

The slab is modeled as a semi-infinite solid which, under a convective effect on its surface, will undergo one-dimensional transient heat conduction. The schematic of the modeled slab is shown in Figure 5.9. The capacitance of the slab, the air and surface nodes connected through convection and the convective and conductive heat transfer are illustrated in (a) while the solid temperature variation with time and position is illustrated in (b). At time $t = 0$, the solid is in uniform temperature T_i . Convective cooling from the incoming air at temperature $T_{stream} < T_i$ causes the temperature of the slab to drop. The temperature gradient in the solid is dependent on the relative convective and conductive thermal resistances.

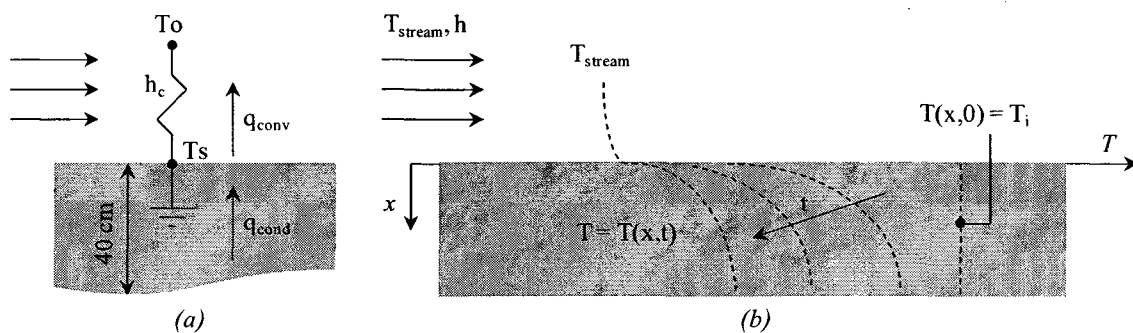


Figure 5.9. Schematic of the modeled slab

To predict the surface temperature of the slab at different distances from the inlet grilles, the corridor was divided in 10 control volumes (Figure 5.10). Air at a certain temperature T_{o_i} and velocity U is entering control volume i located at a distance L_i from the inlet grilles and as it passes over the floor slab, convective heat exchange with the solid is causing a rise in its temperature. The warmer air of temperature T_{i+1} exiting this control volume is entering the next control volume $i+1$ located at L_{i+1} m from the inlet grilles. In addition to that, the convective heat transfer coefficient h_{i+1} in control volume $i+1$ will be lower than h_i in control volume i as the heat transfer coefficient significantly decreases with the increasing length of the slab (for a laminar boundary layer). Under these conditions, the greater the distance from the inlet grilles and the leading edge (referring to the slab receiving the incoming flow stream at $L = 0$), the smaller the surface temperature drop is expected to be.

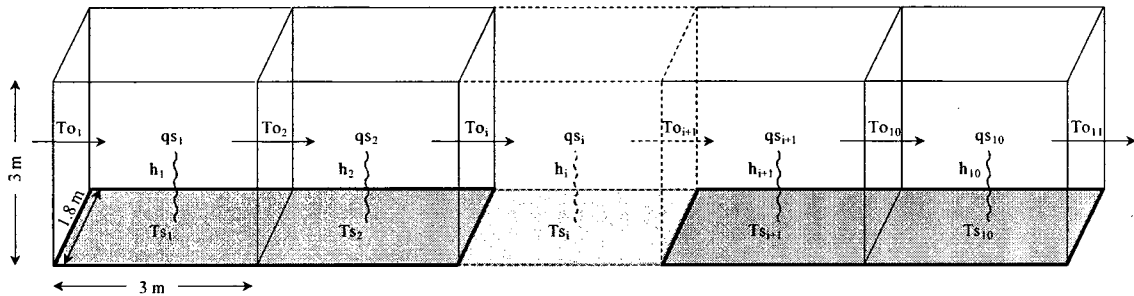


Figure 5.10. Corridor divided in control volumes

The case of the ventilated slab is a complicated problem under transient conditions with many unknown factors. It is not within the scope of the present analysis to accurately simulate the slab subjected to the cool air stream flowing in through the inlet grilles. The purpose of the analytical model is to first examine if the prediction of the slab surface temperature drop at different distances from the inlet grilles is within acceptable limits. Reaching a relatively good agreement between experimental and simulation results can

then allow to use the model for energy calculations. The assumptions and limitations of the analytical model, followed by its mathematical description, are presented below:

- The 40-cm slab was modeled as a semi-infinite slab with a single plane surface ($x = 0$) and its other surfaces distant enough to ignore for time periods of interest in transient analysis.
- One dimensional transient heat conduction was assumed for the slab, with a convective boundary condition; if a uniform boundary condition is applied at $x = 0$, it is reasonable to assume that this case can be analysed as transient one-dimensional conduction (Athienitis A.K. and Santamouris M., 2002).
- The mathematical model only considered the heat exchange between the slab and the air stream without any other heat flux to the surface. The presence of other surfaces, such as the suspended ceiling and ducting network, was not considered in the model. Although this is expected to cause some error, the main heat transfer mechanism is expected to be between the massive floor (hot) and the cool air – with upward heat flow.
- Laminar flow was assumed for all distances from the inlet grilles. Depending on the surface roughness and the turbulence level of the free stream, transition between laminar and turbulent flow can begin at Reynolds numbers as high as 3×10^6 (Incropera and Dewitt, 2002).

The assumption that the 40 cm slab can be simulated as a semi-infinite slab can be justified with the self-admittance of a 40 cm thick massive layer and the self-admittance of a very thick massive layer. Self-admittance is a transfer function relating to the effect

of a heat source at one surface to the temperature of that surface. Substantial insight into building thermal behaviour may be obtained by studying the magnitude and the phase angle of transfer functions such as the self-admittance. For example, a very important result in steady-periodic analysis of building thermal response is that there is a wall thermal mass thickness that will reduce room temperature fluctuations the most and it corresponds to the maximum admittance. For the analysis of variables with a dominant diurnal harmonic such as solar radiation, the diurnal frequency is used (Athienitis et al, 1995).

The self-admittance of a massive wall is given by:

$$Y_{S_x} = A_w \cdot \frac{u+k \cdot \gamma \cdot \tanh(\gamma \cdot L_w)}{\left[\frac{u}{k \cdot \gamma} \cdot \tanh(\gamma \cdot L_w) + 1\right]} \quad (\text{Equation 5.3})$$

In the case of a very thick wall, Equation 5.3 becomes:

$$Y_{S_\infty} = A_w \cdot k \cdot \gamma \cdot \tanh(\gamma \cdot L_w) \quad (\text{Equation 5.4})$$

Also, when the penetration depth is significantly less than the wall thickness then the wall behaves like a semi-infinite solid. The penetration depth is given by:

$$d = \sqrt{\frac{2k}{c \cdot \rho \cdot \omega}} \quad (\text{Equation 5.5})$$

where:

c = specific heat capacity of the massive layer, J/kg·°C

ρ = density of the massive layer, kg/m³

k = thermal conductivity of the massive layer, W/m·°C

u = conductance behind the massive layer, W/m²·°C

L_w = thickness of the massive layer, m

A_w = area of the massive wall, m^2

$$\gamma = (s/\alpha)^{1/2}$$

α = thermal diffusivity of the wall, m^2/sec

s = Laplace transform variable, equal to $i\omega$ for admittance calculations

$$i = \sqrt{-1}$$

$$\omega = 2\pi/P$$

P = period, equal to 86400 sec for diurnal analysis

Defining the properties of the floor slab (Appendix III), Equations 5.3, 5.4 and 5.5 yield:

$$|Y_{s_{40}}| = 13.109 \text{ W/}^\circ\text{C}$$

$$|Y_{s_{\infty}}| = 13.102 \text{ W/}^\circ\text{C}$$

$$d = 18.54 \text{ cm}$$

Given that $|Y_{s_{40}}| \approx |Y_{s_{\infty}}|$ and $d < 40$ cm, it can be reasonably assumed that the floor slab of 40 cm will behave as a very thick massive layer and it can therefore be simulated as a semi-infinite slab.

For a case of no internal generation and the assumption of constant thermal conductivity, the one dimensional transient heat conduction in the slab can be described by (Incropera and Dewitt, 2002):

$$\frac{\partial^2 T}{\partial x^2} = \frac{1}{\alpha} \frac{\partial T}{\partial t} \quad (\text{Equation 5.6})$$

where:

T = temperature of the slab, $^\circ\text{C}$

α = thermal diffusivity of the slab, m^2/sec

x = medium (solid) depth, m

t = time, sec

Heat flux by convection on the semi-infinite solid surface is given by (Incropera and Dewitt, 2002):

$$-k \frac{\partial T}{\partial x} \Big|_{x=0} = h \cdot [T_{\infty} - T(0, t)] \quad (\text{Equation 5.7})$$

where:

x = medium (solid) depth, m

k = thermal conductivity of the solid, W/m·°C

h = convective heat transfer coefficient, W/m²·°C

T_{∞} = temperature of the fluid, °C

$T(0,t)$ = solid temperature at $x=0$ (surface temperature), °C

Equation 5.7 is a reasonable approximation for the early portion of the transient one dimensional heat conduction, during which temperatures in the slab interior (well removed from the surface) are not influenced by the change in surface conditions (Incropera and Dewitt, 2002).

The analytical solution of Equation 5.6 for a semi-infinite solid with surface convection and uniform temperature distribution at $t=0$, is (Athienitis, 1999):

$$T_{i,j} = (T_{e_{i-1}} - T_{i-1,j}) \cdot \left[1 - \operatorname{erf}\left(\frac{x_j}{2\sqrt{a \cdot t_i}}\right) - \exp\left[\frac{h \cdot x_j}{k_s} + \frac{h^2 \cdot a \cdot t}{k_s^2}\right] \cdot \left(1 - \operatorname{erf}\left(\frac{x_j}{2\sqrt{a \cdot t}} + \frac{h \cdot \sqrt{a \cdot t}}{k_s}\right)\right) \right] + T_{i-1,j} \quad (\text{Equation 5.8})$$

where:

$T_{i,j}$ = floor slab temperature at time i and depth j , °C

$T_{e_{i-1}}$ = outdoor temperature – temperature of the air stream at time $(i-1)$, °C

$T_{i-1,j}$ = floor slab temperature at time $i-1$ and depth j , °C

x_j = floor slab depth, m

t = time, hr

α = thermal diffusivity of the floor slab, m²/sec

h = convective heat transfer coefficient, W/m²·°C

k_s = thermal conductivity of the floor slab, W/m·°C

To calculate the convective heat transfer coefficient, the following correlation was used:

$$h = \frac{Nu \cdot k_f}{L} \quad (\text{Equation 5.9})$$

where:

Nu = Nusselt number for laminar boundary layer and external flows for flat plates (*ASHRAE Handbook*)

k_f = thermal conductivity of the air, W/m·°C

L = floor slab characteristic length, m

Nusselt number in Equation 5.9 is equal to:

$$Nu = 0.332 \cdot Re^{1/2} \cdot Pr^{1/3} \quad (\text{Equation 5.10})$$

where:

Re = Reynolds number, equal to: $Re = \frac{U \cdot L}{\nu}$

Pr = Prandtl number, equal to: $Pr = \frac{\nu}{\alpha_{air}}$

U = velocity of the air stream, m/sec

ν = kinematic viscosity of the air, m²/sec

α_{air} = thermal diffusivity of the air, m²/sec

Similar to Equation 5.8, the surface temperature of the slab at different distances away from the inlet grilles was calculated with the following equation:

$$T_{S_{k,i}} = (T_{O_{k-1,i}} - T_{S_{k-1,i}}) \cdot \left[1 - \exp\left[\frac{h_i^2 \cdot a \cdot t}{k_s^2}\right] \cdot \left(1 - \operatorname{erf}\left(\frac{h_i \sqrt{a \cdot t}}{k_s}\right)\right) \right] + T_{S_{k-1,i}} \quad (\text{Equation 5.11})$$

where:

$T_{S_{k,i}}$ = floor surface temperature at time k and control volume i, °C

$T_{O_{k-1,i}}$ = temperature of the air stream at time (k-1) and control volume i, °C

$T_{S_{k-1,i}}$ = surface floor temperature at time k-1 and control volume i, °C

t = time, hr

α = thermal diffusivity of the floor slab, m²/sec

h_i = convective heat transfer coefficient at control volume i, W/m²·°C

k_s = thermal conductivity of the floor slab, W/m·°C

The temperature of the air stream entering a control volume was calculated using Equation 5.12.

$$T_{O_{k,i}} = T_{O_{k,i-1}} - \frac{q_{S_{k,i-1}} \cdot A_{slab}}{\rho_{air} \cdot U \cdot A_{gr} \cdot C_p} \quad (\text{Equation 5.12})$$

where:

$T_{O_{k,i-1}}$ = temperature of the air stream at time k and control volume i-1, °C

$q_{S_{k,i-1}}$ = convective heat flow to floor at time k and control volume i-1, W/m²·°C

A_{slab} = floor slab area per control volume, m²

ρ_{air} = density of the air, kg/m³

U = velocity of the air stream, m/sec

A_{gr} = inlet grilles opening area, m²

C_p = specific heat capacity of the air, J/kg·°C

Finally, the convective heat flow towards the floor in each control volume is given by Equation 5.13 (Athienitis, 1999).

$$q_{S_{k,i}} = h_i \cdot (T_{O_{k,i}} - T_{S_{k,i}}) \cdot \exp \left[\frac{h_i^2 \cdot \alpha \cdot t}{k_s^2} \right] \cdot \left(1 - \operatorname{erf} \left(\frac{h_i \cdot \sqrt{\alpha \cdot t}}{k_s} \right) \right) \quad (\text{Equation 5.13})$$

Basic air and floor slab properties used in the calculations are shown in Table 5.6 while detailed calculation sheets can be found in Appendix III.

Table 5.6. Floor slab and air properties

| Physical properties | Air | Concrete floor slab |
|--|------------------------|-----------------------|
| Density, kg/m ³ | 1.2 | 1700 |
| Thermal conductivity, W/m·°C | 0.0257 | 1.7 |
| Kinematic viscosity, m ² /sec | 1.511·10 ⁻⁵ | - |
| Specific heat capacity, J/kg·°C | 1005 | 800 |
| Thermal diffusivity, m ² /sec | 2.13·10 ⁻⁵ | 1.25·10 ⁻⁶ |

5.3.1 Surface temperature of the slab near the SE and NW façade inlet grilles

Surface floor temperature change over time was calculated for the slab near the inlet grilles of floor 6. Assuming a laminar boundary layer, Equations 5.7 – 5.9 were used. Based on measurements performed on the night of September 10 to 11, an average velocity U for the air stream passing over the floor slab was used while outdoor temperature and the initial floor surface temperature were imposed to increase the accuracy of the predictions. Calculations were done for a time period of 10 hours (20:00 – 6:00). Simulation and experimental results are presented in the graph below.

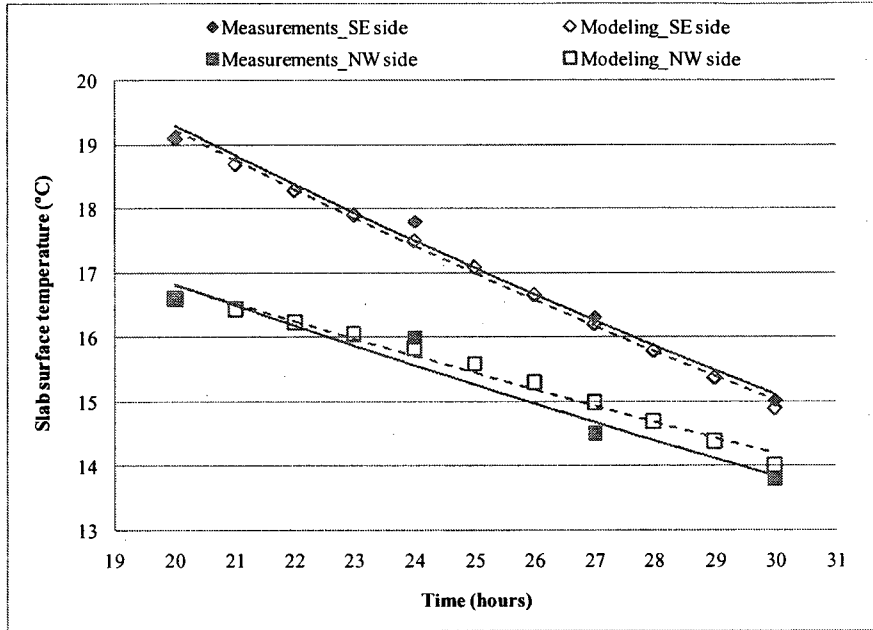


Figure 5.11. Measured and calculated slab surface temperature near the SE and NW inlet grilles on floor 6

As shown in Figure 5.11, measured and calculated values for the slab surface temperature are in good agreement. The surface temperature change as a function of time follows an exponential decay, the initial – almost linear looking – section of which is shown in the graph. The total surface temperature decrease for the floor located near the inlet grilles is well predicted on both the SE and the NW side. Calculated and measured maximum temperature difference for each case is summarized in Table 5.7.

Table 5.7. Calculated and measured slab surface total temperature drop on floor 6

| Date | September 10 – 11 | |
|---|-------------------|-----------|
| Façade | Southeast | Northwest |
| Time period, hours | 10 | 10 |
| Average outdoor temperature, °C | 12.5 | 12.5 |
| Average air velocity, m/sec | 1.3 | 1.2 |
| Initial floor temperature, °C | 19.1 | 16.6 |
| Calculated maximum temperature difference, °C | 4.2 | 2.6 |
| Measured maximum temperature difference, °C | 4.1 | 2.8 |

5.3.2. Surface temperature of the floor slab at different distances from the SE side inlet grilles

The surface temperature of the floor slab along a distance of $L = 30$ m away from the inlet grilles was predicted using Equations 5.10 – 5.12. The SE corridor of floor 6 was divided in ten control volumes (previously shown in Figure 5.10), each of them having dimensions of 3 m long, 1.8 m wide and 3 m high. As already mentioned, the only heat exchange considered was between the air stream and the floor slab. The outdoor temperature was imposed to increase the accuracy of the temperature predictions. An average velocity of the air stream was used, constant for all control volumes, while the flow was considered to be laminar. A uniform initial floor surface temperature was applied for the entire length of the corridor, equal to 19.8 °C, based on measurements performed at four different locations along the corridor.

Night time surface temperature measurements at different lengths along the SE corridor of floor 6 and the corresponding calculated temperatures are shown in Figure 5.12. As mentioned before, over a period of ten hours, only the first almost linear looking part of

the temperature-time exponential decay can be seen. Comparing the simulation data to the experimental data, a relatively good agreement is observed. As expected, the slab surface temperature drops at a decreasing rate when moving away from the leading edge. Table 5.8 summarizes the measured and predicted values of the maximum temperature difference.

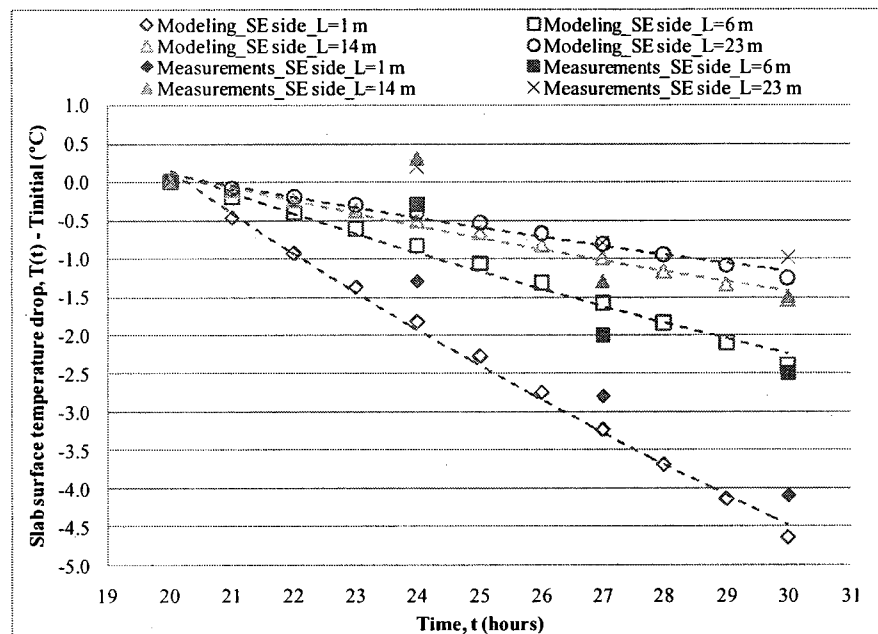


Figure 5.12. Measured and calculated slab surface temperature at different distances from the SE inlet grilles on floor 6

Table 5.8. Measured and predicted slab surface maximum temperature difference at different distances from the SE corridor inlet grilles on floor 6

| Distance from corridor inlet grilles | L = 1 m | L = 6 m | L = 14 m | L = 23 m |
|--|---------|---------|----------|----------|
| Measured maximum temperature difference, °C | 4.1 | 2.5 | 1.5 | 1.0 |
| Predicted maximum temperature difference, °C | 4.6 | 2.4 | 1.5 | 1.2 |

5.3.3. Heat removed from the floor slab

The 10 control volumes approach described in section 5.3.2 and Equations 5.11 – 5.13 were then used to calculate the heat flow at the floor surface and the total heat that was removed from the floor slab. Since stack-driven flow in the building extends from floor 2 to floor 10, the results were extrapolated to estimate the total heat removal that is achieved in 8 floors. These results correspond to a 30 m long slab extending on each side of inlet grilles, a total area of 864 m².

Table 5.9 presents the heat flow rates and the heat removed during a period of 10 hours for each control volume. The total heat removal for an area of 54 m² is 2.4 kWh. This heat removal, corresponding to an outdoor temperature range of 9 – 15 °C, was compared to the heat removal that would have been obtained if different temperature ranges had been applied. An initial surface temperature of 20 °C for the floor was assumed and an average outdoor temperature of 12 °C, 15 °C and 18 °C was applied for each night ventilation schedule. These outdoor temperatures represent the standard night ventilation schedule, schedule #1 and schedule #2 (described in section 5.1.2) respectively. Based on experimental data, the velocity of the air stream was adjusted according to the outdoor temperature.

Table 5.9. Calculated heat flow rate and heat removed from the slab over a 10-hour period

| Control Volume | 1 | 2 | 3 | 4 | 5 | 6 | 7 | 8 | 9 | 10 |
|---|-------|-------|-------|-------|-------|-------|-------|-------|-------|-------|
| Average heat flow rate, W | 49.08 | 33.05 | 26.87 | 23.30 | 20.88 | 19.10 | 17.72 | 16.60 | 15.68 | 14.89 |
| Heat removed over a 10-hour period, kWh | 0.49 | 0.33 | 0.27 | 0.23 | 0.21 | 0.19 | 0.18 | 0.17 | 0.16 | 0.15 |

Heat that can be removed from the slab under different night ventilation temperature ranges was calculated for each control volume of the 30 m long corridor and is shown in Figure 5.13. It is evident that when the air stream is at an average temperature of 12 °C, the heat removed is close to 2 times higher compared to that with an air stream at 15 °C and approximately 5 times higher than the case of an air stream at 18 °C.

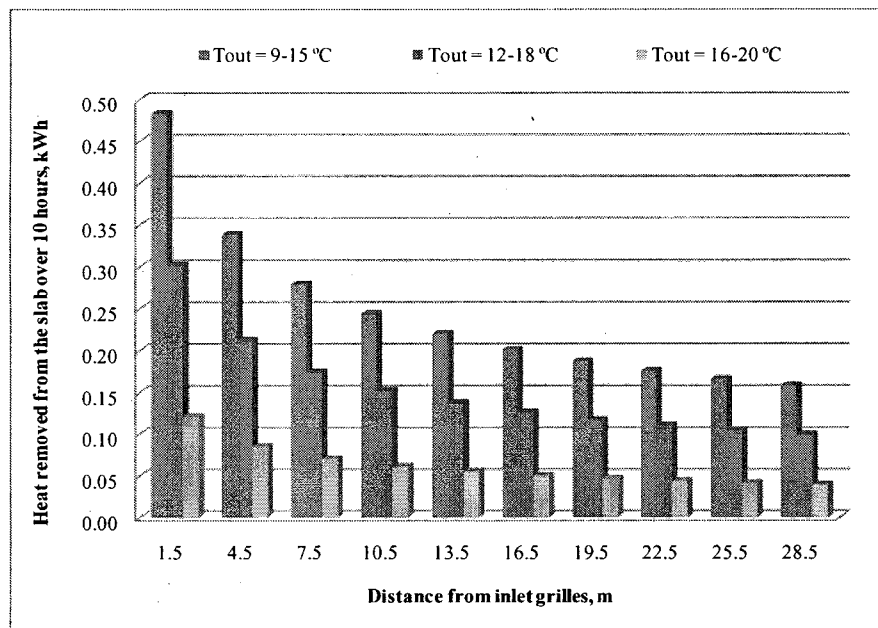


Figure 5.13. Calculated heat removal from the 30 m long slab for a 10 hour period under different outdoor temperature ranges

Table 5.10 presents the heat removed from the slab for an area of 864 m² and the hours of cooling that would have been needed to achieve a heat removal of 25 kWh (approximately the average of the three heat removal values) using each of the three night ventilation schedules. Extending the existing temperature range to as low as 12 °C and 8 °C would result in 3 and 5 times more heat removed from the floor slab respectively. On the other hand, the cooling time period needed to achieve a 25 kWh heat removal would have been 53 hours using the standard night schedule as opposed to 12 and 6 hours if night schedules at lower outdoor temperatures had been employed.

Table 5.10. Heat removed from 864 m² of slab area and cooling time needed under different outdoor temperatures

| Night ventilation schedule | Standard (average $T_{out} = 18\text{ }^{\circ}\text{C}$) | Schedule #1 (average $T_{out} = 15\text{ }^{\circ}\text{C}$) | Schedule #2 (average $T_{out} = 12\text{ }^{\circ}\text{C}$) |
|---|--|---|---|
| Heat removed over a 10-hour period, kWh | 7.6 | 22.1 | 39.2 |
| Period of cooling needed to achieve heat removal of 25 kWh, hours | 53 | 12 | 6 |

These results are limited to the corridor area of 8 floors (864 m²) and do not consider the cooling of the indoor air, the heat removed from the slab in zones further away from the inlet grilles and the cooling effect in the upper building levels (floors 11-16). Nonetheless, the calculated amounts of cooling stored in the slab can be compared to the cooling requirements in the atria, as indicated by monitoring data. For the month of September, measurements showed that an average 14 kWh of heat removed was needed for a 6-hour period (12:00 – 18:00) in the top atrium, approximately a total of 70 kWh for the five building atria. Employing a night ventilation schedule that would operate for outdoor temperatures as low as 8 °C during the night – resulting in a total 39 kWh of heat removed – could significantly contribute to the atria cooling requirements of the following day. A control strategy, together with weather prediction for the following day and a variable temperature range, should be implemented in the building to optimize the benefits of night cooling and avoid overcooling problems and discomfort to occupants. A similar approach for load control using building thermal mass and night pre-cooling is used in buildings with mechanical ventilation (e.g. Braun, 2003).

5.4. Summary

Three different night ventilation strategies were compared. At outdoor temperatures in the 12 – 25 °C and 8 – 25 °C ranges, night ventilation time can increase by 30% (for both 2007 and 2008 cooling seasons) and 54% (2007) or 95% (2008) respectively, compared to the 15 – 25 °C temperature range condition presently in use. This additional night ventilation time reflects the night cooling potential, particularly during the months of April, May, September and October.

Surface temperature of the ventilated slab located near the corridor inlet grilles on floor 6 was measured at night time. For a time period of 10 hours, at an outdoor temperature of 9 – 15 °C, a surface temperature drop of 4 °C was observed. Air velocity night measurements at the corridor inlet grilles on floors 4 – 10 were used as inputs (together with measured outdoor temperatures and initial slab surface temperature) in a simple analytical model to predict the surface temperature change of the slab located near and at different distances from the inlet grilles. Theoretical and experimental results are in relatively good agreement. The same model approach was then followed to estimate the heat removed from the slab under different outdoor temperatures. Results indicate that the inflowing air stream at lower temperatures has increased cooling capacity resulting in higher amounts of cooling stored in the thermal mass; the heat removed with an air stream at an average 12 °C (corresponding to a 9 – 15 °C outdoor temperature variation) is 5 times greater than an air stream at an average 18 °C (for a 16 – 20 °C outdoor temperature variation) while the cooling time needed to remove 25 kWh of heat at 18 °C is 9 times more than the time needed at 12 °C. With the present hybrid ventilation schedule, the daytime cooling demand in the atria for the month of September is very

comparable to the cooling that can be stored in the slab during the night, at typical September outdoor temperatures. However, weather forecast and thermal comfort (i.e. risk of overcooling) are issues to be further investigated should a modified night ventilation schedule be adopted.

6. CONCLUSIONS AND RECOMMENDATIONS

6.1. Summary and conclusions

The present thesis investigated the natural ventilation system performance of Concordia University Engineering building. Thermal and airflow long-term monitoring and manual measurements were employed to assess the indoor environmental conditions and estimate the free cooling obtained by the operation of the natural ventilation system. Additionally, experimental data for the slab surface temperature and stack-driven ventilation rates, combined with a mathematical model, were used in order to examine the cooling potential when different night ventilation strategies are used.

It was found that, under the climatic conditions for the city of Montreal and according to its design parameters, the natural ventilation system operated for 35 % and 26 % of the time during the 2007 and 2008 cooling seasons respectively (April – October). Energy calculations showed that the free cooling received by the natural ventilation schedule currently in use can cover only part of the building's requirements in cooling (approximately 30%, based on a 6-hour workday time period during the months of August – October).

The analysis of various temperature data (focusing on clear days) indicates that when the building is under natural ventilation mode, indoor conditions in the atrium space are maintained within acceptable limits and overheating is avoided. Indoor temperature in the atrium is strongly dependent on solar radiation, with the maximum thermal stratification on a clear day being typically around 3-4 °C near the façade and 2-3 °C in the space.

Monitoring of air velocity and pressure difference across the corridor inlet grilles verified the strong dependence between stack and/ or wind effect and the amount of air flowing in or out of the building. On the top building levels (floors 14 – 16), the stack effect generally induces an outflow (negative ΔP) through the corridor inlet grilles while inflow on these levels is usually wind-driven. Air velocity measurements at the corridor inlet grilles of floors 4 – 13 indicated that the neutral pressure level of the building is near floor 10. It was found that airflows driven by the stack effect are theoretically overestimated, especially at lower building heights.

Regarding the night cooling potential of the natural ventilation system, different night ventilation strategies, that were originally suggested but not adopted in the design of the building, were studied. It was shown that at outdoor temperatures in the ranges 12 – 25 °C and 8 – 25 °C, night ventilation time can increase by 30% (for both 2007 and 2008 cooling seasons) and 54% (2007) or 95% (2008) respectively, compared to the 15 – 25 °C temperature range condition presently in use. This additional night ventilation time indicates a significant cooling potential, particularly during the months of April, May, September and October. Experimental data for the night time ventilation rates and surface temperatures of the concrete slab located near the inlet grilles were used as inputs and for the validation of a simple mathematical model that was developed to estimate the cooling capacity of the slab. Results indicated that the inflowing air stream at lower temperatures has increased cooling capacity resulting in higher amounts of cooling stored in the thermal mass. More specifically, the amount of heat removed by convection with an air stream at an average outdoor temperature of 12 °C was estimated to be 5 times greater than with an air stream at an average temperature of 18 °C.

Based on the findings of the study, it can be concluded that:

- Atria should be considered in the design of a building's natural ventilation system. The tall atrium space and solar radiation transmitted in the room promote temperature stratification and consequently enhance buoyancy-driven flows in the building. To avoid thermal/visual discomfort and overheating problems by excessive heat stored in the thermal mass, attention should be given to the incoming solar radiation, i.e. by proper controlled use of the roller shades designed with optimal optical properties.
- Given the unpredictability of wind forces and the dependence of inflows in the upper building levels on the wind effect, a variable speed fan assisting the stack-driven flows in natural ventilation is required in order to raise the neutral pressure level of the building at the roof level and increase the ventilation rates.
- The location and the opening area of the inlet grilles should be considered based on the desired ventilation rates in the building and the maximum allowable air velocities for thermal comfort. In this case study, although air velocities greater than 1 m/sec at the lower building levels are expected at outdoor temperatures near 15 °C, thermal discomfort is believed to be avoided because of the location of the inlet grilles (far from occupants).
- When natural ventilation during daytime does not sufficiently cover the building cooling load, night ventilation can be employed. A predictive control strategy is necessary in order to maximize the cooling effect of night ventilation without compromising the indoor thermal comfort. Such operating strategies can be generalized for similar hybrid ventilation systems in buildings with high amounts of

exposed thermal mass and guidelines can be adopted in both the design and optimal operation of such buildings.

6.2. Design and future work recommendations

Based on results of the present study, it can be recommended to:

- Optimize the operation of mixed mode ventilation systems allowing for the mechanical system to assist in the cooling from natural ventilation so that indoor conditions are tempered and peak cooling loads are minimized.
- Introduce a variable temperature range and weather predictive control in the operation of natural ventilation systems at night time. In the absence of such a control strategy, there is a risk of overcooling resulting in a) indoor operative temperatures too low to be acceptable for thermal comfort, and b) possible heating demand to compensate for the increased cooling of the thermal mass.
- Develop an energy simulation model for the atrium and the building that will allow the examination and optimization of different control strategies for the passive cooling of the building (e.g. modulated flow at corridor inlet grilles, atrium shading control, necessary amount of cooling to be stored in the building mass) and use existing experimental data to enhance its accuracy. The energy simulation model would also allow optimize control strategies for the passive heating of the building.
- Investigate the effects of any control strategies and modifications introduced in the existing ventilation and cooling strategies on the energy consumption of mixed mode ventilated buildings.

REFERENCES

- Abdullah, A.H., Meng, Q., Zhao, L., Wang, F. (2009). Field study on indoor thermal environment in an atrium in tropical climates. *Building and Environment*, 44, (2), 431-436.
- Aiulfi, D. (1994). Overview of the use of Flovent in the Swiss energy saving research. IEA task 12 Atria Model Development, *Proceedings of Atria Model Development*.
- Altan, H., Ward, I., Mohelnikova, J., Vajkay, F. (2009). An internal assessment of the thermal comfort and daylighting conditions of a naturally ventilated building with an active glazed façade in a temperate climate. *Energy and Buildings*, 41, 36-50.
- ASHRAE. (2005). *Handbook of fundamentals*. Atlanta: American Society of Heating, Refrigerating, and Air-Conditioning Engineers, Inc.
- Athienitis, A.K. (1999). *Building thermal analysis*. Electronic Mathcad Book (2nd Edition) in Civil Eng. Library, Mathsoft Inc., Boston, U.S.A.
- Athienitis, A.K., Berger, X., Santamouris, M. (1995). *Thermal analysis for summer comfort in buildings*, Central Institution for Energy Efficiency Education (CIENE), Athens, Greece.
- Athienitis, A.K., Santamouris, M. (2002). *Thermal analysis and design of passive solar buildings*, James and James, London, UK.
- Awad, A.S., Calay, R.K., Badran, O.O., Holdo A.E. (2008). An experimental study of stratified flow in enclosures. *Applied Thermal Engineering*, 28, 2150-2158.

- Axley, J.W., Emmerich, S.J. (2002). A method to assess the suitability of a climate for natural ventilation of commercial buildings. *Proceedings of Indoor Air 9th International Conference on Indoor Air Quality and Climate, Volume 2. June 30-July 5, 2002, Monterey, CA, 854-859 pp, 2002.*
- Axley, J.W., Emmerich, S.J., Walton G.N. (2002). Modeling the performance of a naturally ventilated commercial building with a multizone coupled thermal/ airflow simulation tool. *Proceedings of ASHRAE Transactions Annual Meeting. 2002, Honolulu, HI, 1-16 pp, 2002. ASHRAE Transactions, Vol. 108, No. 2,*
- Basarir, M., Oosthuizen, P.H., Lightstone, M. (2009). Numerical simulation of the airflow and temperature distribution in an atrium and a comparison of the results with measurements. *Proceedings of the 4th Canadian Solar Buildings Research Network conference, Toronto, 2009.*
- Braun, J.E. (2003). Load control using building thermal mass. *Journal of Solar Energy Engineering, 125, 292-303.*
- Bourgeois, D., Haghghat, F., Potvin, A. (2002). On the applicability of Hybrid ventilation in Canadian office and educational buildings: Part 1 – Barriers and opportunities stemming from building regulation. *Proceedings of the 4th International Forum on Hybrid ventilation, Montreal, 2002.*
- Cable, M., Oosthuizen, P.H., Lightstone, M. (2007). An evaluation of turbulent models for the numerical study of mixed and natural forced convective flow in atria. *Proceedings of the 2nd Canadian Solar Buildings Research Network conference, Calgary, 2007.*

- Carrilho da Graça, G., 2003. Simplified models for heat transfer in rooms. Ph.D. Thesis, Engineering Physics, University of California, San Diego.
- Carrilho da Graça, G., Linden, P.F., McConahey, E., Haves, P. (2003). Design and testing of a control strategy for a large naturally ventilated office building. *Proceedings of Building Simulation, 2003, Eindhoven, Netherlands.*
- CIBSE 2005 TM36. Climate change and the indoor environment: impacts and adaptation. *Technical Memorandum no. 36, Chartered Institution of Building Services Engineers, London.*
- De Dear, R.J., Brager, G.S. (2002). Thermal comfort in naturally ventilated buildings: revisions to ASHRAE standard 55. *Energy and Buildings 34*, 549-561.
- Djunaedy, E. (2005). External coupling between building energy simulation and computational fluid dynamics. PhD Thesis, Technische Universiteit Eindhoven, Eindhoven.
- Elmualim, A. A. (2006). Effect of damper and heat source on wind catcher natural ventilation performance. *Energy and Buildings*, 38, (8), 939-948.
- Gocer, O., Tavit, A., Ozkan, E. (2006). Thermal performance simulation of an atrium building. *Proceedings of eSim 2006 Building Performance Simulation Conference.*
- Heiselberg, P. (2002). Principles of hybrid ventilation. Annex 35 report. Hybrid ventilation in new and retrofitted buildings, Hybrid Ventilation Centre, Aalborg University, Denmark.

- Holford, J.M., Hunt, G.R. (2003). Fundamental atrium design for natural ventilation. *Building and Environment*, 38, 409-426.
- Holmes, M.J., Hacker J.N. (2007). Climate change, thermal comfort and energy: Meeting the design challenges of the 21st century. *Energy and Buildings*, 39, 802-814.
- Horan, J.M., Finn, D.P. (2008). Sensitivity of air change rates in a naturally ventilated atrium space, subject to variations in external wind speed and direction. *Energy and Buildings*, 40, 1577-1585.
- Hunt, G.R., Linden, P.F. (1999). The fluid mechanics of natural ventilation – displacement ventilation by buoyancy-driven flows assisted by wind. *Building and Environment*, 34, 707-720.
- Incropera, F.P., Dewitt D. P. (2002). *Fundamentals of Heat and Mass Transfer* (5th ed.), J.Wiley & Sons, New York.
- Jayaraman, B., Finlayson, E.U., Sohn, M.D., Thatcher, T.L., Price, N.P., Wood, E.E., Sextro, R.G., Gadgil, A.J. (2006). Tracer gas transport under mixed convection conditions in an experimental atrium: Comparison between experiments and CFD predictions. *Atmospheric Environment*, 40, 5236-5250.
- Ji, Y., Cook, M.J., Hanby, V. (2007). CFD modelling of natural displacement ventilation in an enclosure connected to an atrium. *Building and Environment*, 42, 1158-1172.
- Laouadi, A., Atif, M.R. (1999). Comparison between computed and field measured parameters in an atrium building. *Building and Environment*, 34, 129-138.

- Joubert, P.H., Mathews, E.H. (1989). Quick TEMP – A thermal analysis program for designers of naturally ventilated buildings. *Building and Environment*, 24, (2), 155-162.
- Karava, P., Stathopoulos, T., Athienitis, K.A. (2007). Wind-induced natural ventilation analysis. *Solar Energy*, 81, 20-30.
- Kolokotroni, M. (1998). Night ventilation for office buildings. *BRE information paper 4/98. CRC, 1998.*
- Kolokotroni, M., Perera, M.D.A.E.S., Azzi, D., Virk, G.S. (2001). An investigation of passive ventilation cooling and control strategies for an educational building. *Applied Thermal Engineering*, 21, 183-199.
- Krause, B., Cook, M., Lomas, K. (2007). Environmental performance of a naturally ventilated city centre library. *Energy and Buildings*, 39, 792-801.
- Li, Y. (2000). Buoyancy driven natural ventilation in a thermally stratified one-zone building. *Building and Environment*, 35, 207-214.
- Li, Y., Delsante, A., Chen, Z., Sandberg, M., Andersen, A., Bjerre, M., Heiselberg, P. (2001). Some examples of solution multiplicity in natural ventilation. *Building and Environment*, 36, 851-858.
- Mouriki, E., Karava, P., Athienitis, A.K., Park, K.W., Stathopoulos, T. (2008). Full scale-study of an atrium integrated with a hybrid ventilation system. *Proceedings of the 3rd Canadian Solar Buildings Research Network conference, Fredericton, 2008.*

- Park, K.W., O'Neill, B., Karava, P., Mouriki, E., Athienitis, A.K. (2008). A control algorithm for motorized roller blinds in an atrium integrated with a hybrid ventilation system. *Proceedings of the 3rd Canadian Solar Buildings Research Network conference, Fredericton, 2008.*
- Reardon, J.T., Atif, M.R., Shaw, C. (2002). Tracer gas measurements for ventilation, air movement and air infiltration in a four-sided atrium office building. *International Journal of Ventilation, 1, (1), 13-22.*
- Ren, Z., Stewart, J. (2003). Simulating air flow and temperature distribution inside buildings using a modified version of COMIS with sub-zonal divisions. *Energy and Building, 35, 275-271.*
- Rousseau, P.G., Mathews, E.H. (1996). A new integrated design tool for naturally ventilated buildings. *Energy and Building, 23, 231-236.*
- Spindler, H.C., Norford, L.K. (2009). Naturally ventilated and mixed-mode buildings – Part I: Thermal modeling. *Building and Environment, 44, 736-749.*
- Tan, G., Glicksman, L.R. (2005). Application of integrating multi-zone model with CFD simulation to natural ventilation prediction. *Energy and Buildings, 37, 1049-1057.*
- Tovar, R., Linden, P.F., Thomas, L.P. (2007). Hybrid ventilation in two interconnected rooms with a buoyancy source. *Solar Energy, 81, 683-691.*
- Tzempelikos, A., Athienitis, K.A., Karava, P. (2007). Simulation of façade and envelope design options for a new institutional building. *Solar Energy, 81, 1088-1103.*

Urban, B.J. (2007). The MIT Design Advisor: Simple and rapid energy simulation of early stage building designs. Mechanical Engineering SM Thesis. MIT. Cambridge, MA.

Voeltzel, A., Carrie, F.R., Guarracino, G. (2001). Thermal and ventilation modeling of large highly-glazed spaces. *Energy and Buildings*, 33, 121-132.

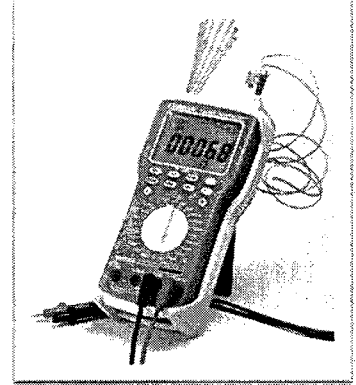
Walker, C.E., Glicksman, L.R., (2006). Reduced-scale air modeling technique for naturally ventilated buildings. *Research in Building Physics and Building Engineering – Fazio, Ge, Rao & Desmarais (eds) 2006 Taylor and Francis Group, London, ISBN 0-415-41675-2.*

Wall, M. (1996). Climate and energy use in atria. Energy and Building Design, Lund University.

APPENDIX I: Instrumentation

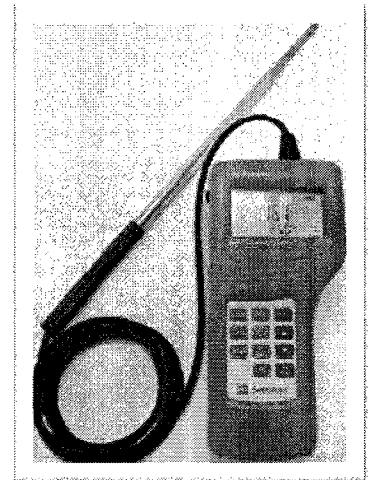
HHM290 Omega Supermeter

The HHM290 is a low cost digital multimeter & thermometer. It has a built-in infrared sensor and laser sighting for non-contact temperature measurement. The optical field of view is 10 to 1. This multimeter also measures and displays voltage, current, resistance, inductance, capacitance and frequency. It also has dual K-type thermocouple inputs (non-isolated) for temperature measurements. Temperature readings with the K-type thermocouple are 2% of reading or 2°C. Special features include T1-T2, min, max and average readings, manual/auto range and a built-in timer.



KANOMAX Anemomaster Model A031 Series

This velocity meter is used for HVAC testing, IAQ investigations, filter face velocity measurements, cleanroom studies and industrial hygiene applications. It has a velocity range of 0.10 – 30.0 m/sec, with an accuracy of +/- of reading or +/-0.015 m/sec (whichever is greater).



Some of the features of this type of velocity meter are:

- Single probe capable of measuring air flow and temperature simultaneously
- Built-in memory allows storage of measured data
- Highly- visible LCD is capable of displaying air flow and temperature simultaneously

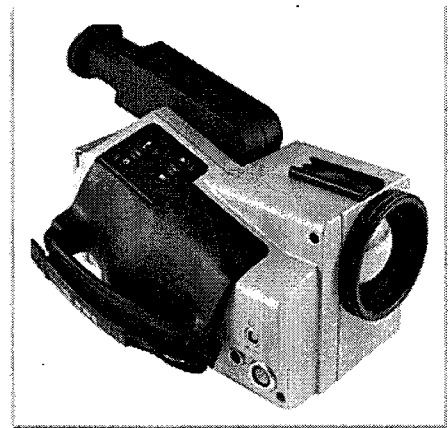
- RS232 and Analog (option) outputs are available

Its benefits include the following:

- Data can be reviewed on-screen, printed, or downloaded to a computer
- Articulating probe for various applications
- Etched length increments on the telescopic probe make duct traverse measurements easier
- Telescopic probe for hard-to-reach areas and in-duct measurements

FLIR SYSTEMS Infrared Camera

The thermaCAM PM595 infrared condition monitoring system consists of an IR-camera with a built-in 24° lens, a removable battery pack and a range of accessories. The IR-camera measures and images the emitted infrared radiation from an object.

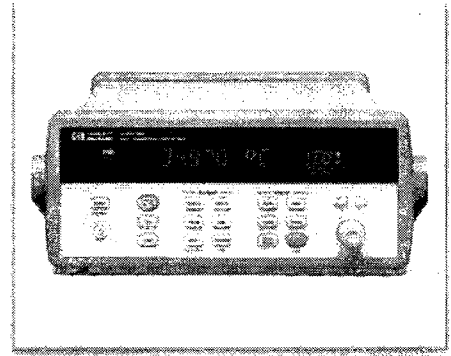


The fact that radiation is a function of object surface temperature makes it possible for the camera to calculate and display this temperature. The images can be analyzed either in the field by using the real time measurement functions built into the camera or in a PC by using the AGEMA Report Software. The measurement accuracy is +/-2% of readings or 2 °C.

34970A Agilent Data Acquisition

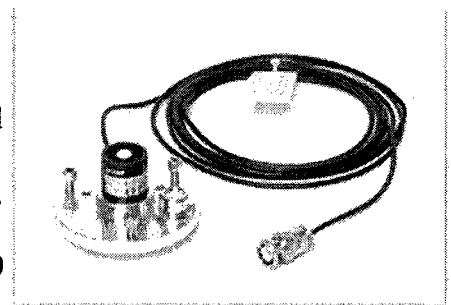
Some of the key features and specifications of the data acquisition system are:

- 3-slot mainframe, offers up to 96 matrix crosspoints or 120 single-ended channels
- 6 ½-digit (22-bit) internal DMM measures 11 functions without external signal conditioning
- 8 switch and control plug-in modules
- Agilent BenchLink Data Logger software included
- 50k readings of non-volatile memory holds data when power is removed
- Built-in Agilent-IB and RS-232 interfaces
- Scaling function for converting raw inputs into user-defined units
- Monitor display mode lets you keep an eye on tests in progress
- HI/LO alarm limits on each input channel, plus 4 TTL alarm outputs
- Battery-backed real-time clock for pacing scans and time-stamping readings



Li-cor Pyranometer

The LI-200 Pyranometer is designed for field measurement of global solar radiation in agricultural, meteorological, and solar energy studies. The LI-200



features a silicon photovoltaic detector mounted in a fully cosine-corrected miniature head. Current output, which is directly proportional to solar radiation, is calibrated

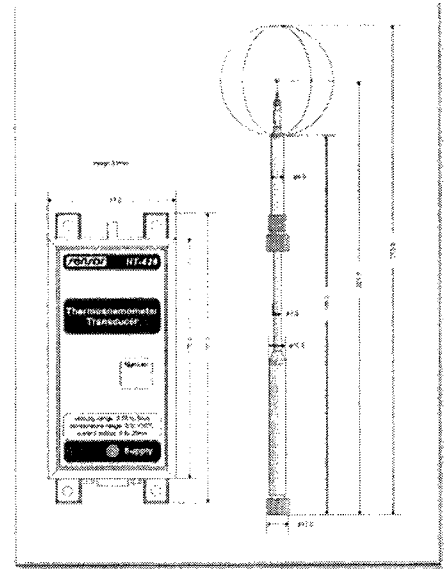
against an Eppley Precision Spectral Pyranometer (PSP) under natural daylight conditions in units of W per square meter (W/m^2). Under most conditions of natural daylight, the error is $< 5\%$.

The specifications of the LI-200 pyranometer are:

- Calibration: Calibrated against an Eppley Precision Spectral Pyranometer (PSP) under natural daylight conditions. Typical error under these conditions is $\pm 5\%$.
- Sensitivity: Typically $90 \mu A$ per $1000 W m^{-2}$.
- Linearity: Maximum deviation of 1% up to $3000 W m^{-2}$.
- Stability: $< \pm 2\%$ change over a 1 year period.
- Response Time: $10 \mu s$.
- Temperature Dependence: 0.15% per $^{\circ}C$ maximum.
- Cosine Correction: Cosine corrected up to 80° angle of incidence.
- Azimuth: $< \pm 1\%$ error over 360° at 45° elevation.
- Tilt: No error induced from orientation.
- Operating Temperature: -40 to $65^{\circ}C$.
- Relative Humidity: 0 to 100% .
- Detector: High stability silicon photovoltaic detector (blue enhanced).
- Sensor Housing: Weatherproof anodized aluminum case with acrylic diffuser and stainless steel hardware.
- Size: 2.38 Dia. x 2.54 cm H ($0.94''$ x $1.0''$).
- Weight: 28 g (1 oz).
- Cable Length: 3.0 m (10 ft)

ThermoAnemometer Measurements System HT-400 (Transducer unit HT-426-0 with probe HT-412)

This system is based on omnidirectional thermoanemometer sensors. It can be used to take air temperature and low air velocity measurements in rooms and inside air supply devices. The HT-400 measuring system complies with the requirements in



the future standards for low velocity measuring instruments as described in ASHRAE Transaction Vol. 1, 1998, paper No SF-98-20-5.

The system provides the high level of accuracy and sensitivity recommended for low velocity measurements that are typical of indoor environments. The sensors provide a short response time which is critical in measuring velocity fluctuations. Each transducer is calibrated in a wind tunnel with LDA reference. The software used for data acquisition compensates for the impact of barometric pressure on velocity measurements and collects and stores data to computer disks.

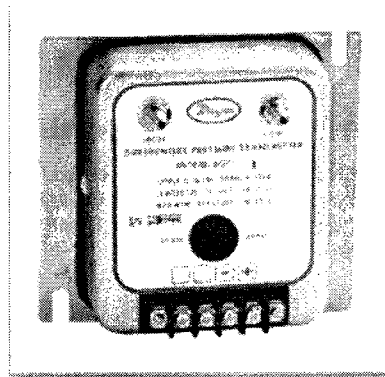
The system has the following technical properties:

- type of velocity sensor: omnidirectional, spherical
- diameter of velocity sensor: 2mm
- measurement velocity range: 0.05 to 5 m/s
- repeatability:
 - range of 0,05 to 1m/sec ± 0.02 m/sec $\pm 1\%$ of readings

- range of 1 to 5m/sec $\pm 3\%$ of readings
- automatic temperature compensation accuracy: better than $\pm 0.1\%/K$
- upper frequency f_{up}): min. 0,5Hz
- mean velocity directional sensitivity MDS *2): -4%
- turbulence intensity directional sensitivity TDS *3): 7%
- temperature range: -10 to +50 °C
- accuracy of temperature measurement: 0.2 °C
- outputs: analogue current $I_v = 0-20mA$; $I_t = 0-20mA$ (converted to voltage in the multichannel power supply HT-430 or connector unit HT-440)
 - temperature: linear $t [^{\circ}C] = 2,5 \cdot I_t [mA]$
 - velocity: non-linear (set of equations) $V [m/s] = f(0,25 \cdot I_v)$
- max output resistance: 450 Ohm
- max length of probe cable *4): 5 m
- power supply: 12VDC/200mA

Dwyer Series 607 Differential Pressure Transmitter

Series 607 differential pressure transmitter combines very low ranges with exceptional stability, reliability and either $\pm 0.25\%$ or $\pm 0.5\%$ accuracy for the most demanding applications. Ranges from 0-0.1" W.C and has an ultra thin glass clad silicon diaphragm design that



resists shock and vibration, practically eliminating drift. Certification to NIST standards is included with each unit.

The system's specifications are:

- Service: Air and nonconductive, non-corrosive gases..
- Accuracy: $\pm 0.5\%$ or $\pm 0.25\%$ F.S.
- Stability: $\pm 0.5\%$ F.S.O./yr.
- Temperature Limits: -20 to 160°F (-29 to 71°C), 10 to 95% RH.
- Pressure Limits: 10 psig (0.69 bar).
- Compensated Temp. Range: 35 to 135°F (2 to 57°C).
- Thermal Effects: $\pm 0.015\%$ FS/ $^{\circ}\text{F}$ (zero and span).
- Power Requirements: 12-36 VDC.
- Output Signal: 4 to 20 mA DC, 2-wire.
- Zero & Span Adjustments: Externally accessible potentiometers, non-interactive, $\pm 10\%$ F.S. adjustment.
- Response Time: 250 msec max.
- Loop Resistance: 0 to 1045 ohms

- $V_{min} = 12V + [(0.22A)(RL)]$.
- Current Consumption: 3.6 mA (min).
- Electrical Connection: Screw terminals.
- Process Connection: Barbed stainless steel for 3/16" I.D. tubing.
- Housing: 300 Series SS (NEMA 2).
- Weight: 1.04 lb (472 g).

APPENDIX II: Indoor and outdoor conditions

Graphs in Appendix II provide data on the outdoor conditions along with surface and indoor air temperatures for the days presented in the results. The days are divided in three sections referring to the thermal monitoring, the airflow monitoring and the night time measurements analysis and they are in chronological order.

1. Thermal monitoring

August 2, 2007

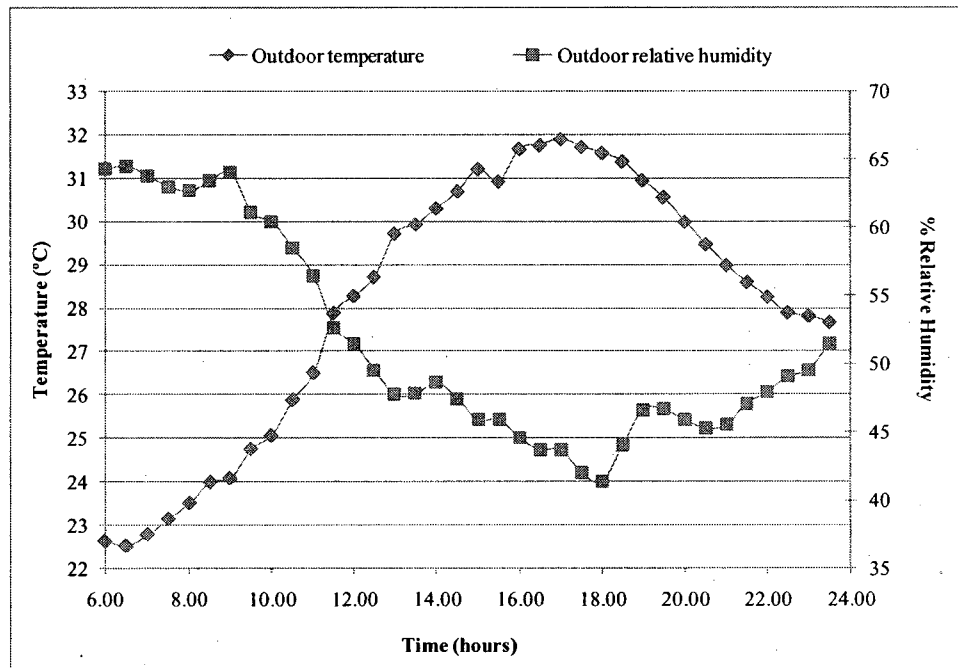


Figure II. 1. Outdoor temperature and relative humidity
(EV roof weather station data for August 2, 2007)

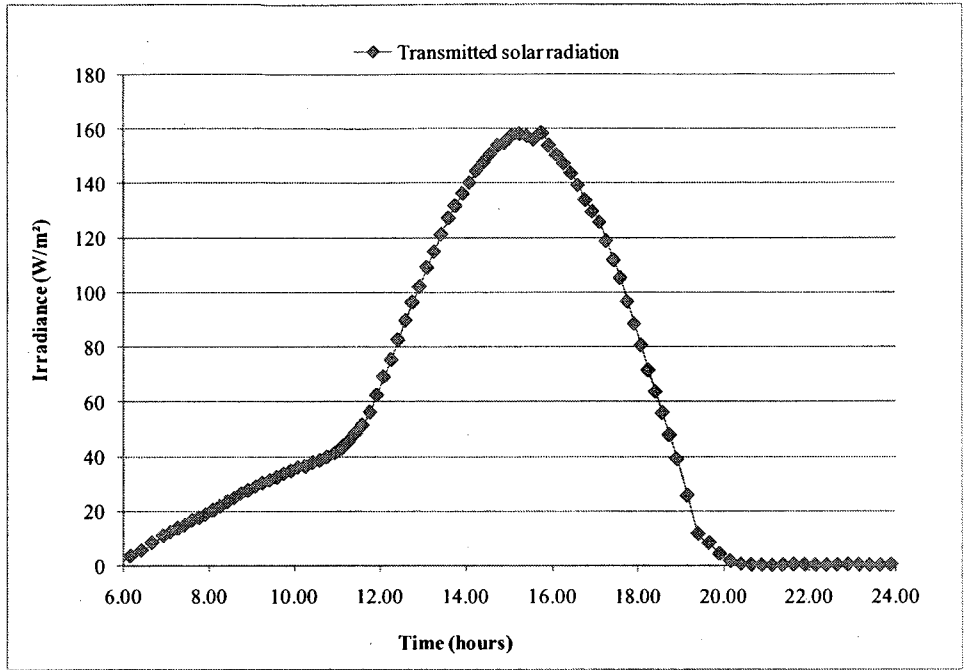


Figure II. 2. Solar radiation transmitted through the glass (atrium monitoring data for August 2, 2007)

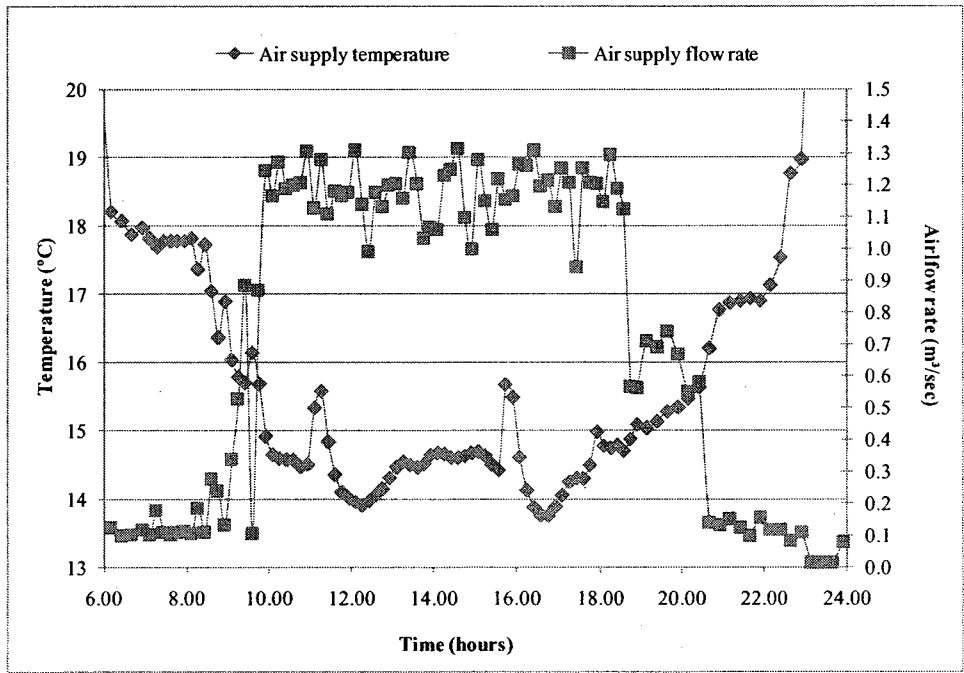


Figure II. 3. Air supply temperature and flow rate (atrium monitoring data for August 2, 2007)

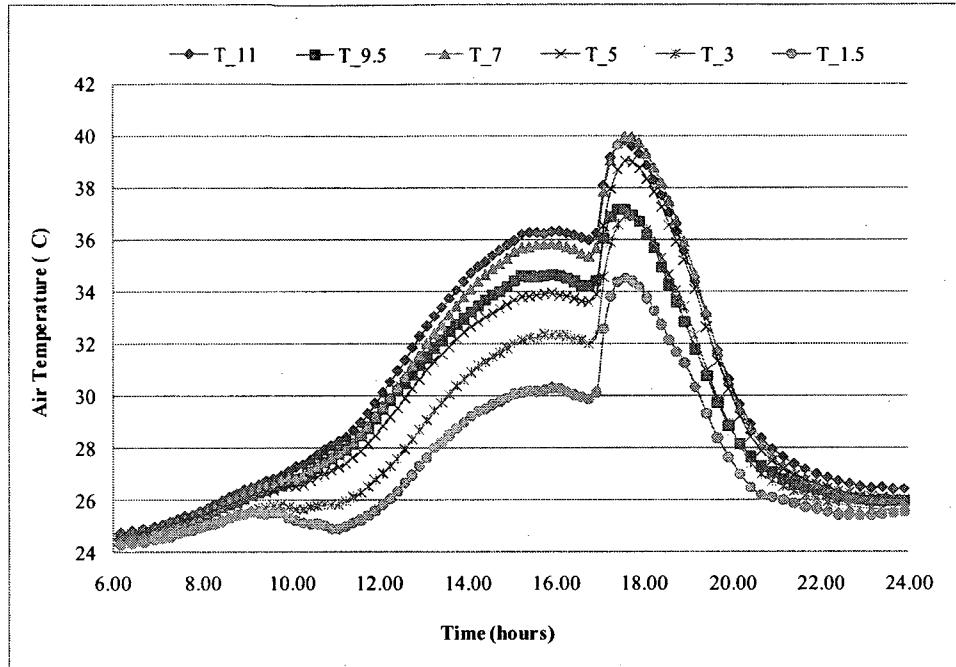


Figure II. 4. Glass temperature in the middle façade section (atrium monitoring data for August 2, 2007)

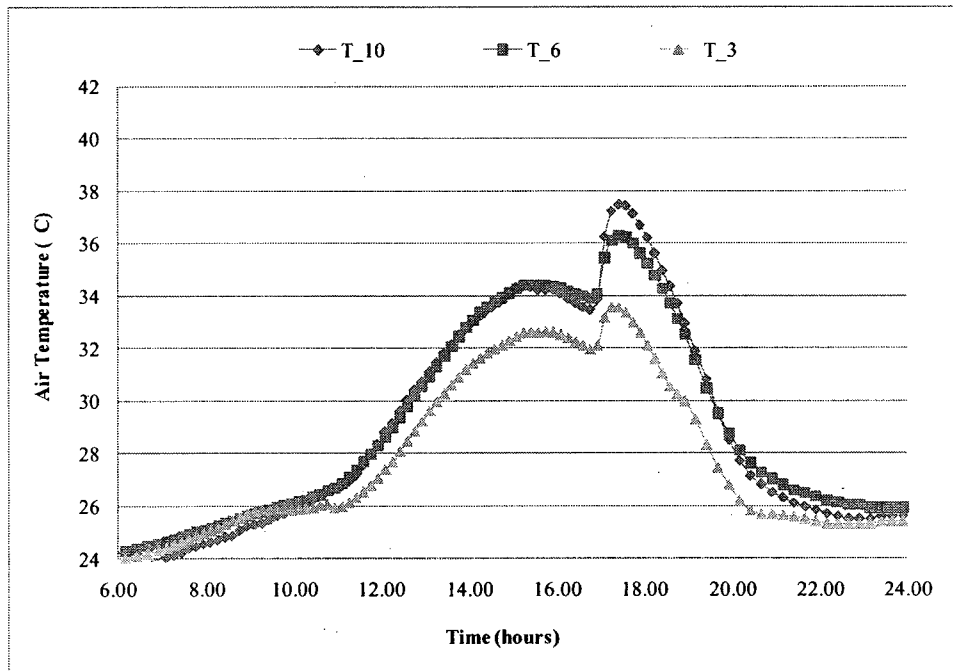


Figure II. 5. Glass temperature in the right façade section (atrium monitoring data for August 2, 2007)

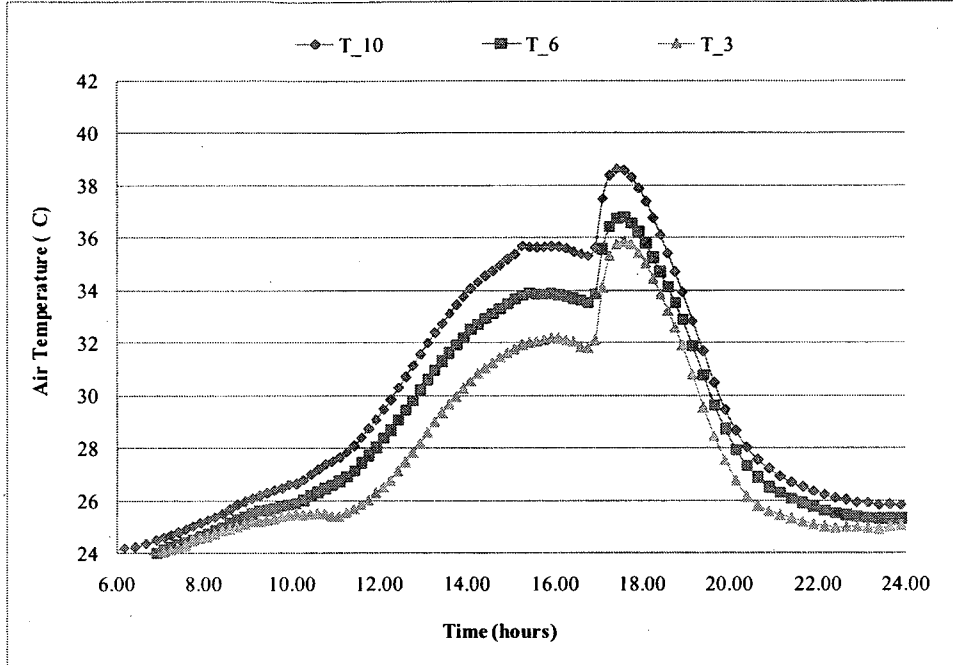


Figure II. 6. Glass temperature in the right façade section (atrium monitoring data for August 2, 2007)

September 1, 2007

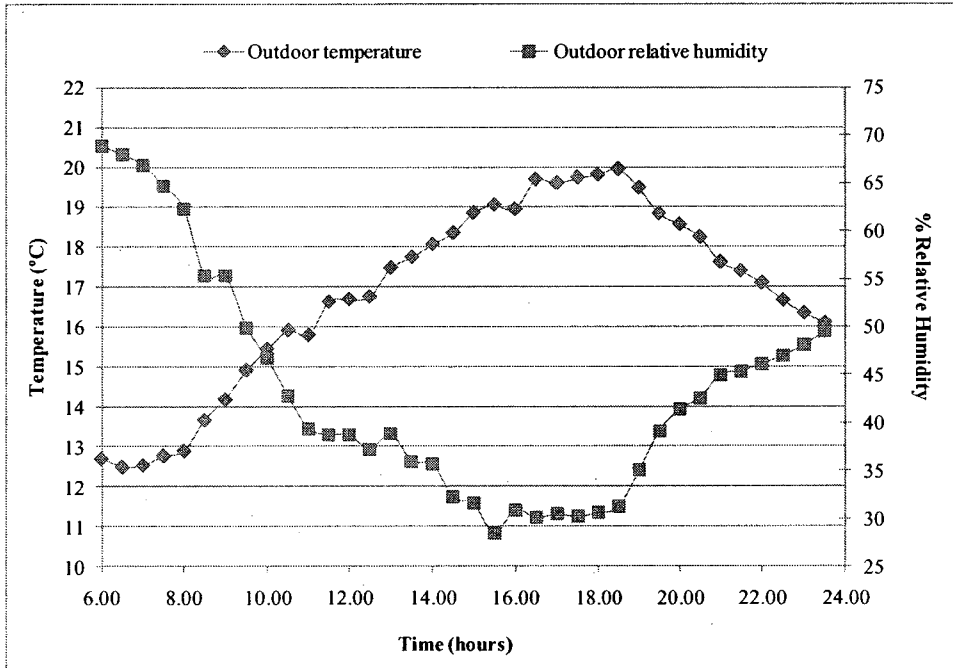


Figure II. 7. Outdoor temperature and relative humidity (EV roof weather station data for September 1, 2007)

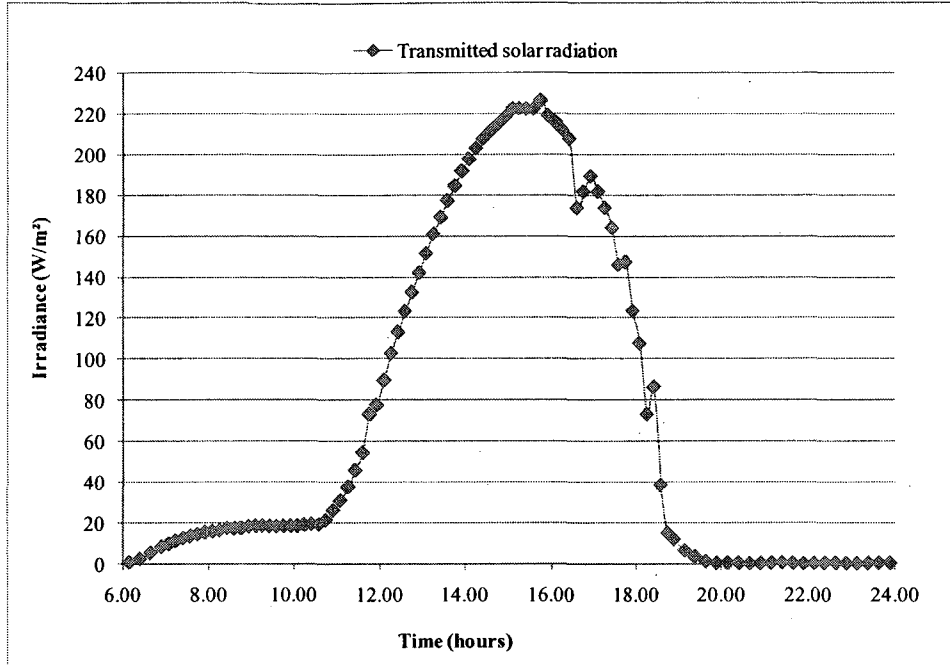


Figure II. 8. Solar radiation transmitted through the glass (atrium monitoring data for September 1, 2007)

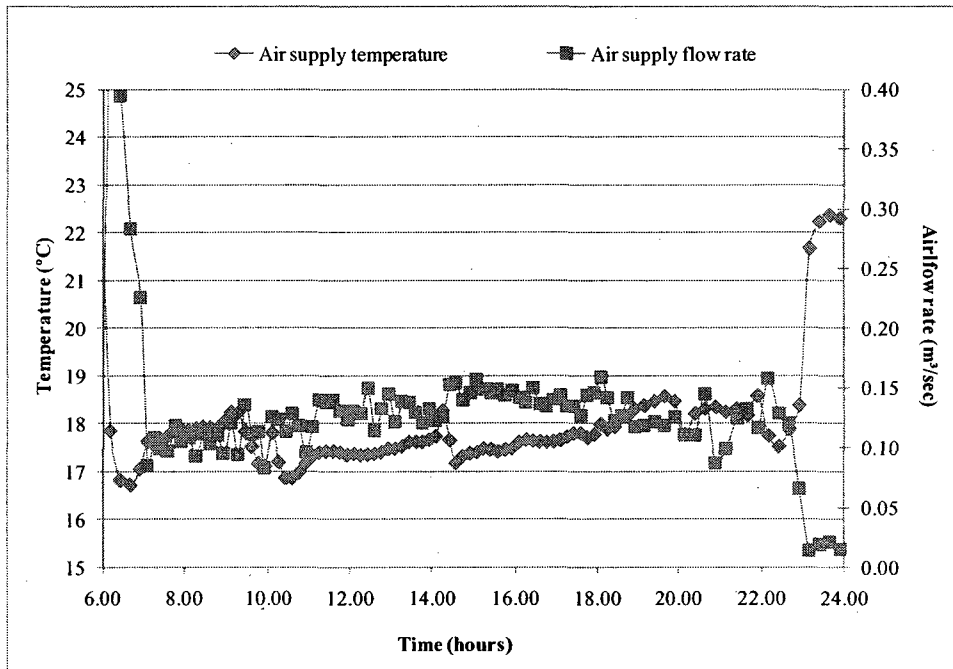


Figure II. 9. Air supply temperature and flow rate (atrium monitoring data for September 1, 2007)

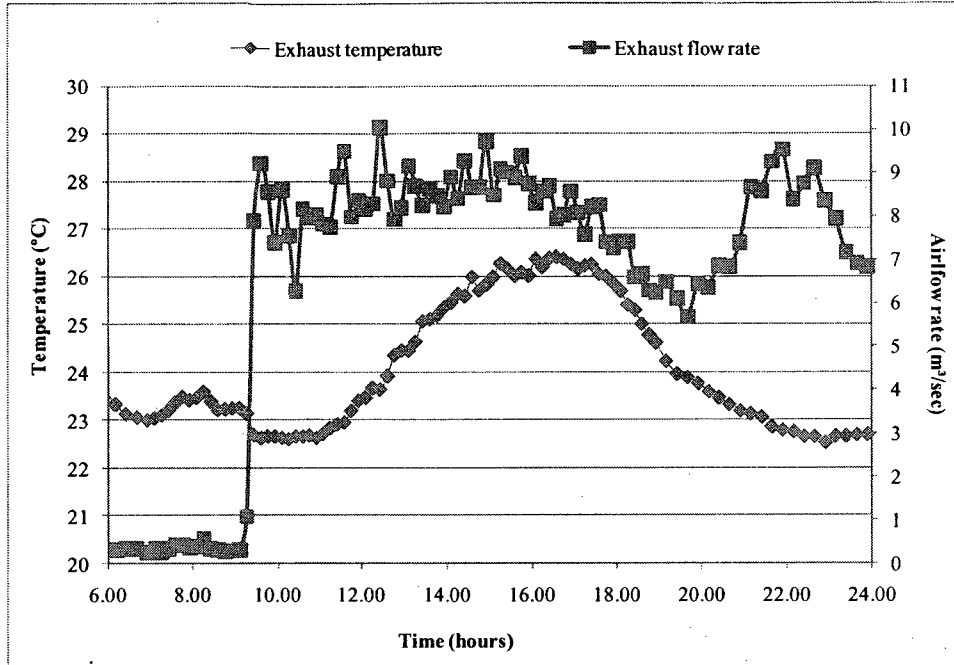


Figure II. 10. Exhaust air temperature and flow rate (atrium monitoring data for September 1, 2007)

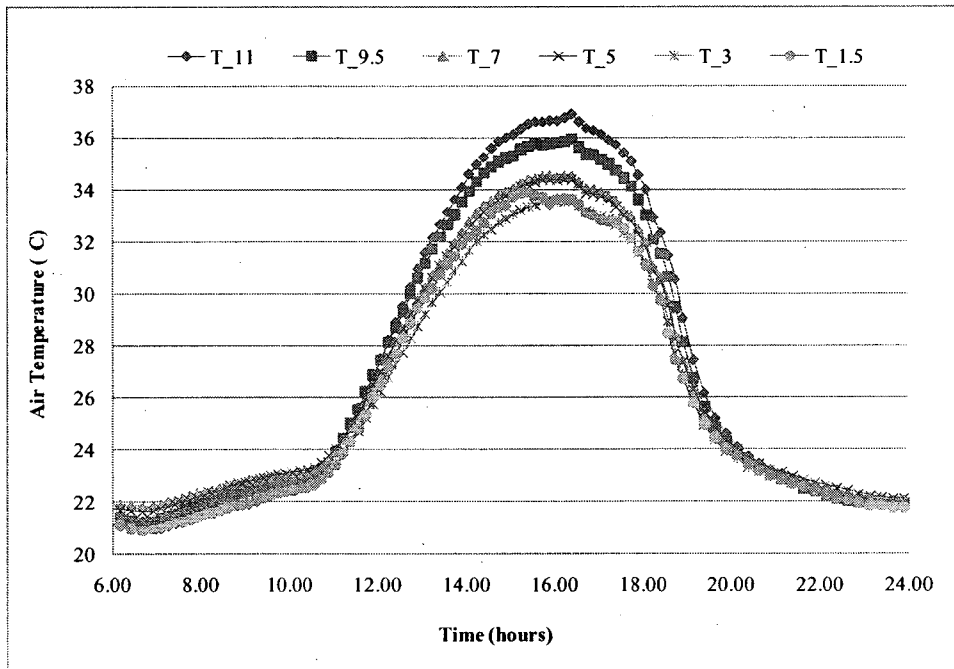


Figure II. 11. Glass surface temperature in the middle façade section (atrium monitoring data for September 1, 2007)

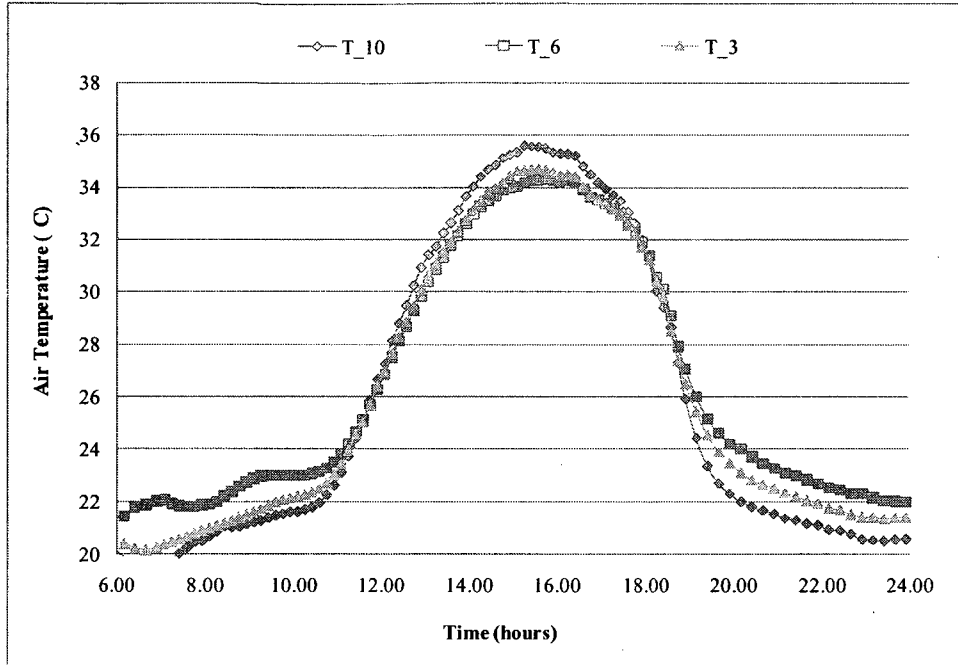


Figure II. 12. Glass surface temperature in the right façade section (atrium monitoring data for September 1, 2007)

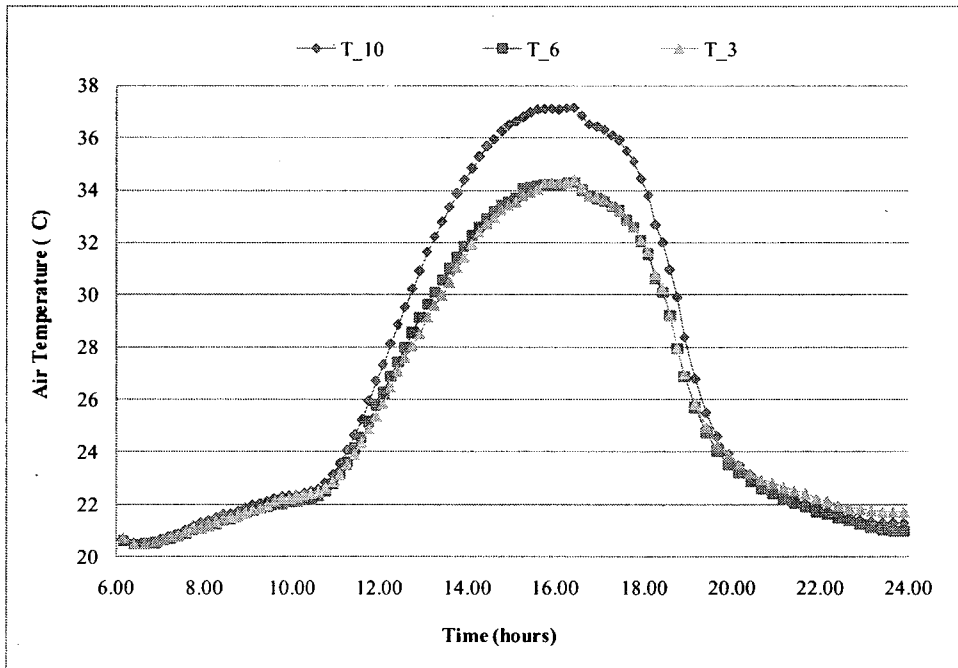


Figure II. 13. Glass surface temperature in the left façade section (atrium monitoring data for September 1, 2007)

September 23, 2007

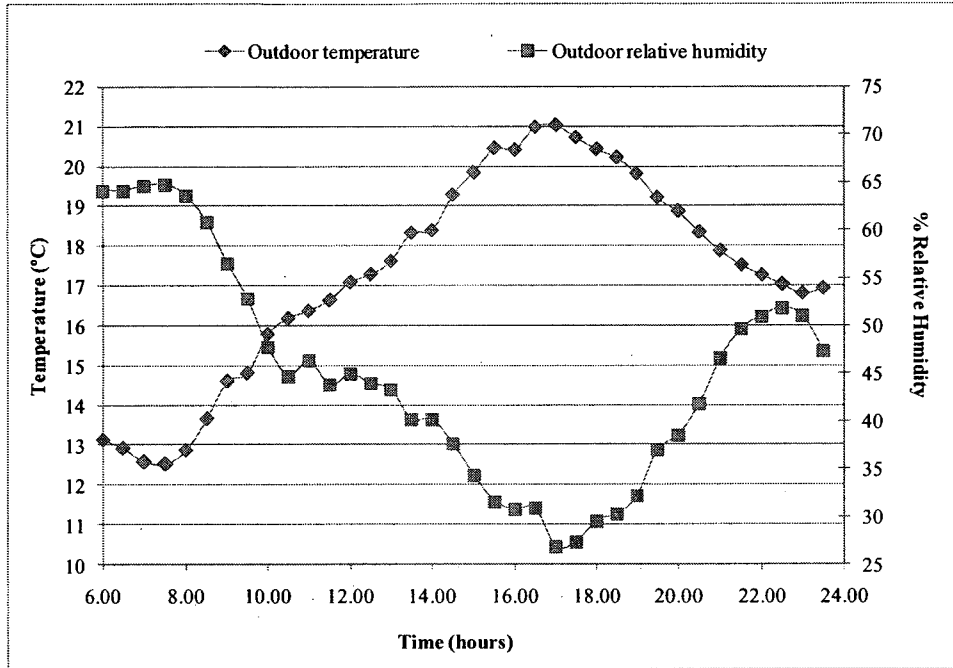


Figure II. 14. Outdoor temperature and relative humidity (EV roof weather station data for September 23, 2007)

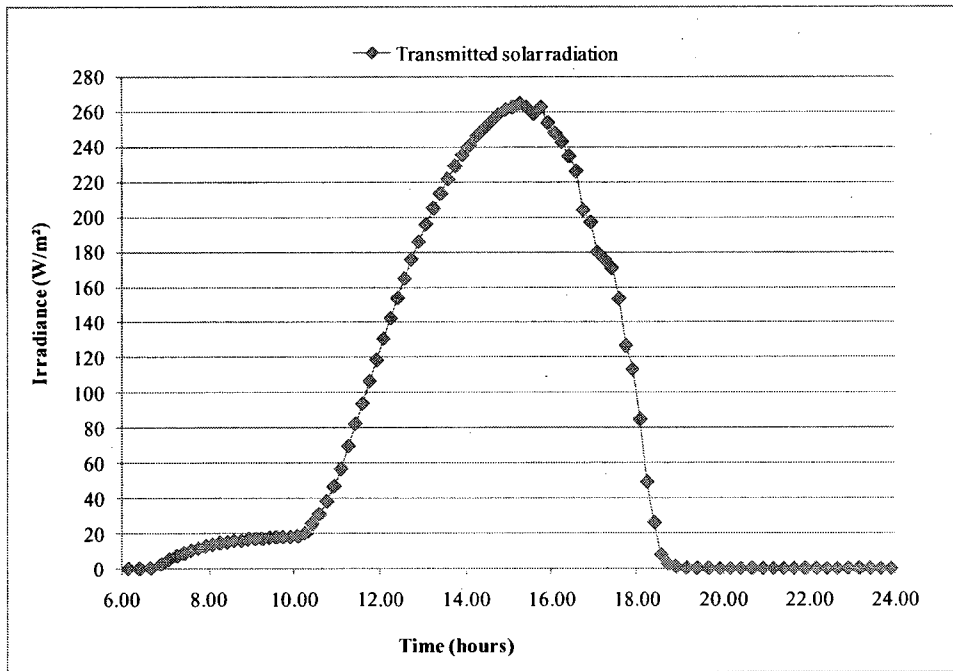


Figure II. 15. Solar radiation transmitted through the glass (atrium monitoring data for September 23, 2007)

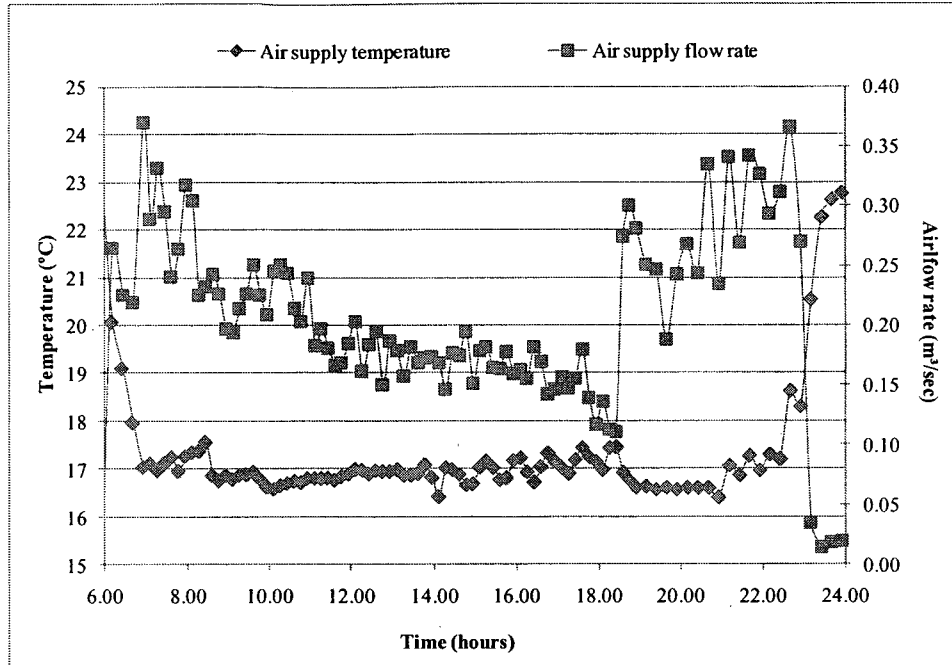


Figure II. 16. Air supply temperature and flow rate (atrium monitoring data for September 23, 2007)

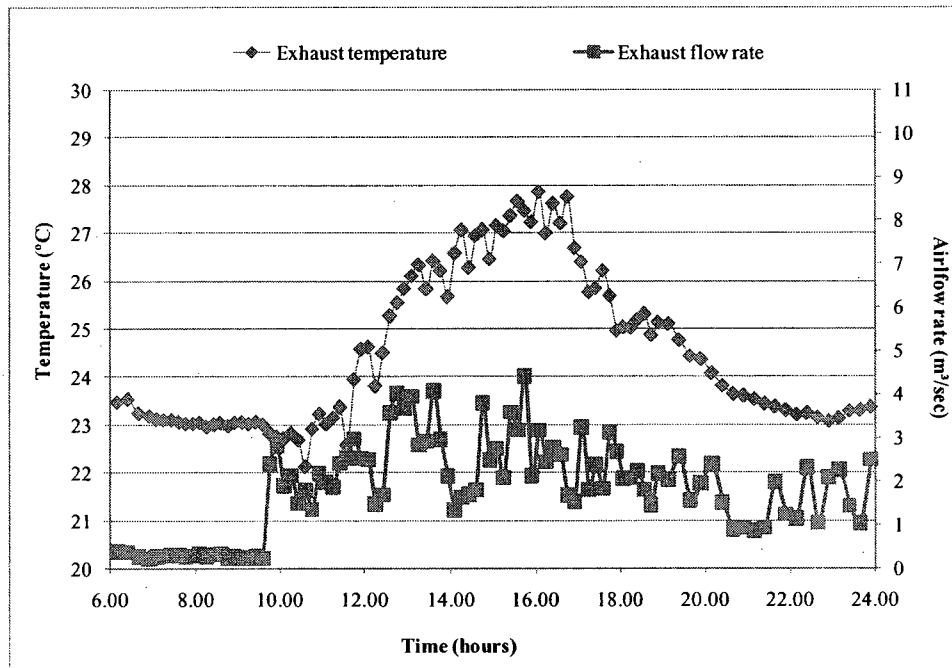


Figure II. 17. Exhaust air temperature and flow rate (atrium monitoring data for September 23, 2007)

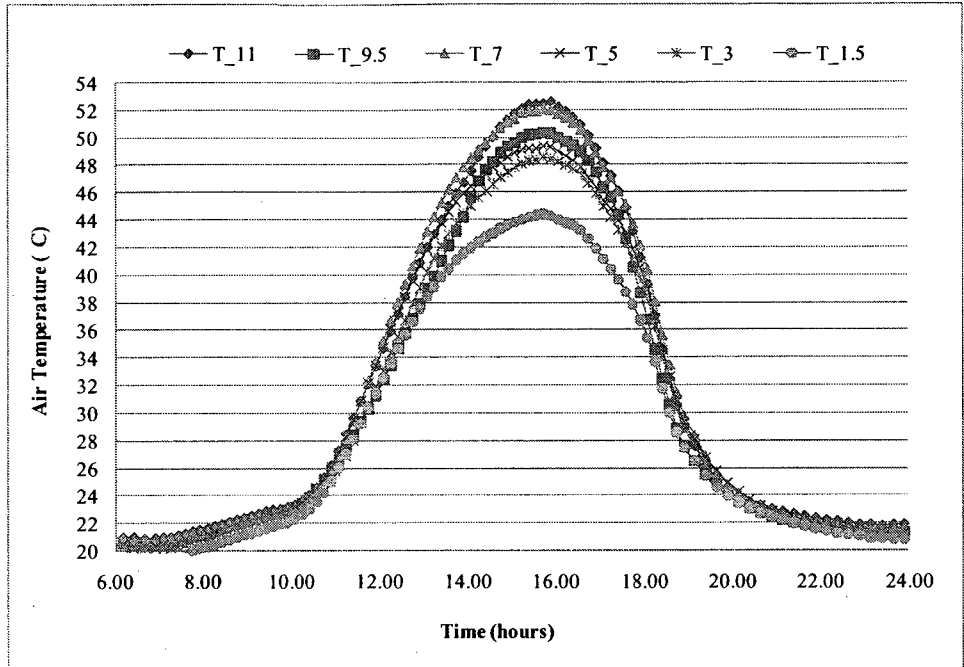


Figure II. 18. Glass surface temperature in the middle façade section (atrium monitoring data for September 23, 2007)

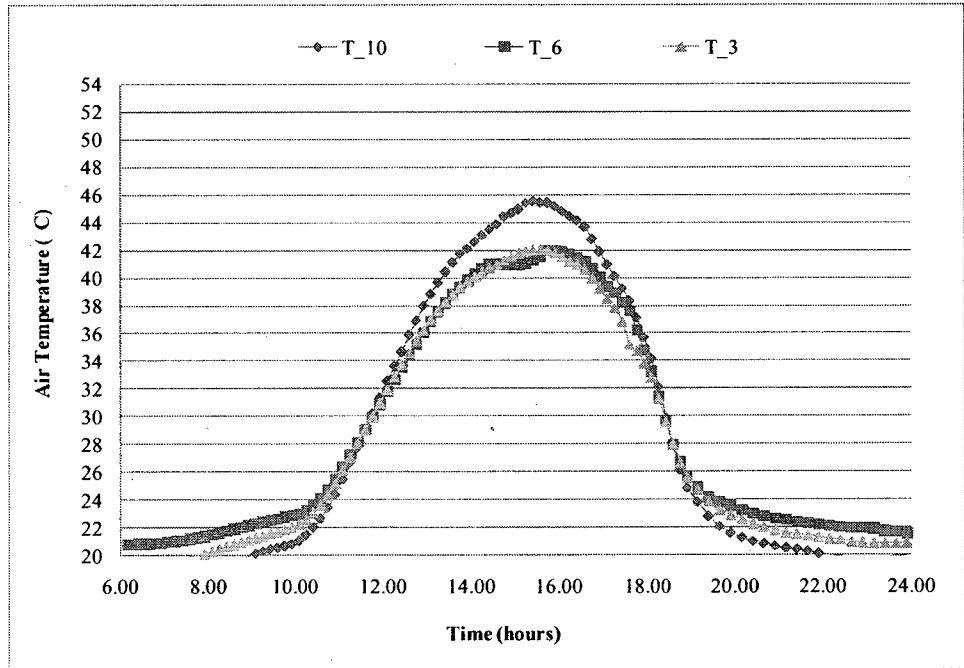


Figure II. 19. Glass surface temperature in the right façade section (atrium monitoring data for September 23, 2007)

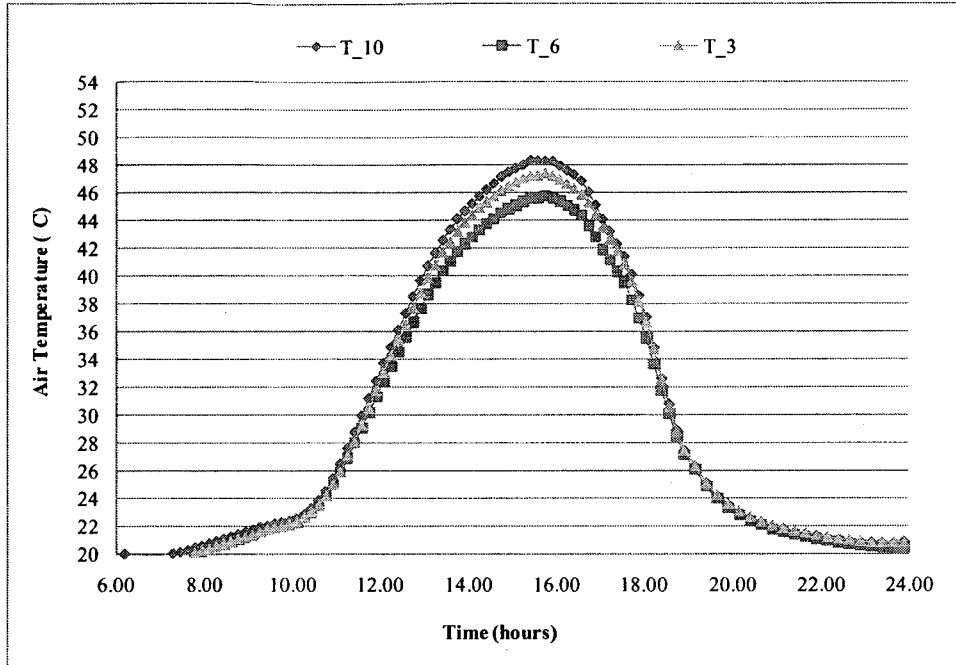


Figure II. 20. Glass surface temperature in the left façade section (atrium monitoring data for September 23, 2007)

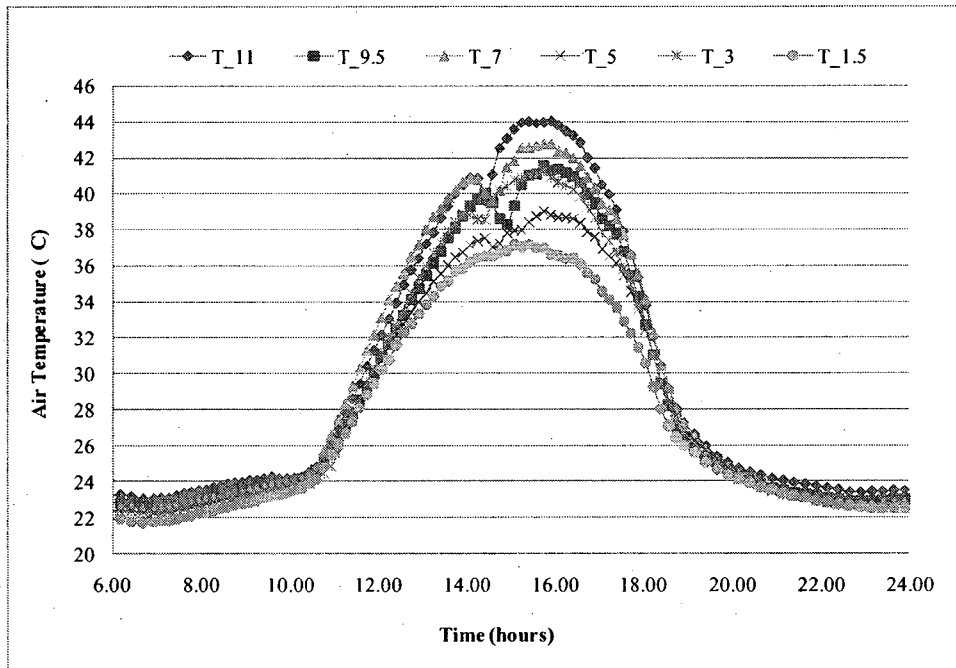


Figure II. 21. Blind surface temperature in the middle façade section (atrium monitoring data for September 23, 2007)

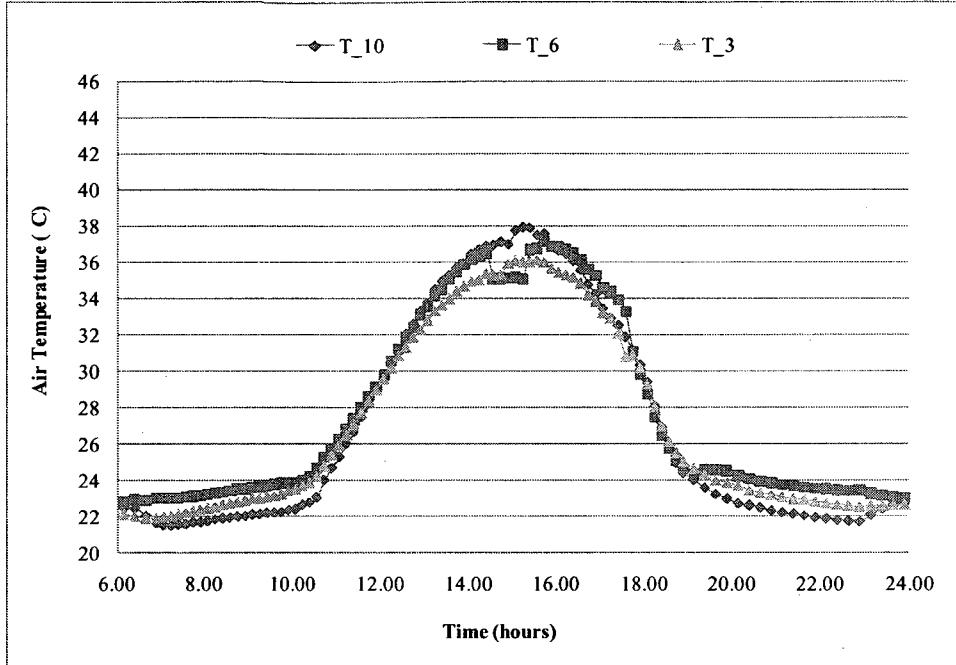


Figure II. 22. Blind surface temperature in the right façade section (atrium monitoring data for September 23, 2007)

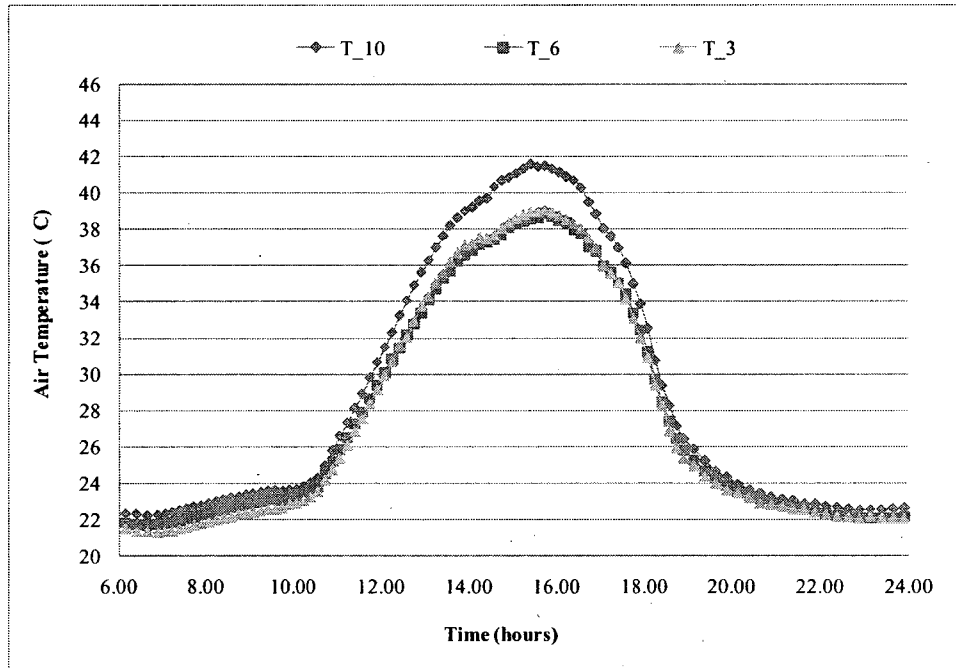


Figure II. 23. Glass temperature in the left façade section (atrium monitoring data for September 23, 2007)

November 2, 2007

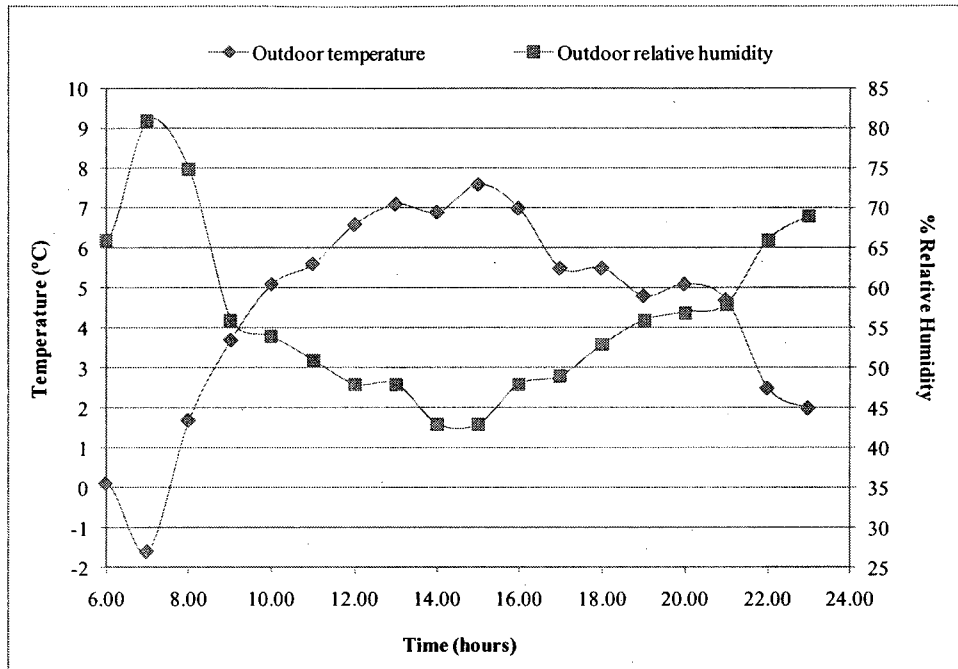


Figure II. 24. Outdoor temperature and relative humidity (Montreal Trudeau Int'l airport weather station data for November 2, 2007)

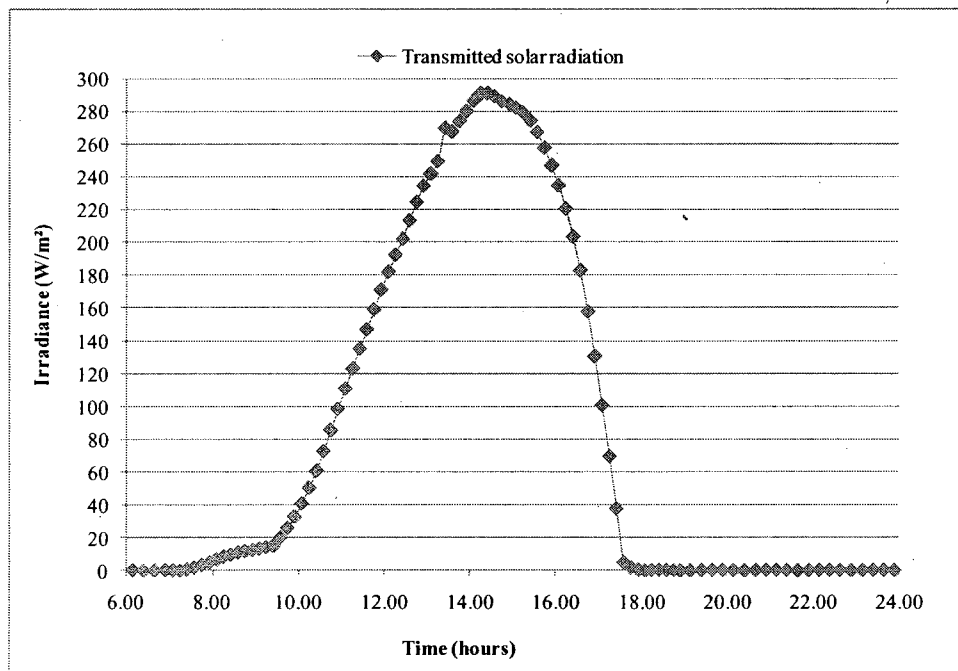


Figure II. 25. Solar radiation transmitted through the glass (atrium monitoring data for November 2, 2007)

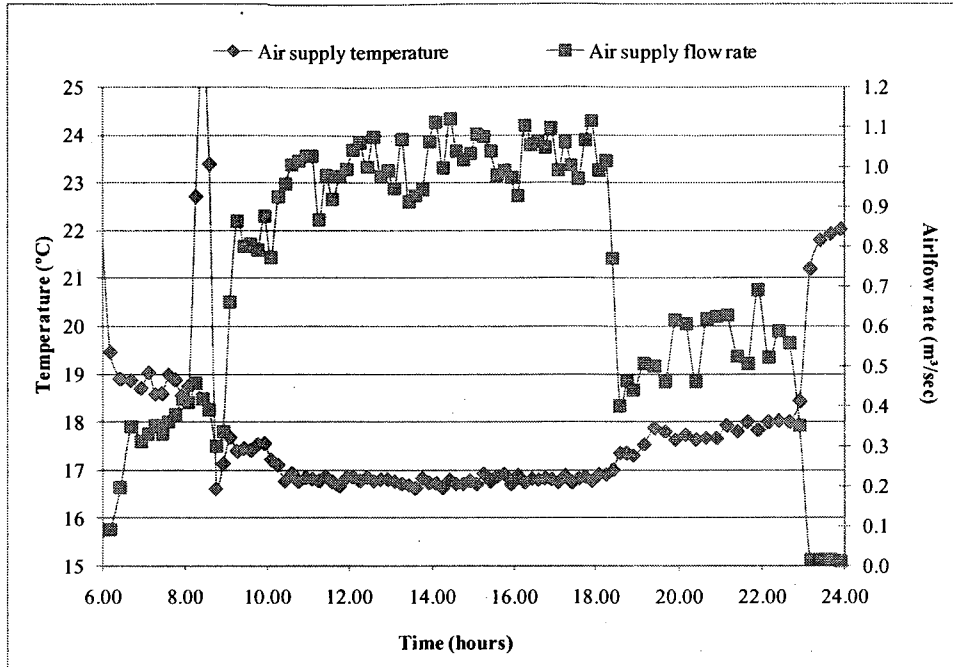


Figure II. 26. Air supply temperature and flow rate (atrium monitoring data for November 2, 2007)

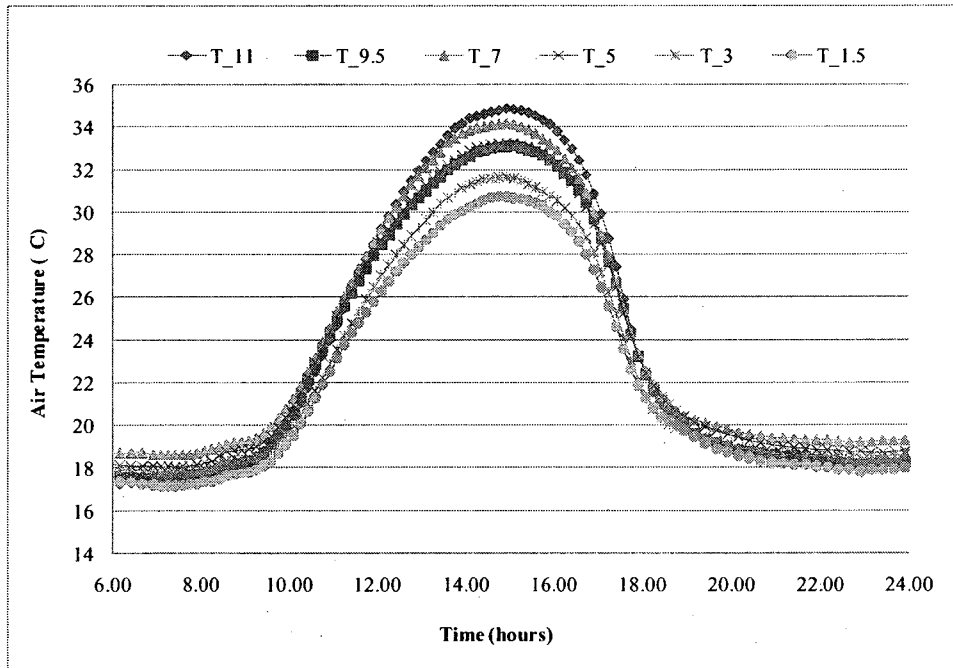


Figure II. 27. Glass temperature in the middle façade section (atrium monitoring data for November 2, 2007)

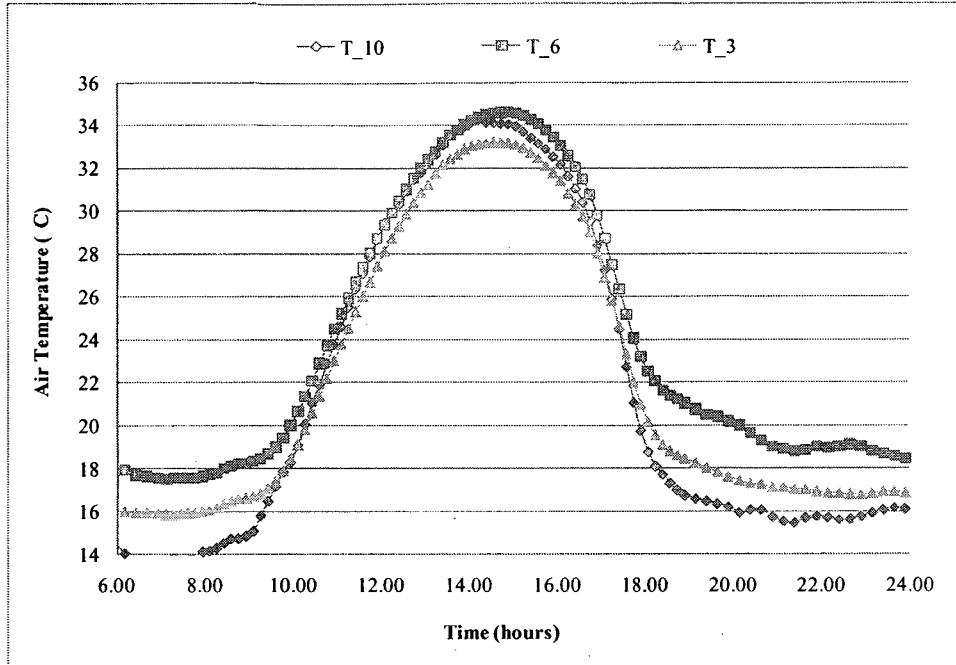


Figure II. 28. Glass temperature in the right façade section (atrium monitoring data for November 2, 2007)

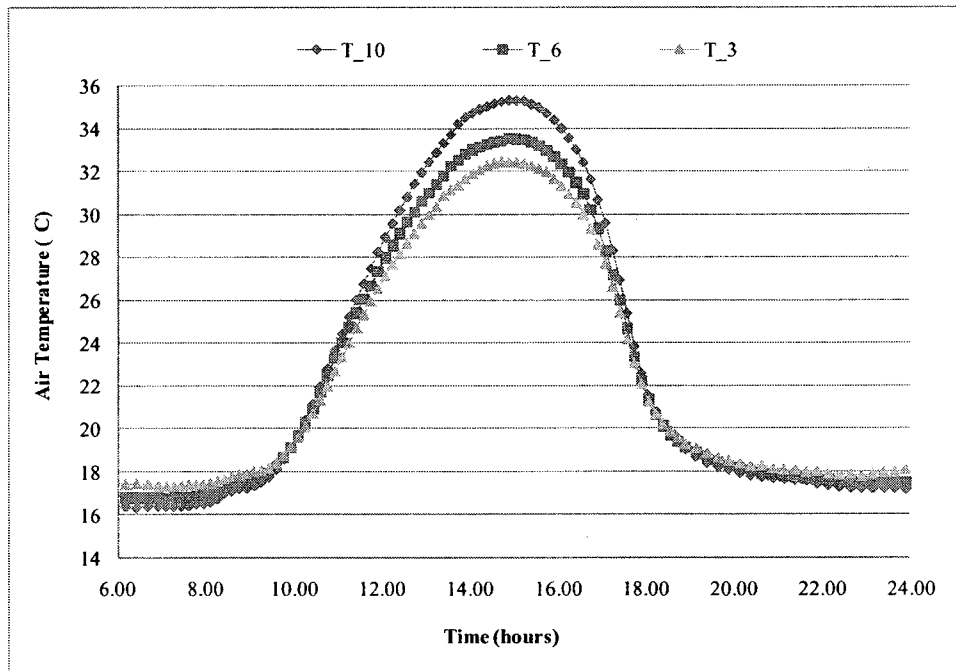


Figure II. 29. Glass temperature in the left façade section (atrium monitoring data for November 2, 2007)

2. Airflow monitoring

September 23, 2007

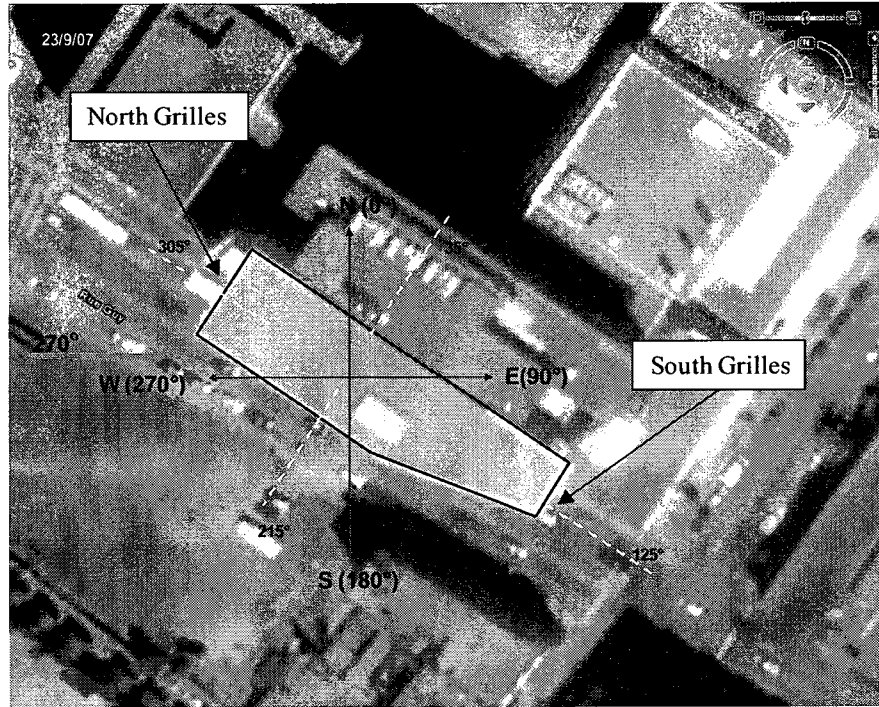


Figure II. 30. Prevailing wind direction around the Concordia Engineering building (September 23, 2007)

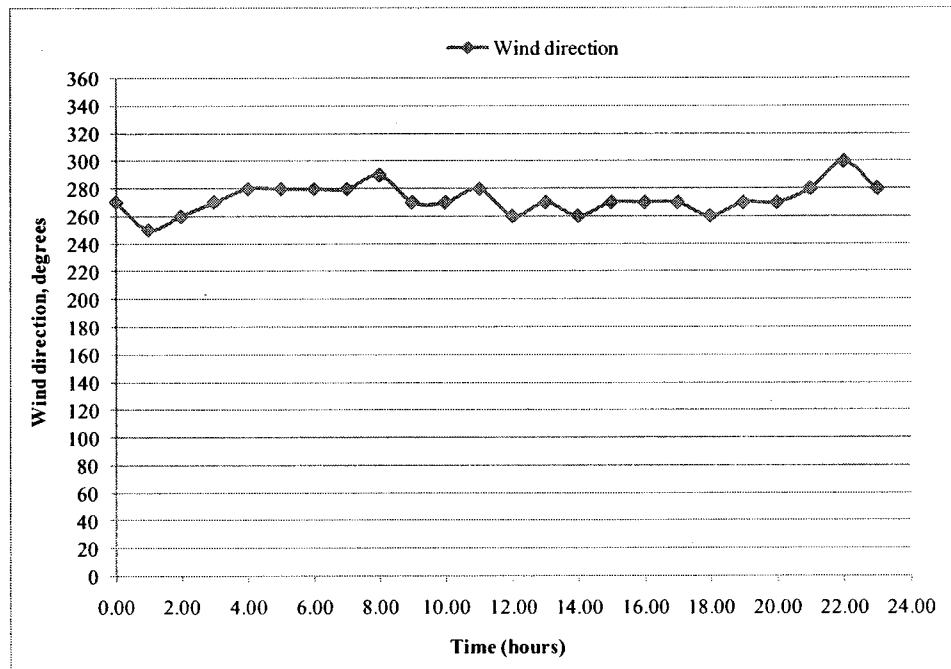


Figure II. 31. Wind direction
(Montreal Int'l airport weather station data for September 23, 2007)

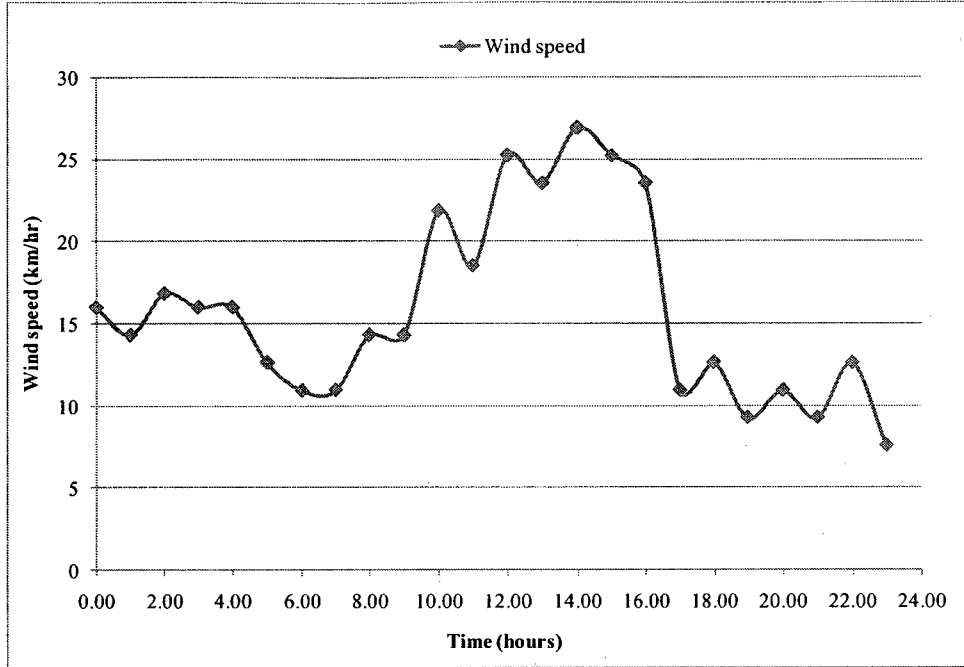


Figure II. 32. Wind speed for city conditions
(Montreal Int'l airport weather station data for September 23, 2007)

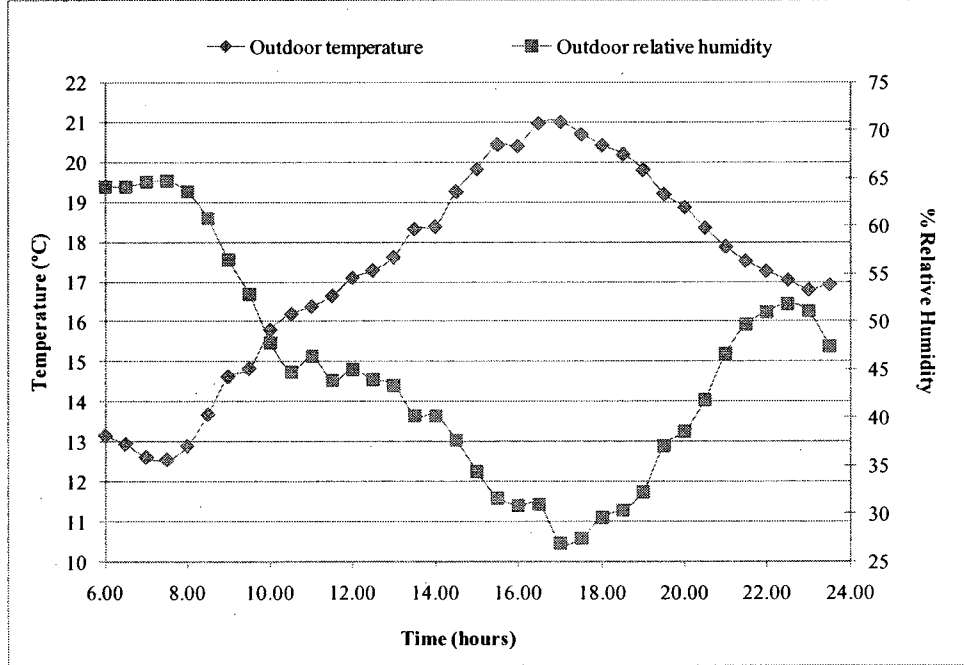


Figure II. 33. Outdoor temperature and relative humidity
(EV roof weather station data for September 23, 2007)

September 30, 2007

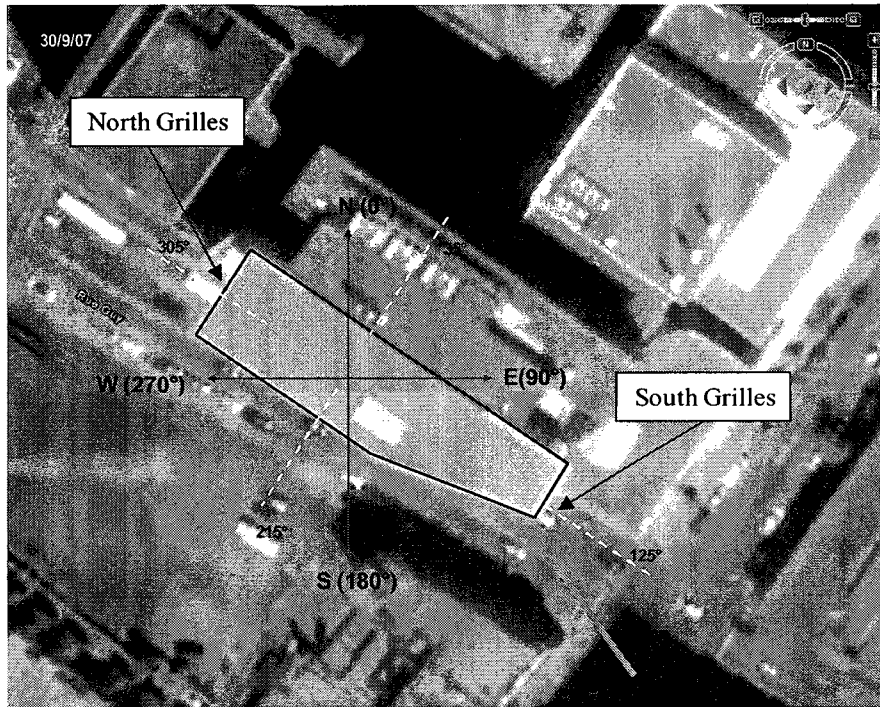


Figure II. 34. Prevailing wind direction around the Concordia Engineering building (September 30, 2007)

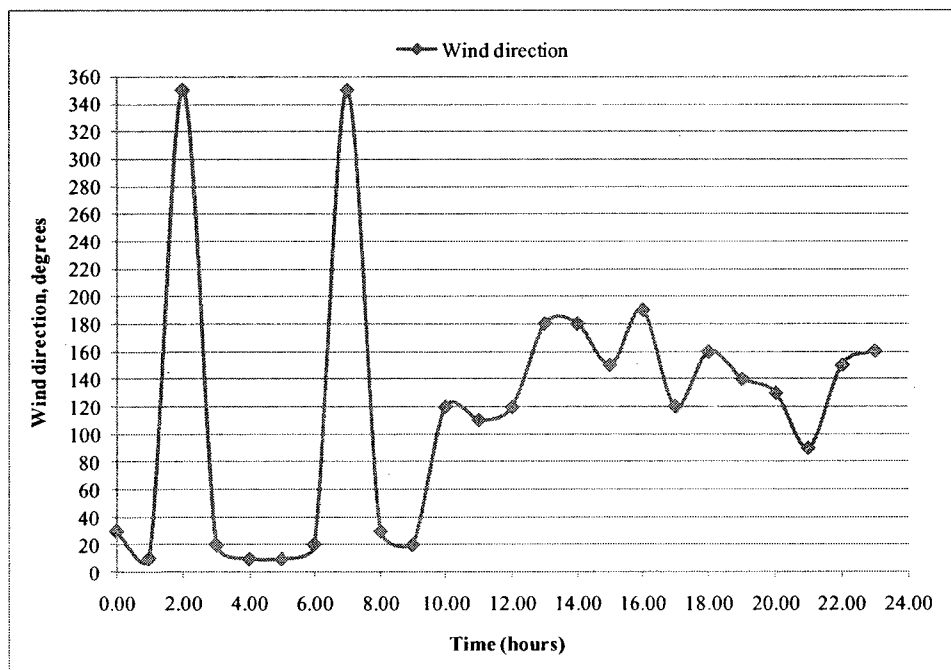


Figure II. 35. Wind direction
(Montreal Int'l airport weather station data for September 30, 2007)

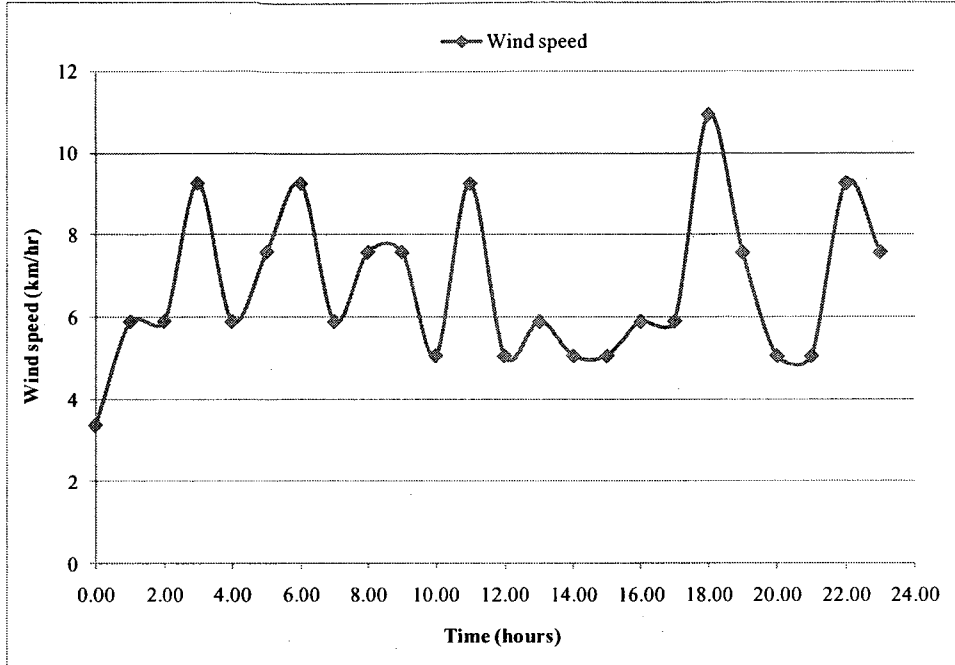


Figure II. 36. Wind speed for city conditions
(Montreal Int'l airport weather station data for September 30, 2007)

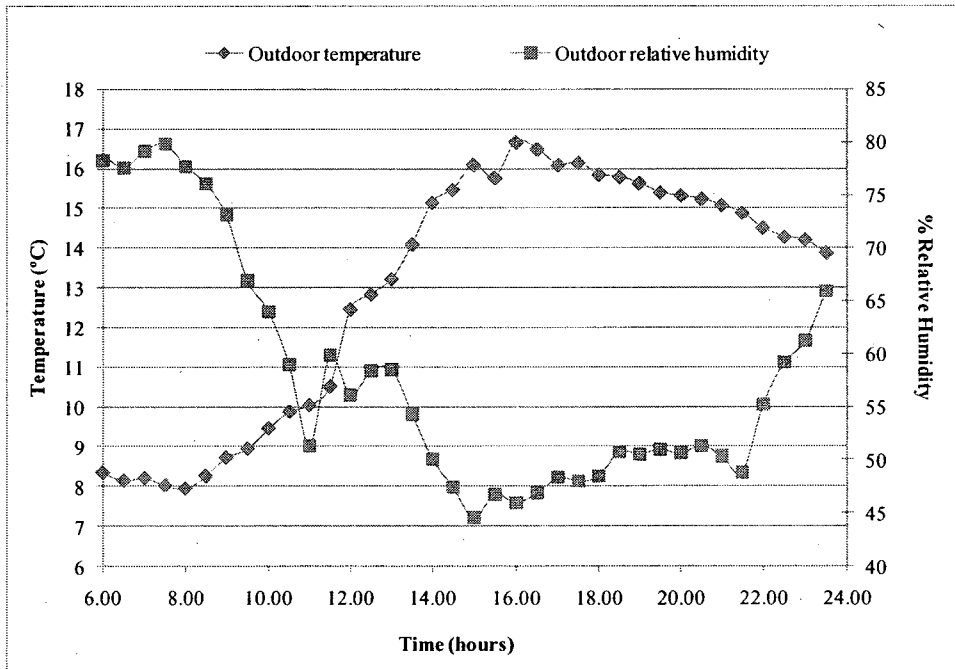


Figure II. 37. Outdoor temperature and relative humidity
(EV roof weather station data for September 30, 2007)

October 5, 2007

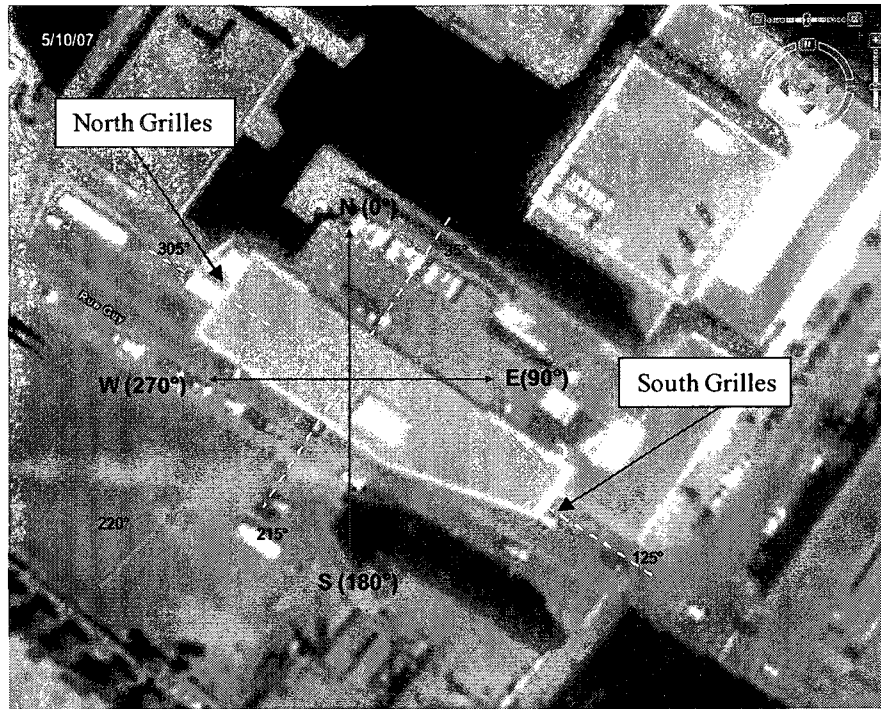


Figure II. 38. Prevailing wind direction around the Concordia Engineering building (October 5, 2007)

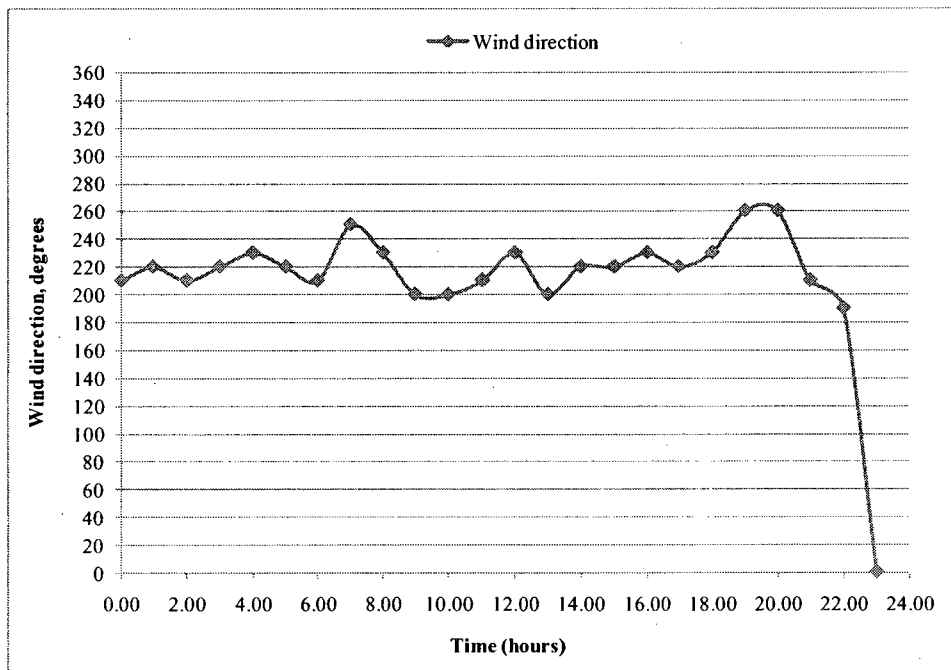


Figure II. 39. Wind direction
(Montreal Int'l airport weather station data for October 5, 2007)

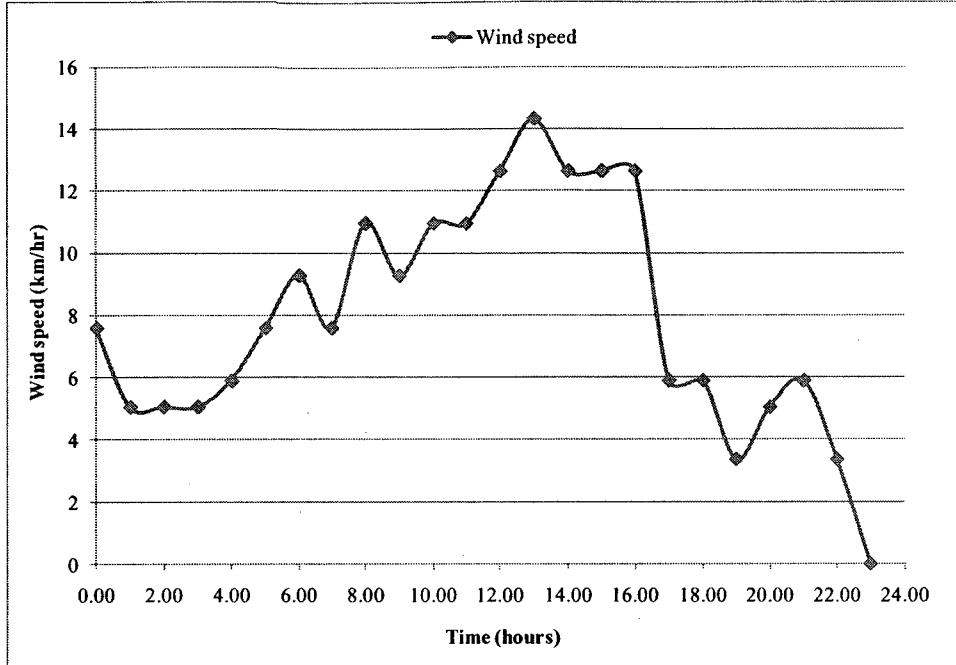


Figure II. 40. Wind speed for city conditions
(Montreal Int'l airport weather station data for October 5, 2007)

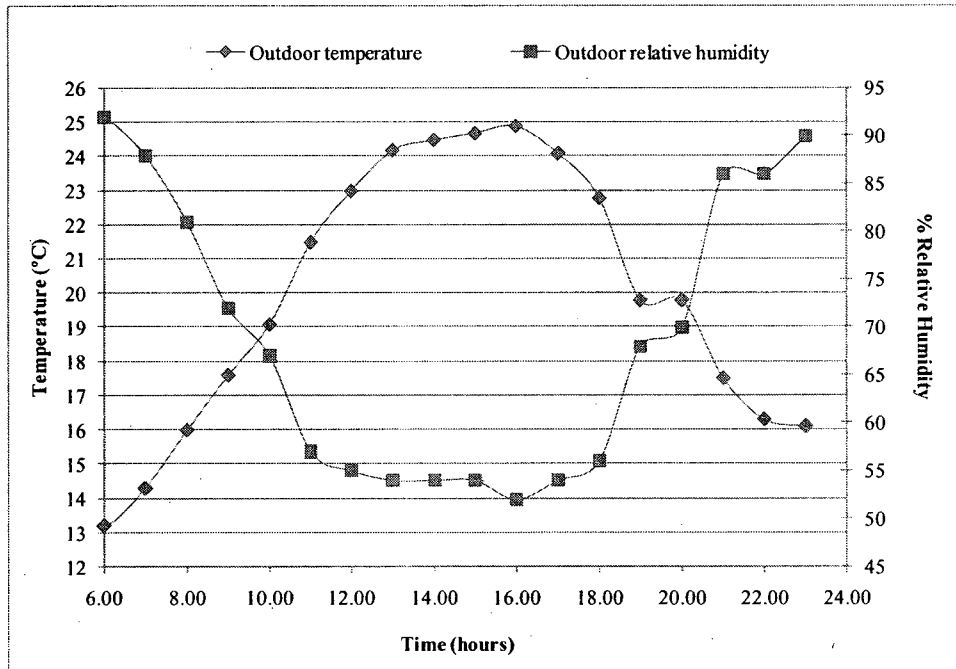


Figure II. 41. Outdoor temperature and relative humidity
(Montreal Trudeau Int'l airport weather station data for October 5, 2007)

3. Night time measurements

September 10–11, 2008

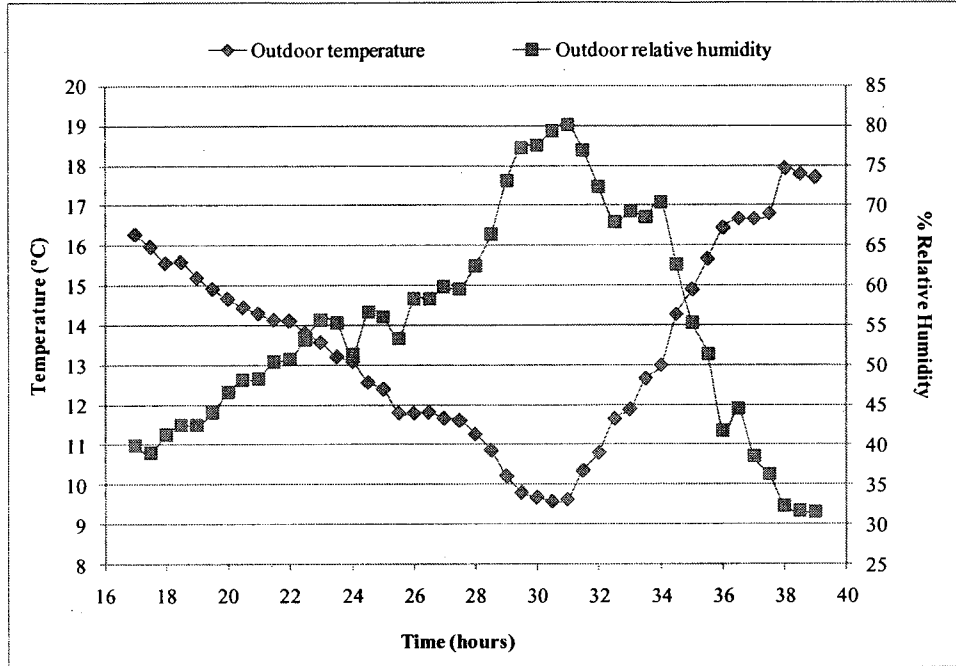


Figure II. 42. Outdoor temperature and relative humidity (EV roof weather station data for September 10-11, 2008)

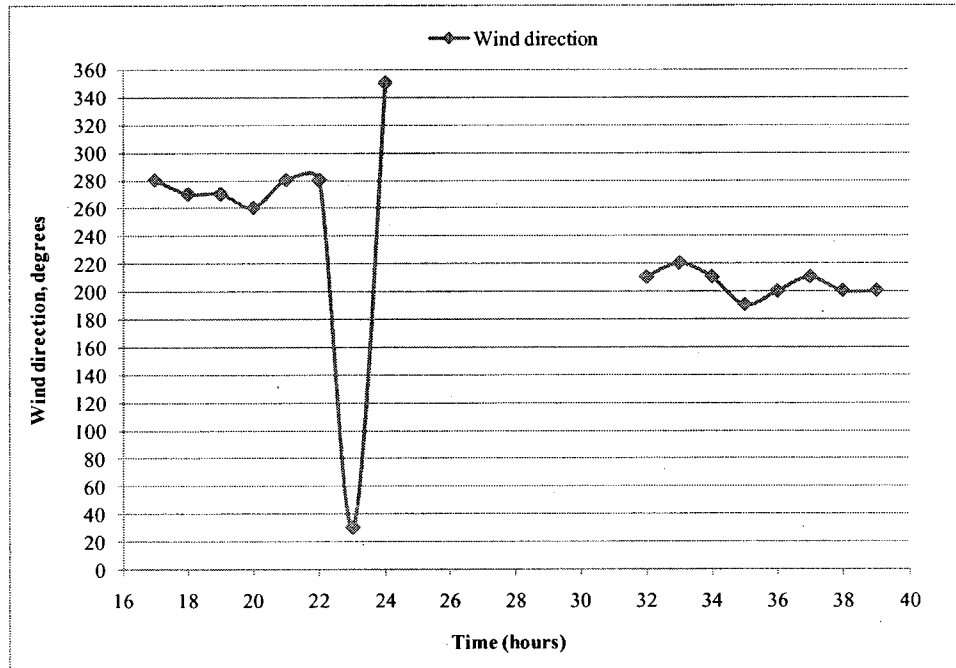


Figure II. 43. Wind direction (Montreal Int'l airport weather station data for September 10-11, 2008)

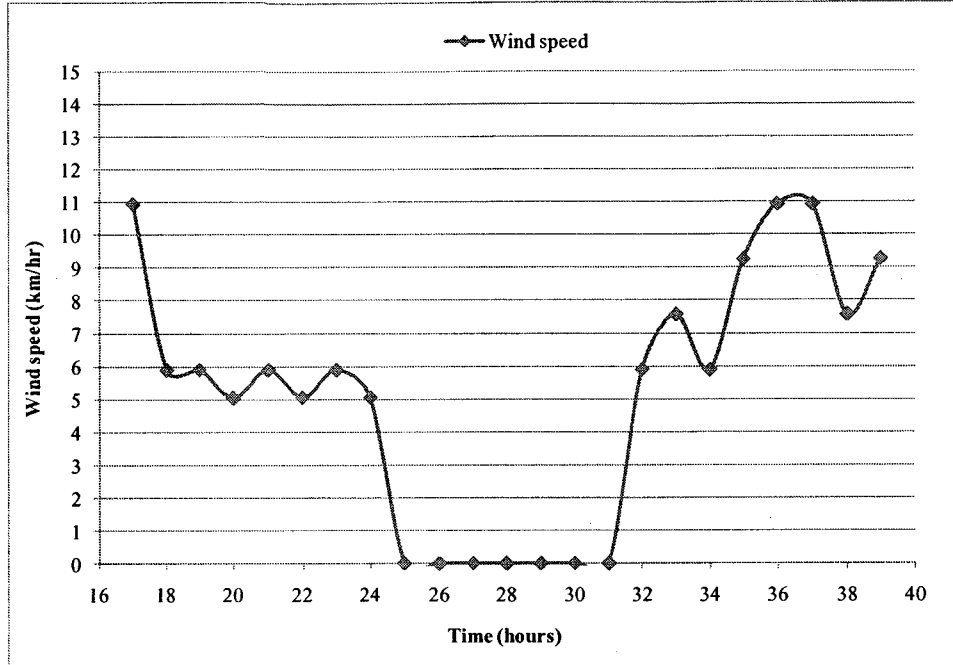


Figure II. 44. Wind speed
(Montreal Int'l airport weather station data for September 10-11, 2008)

September 24–25, 2008

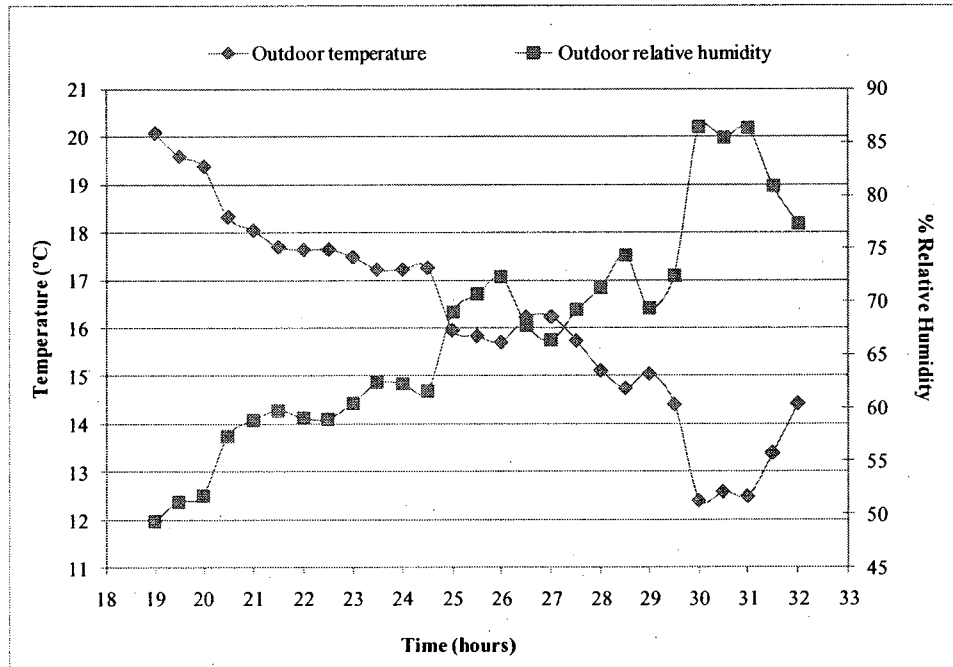


Figure II. 45. Outdoor temperature and relative humidity
(EV roof weather station data for September 24-25, 2008)

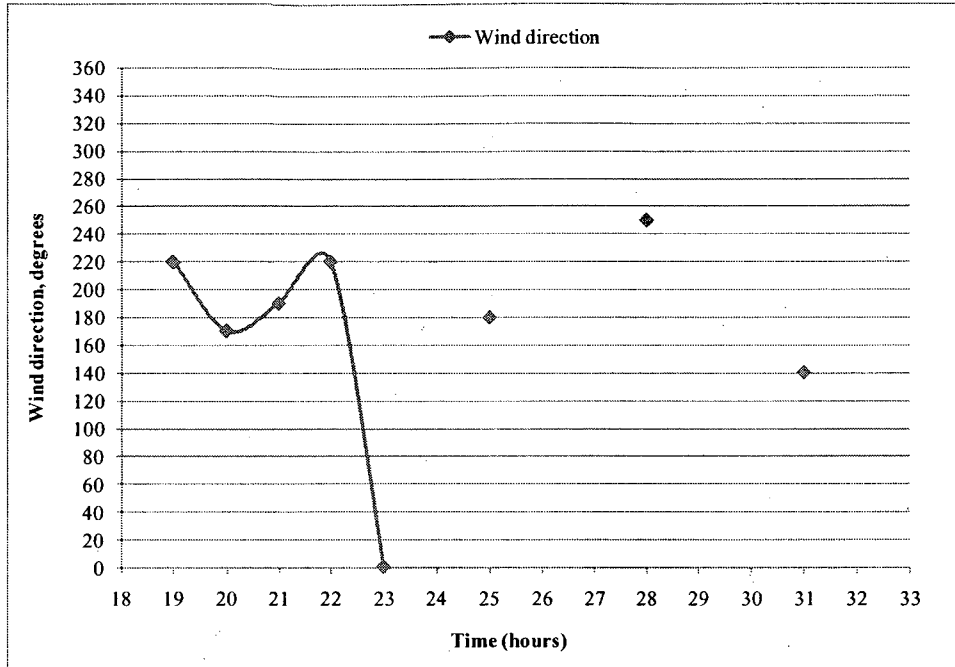


Figure II. 46. Wind direction
(Montreal Int'l airport weather station data for September 24-25, 2008)

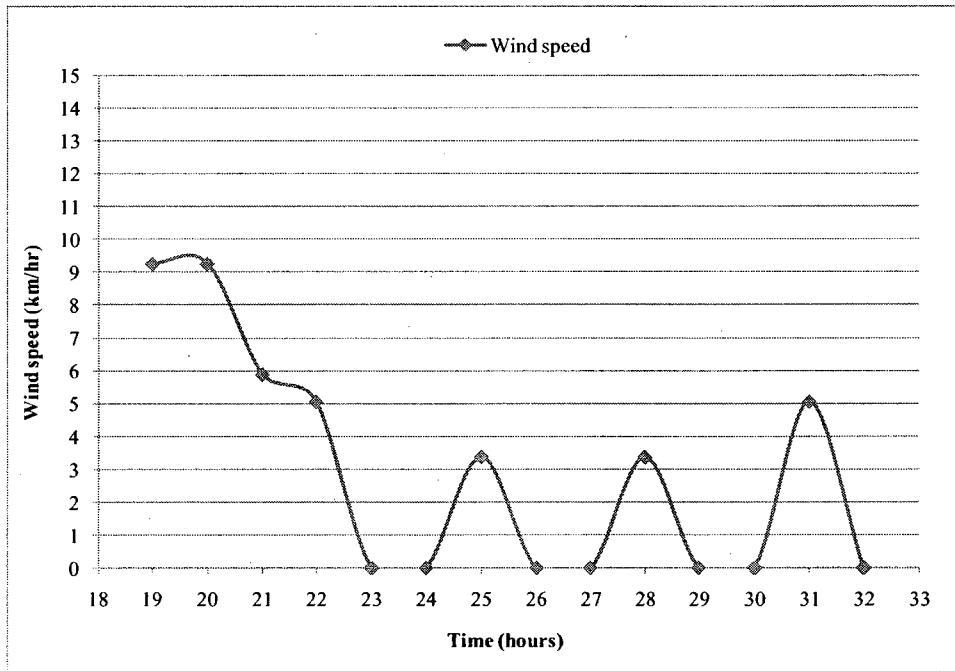


Figure II. 47. Wind direction
(Montreal Int'l airport weather station data for September 24-25, 2008)

APPENDIX III: Mathcad calculation sheet

Appendix III presents the calculation procedure that was followed for three cases:

- a) a mathematical model to predict the temperature of the ventilated slab near the inlet grilles.
- b) the temperature of the ventilated slab at different distances from the grilles and the cooling stored in the slab.
- c) the night time heat removal from the building's thermal mass based on a theoretical equation; some indicative values of U , ΔT_o and T_{om} are given while in the actual calculation procedure these values were adjusted according to each month's weather conditions which are given in the table included in the sheet.

Ventilated lab surface temperature

Properties of the air (for $T=20$ degC):

$$\text{degC} \equiv 1$$

$$\rho_{\text{air}} := 1.2 \frac{\text{kg}}{\text{m}^3} \quad \text{density of air}$$

$$k_f := 0.0257 \frac{\text{watt}}{\text{m} \cdot \text{degC}} \quad \text{thermal conductivity}$$

$$C_{p\text{air}} := 1005 \frac{\text{joule}}{\text{kg} \cdot \text{degC}} \quad \text{specific heat capacity}$$

$$\nu := 0.00001511 \frac{\text{m}^2}{\text{sec}} \quad \text{kinematic viscosity}$$

$$\alpha_{\text{air}} := \frac{k_f}{\rho_{\text{air}} \cdot C_{p\text{air}}} \quad \text{thermal diffusivity}$$

$$\text{Pr} := \frac{\nu}{\alpha_{\text{air}}} \quad \text{Prandtl Number}$$

Calculation of the heat transfer coefficient:

$$U := 1.3 \frac{\text{m}}{\text{sec}} \quad \text{air velocity at inlet grilles}$$

$$L := 1\text{m} \quad \text{characteristic length}$$

$$\text{Re} := \frac{U \cdot L}{\nu} \quad \text{Reynolds Number}$$

$$\text{Nu} := 0.332 \cdot (\text{Re})^{\frac{1}{2}} \cdot \text{Pr}^{\frac{1}{3}} \quad \text{Nusselt number for laminar boundary layer, external flows for flat plate, average velocity}$$

$$h := \frac{\text{Nu} \cdot k_f}{L} \quad \text{convective heat transfer coefficient}$$

Outdoor temperature:

$$\begin{pmatrix} \text{Te}_0 \\ \text{Te}_1 \\ \text{Te}_2 \\ \text{Te}_3 \\ \text{Te}_4 \\ \text{Te}_5 \\ \text{Te}_6 \\ \text{Te}_7 \\ \text{Te}_8 \\ \text{Te}_9 \\ \text{Te}_{10} \end{pmatrix} := \begin{pmatrix} 14.655 \\ 14.29 \\ 14.095 \\ 13.56 \\ 13.075 \\ 12.395 \\ 11.785 \\ 11.66 \\ 11.265 \\ 10.21 \\ 9.67 \end{pmatrix} \text{degC}$$

Properties of floor slab:

$$\rho := 1700 \frac{\text{kg}}{\text{m}^3} \quad \text{density}$$

$$k := 1.7 \frac{\text{watt}}{\text{m} \cdot \text{degC}} \quad \text{thermal conductivity}$$

$$c := 800 \frac{\text{joule}}{\text{kg} \cdot \text{degC}} \quad \text{specific heat capacity}$$

$$\alpha := \frac{k}{\rho \cdot c} \quad \text{thermal diffusivity}$$

Calculation of the slab surface temperature:

$$i := 1..10 \quad t := 1 \text{hr}$$

$$j := 0, 1..3 \quad x_j := j \cdot 0.1 \text{m}$$

$$T_{0,j} := 19.1 \text{degC} \quad \text{initial slab surface temperature}$$

The temperature at depth x and time t for a semi-infinite slab with convective boundary condition is given by:

$$T_{i,j} := \left[T_{e,i-1} - T_{i-1,j} \right] \cdot \left[1 - \text{erf} \left[\frac{x_j}{2 \cdot \sqrt{\alpha \cdot t}} \right] - \exp \left[\frac{h \cdot x_j}{k} + \frac{(h)^2 \cdot \alpha \cdot t}{k^2} \right] \cdot \left(1 - \text{erf} \left(\frac{x_j}{2 \cdot \sqrt{\alpha \cdot t}} + \frac{h \cdot \sqrt{\alpha \cdot t}}{k} \right) \right) \right] + T_{i-1,j}$$

Cooling stored in the slab (10 control volumes)

Properties of the air (for $T=20$ degC):

$$\text{degC} = 1$$

$$\rho_{\text{air}} := 1.2 \frac{\text{kg}}{\text{m}^3} \quad \text{density of air}$$

$$k_f := 0.0257 \frac{\text{watt}}{\text{m} \cdot \text{degC}} \quad \text{thermal conductivity}$$

$$C_{p\text{air}} := 1005 \frac{\text{joule}}{\text{kg} \cdot \text{degC}} \quad \text{specific heat capacity}$$

$$\nu := 0.00001511 \frac{\text{m}^2}{\text{sec}} \quad \text{kinematic viscosity}$$

$$\alpha_{\text{air}} := \frac{k_f}{\rho_{\text{air}} \cdot C_{p\text{air}}} \quad \text{thermal diffusivity}$$

$$\text{Pr} := \frac{\nu}{\alpha_{\text{air}}} \quad \text{Prandtl Number}$$

Outdoor temperature for 10 hours, entering 1st C.V. :

$$\begin{pmatrix} T_{0,1} \\ T_{1,1} \\ T_{2,1} \\ T_{3,1} \\ T_{4,1} \\ T_{5,1} \\ T_{6,1} \\ T_{7,1} \\ T_{8,1} \\ T_{9,1} \\ T_{10,1} \end{pmatrix} := \begin{pmatrix} 14.655 \\ 14.29 \\ 14.095 \\ 13.56 \\ 13.075 \\ 12.395 \\ 11.785 \\ 11.66 \\ 11.265 \\ 10.21 \\ 9.67 \end{pmatrix} \text{degC}$$

Calculation of the heat transfer coefficient:

$$U := 1.3 \frac{\text{m}}{\text{sec}} \quad \text{air velocity at inlet grilles}$$

$$i := 2..11$$

$$A_{\text{gr}} := 1.4 \text{m}^2 \quad \text{Opening area of grilles}$$

$$A_{\text{slab}} := 5.4 \text{m}^2 \quad \text{Slab area per control volume}$$

$$C_p := 1005 \frac{\text{joule}}{\text{kg} \cdot \text{degC}} \quad \text{specific heat capacity}$$

$$\text{Re}_{i-1} := \frac{U \cdot L_{i-1}}{\nu} \quad \text{Reynolds Number}$$

characteristic length for 10 control volumes:

$$\begin{pmatrix} L_1 \\ L_2 \\ L_3 \\ L_4 \\ L_5 \\ L_6 \\ L_7 \\ L_8 \\ L_9 \\ L_{10} \end{pmatrix} := \begin{pmatrix} 1.5 \\ 4.5 \\ 7.5 \\ 10.5 \\ 13.5 \\ 16.5 \\ 19.5 \\ 22.5 \\ 25.5 \\ 28.5 \end{pmatrix} \text{m}$$

$$Ts_{0,i-1} := 19.8 \text{degC}$$

Initial surface temperature of the slab for 10 control volumes

$$Nu_{i-1} := 0.332 \cdot \left(Re_{i-1} \right)^{\frac{1}{2}} \cdot Pr^{\frac{1}{3}}$$

Nusselt number for laminar boundary layer, external flows for flat plate, average velocity

$$h_{i-1} := \frac{Nu_{i-1} \cdot k_f}{L_{i-1}}$$

convective heat transfer coefficient

Properties of floor slab:

$$\rho := 1700 \frac{\text{kg}}{\text{m}^3}$$

density

$$k_s := 1.7 \frac{\text{watt}}{\text{m} \cdot \text{degC}}$$

thermal conductivity

$$c := 800 \frac{\text{joule}}{\text{kg} \cdot \text{degC}}$$

specific heat capacity

$$\alpha := \frac{k_s}{\rho \cdot c}$$

thermal diffusivity

Calculation of the slab surface temperature and heat transfer:

$$k := 1..10$$

$$t_k := k \cdot 1 \text{hr}$$

$$t := 1 \text{hr}$$

$$qs_{k-1,i-1} := h_{i-1} \cdot \left(To_{0,1} - Ts_{0,i-1} \right) \cdot \exp \left[\frac{h_{i-1}^2 \cdot \alpha \cdot t}{k_s^2} \right] \cdot \left(1 - \text{erf} \left(\frac{h_{i-1} \cdot \sqrt{\alpha \cdot t}}{k_s} \right) \right)$$

Define initial conditions. Heat flow to slab of C.V. 1 at time 0

$$To_{k-1,i} := To_{k-1,i-1} - \frac{qs_{k-1,i-1} \cdot A_{\text{slab}}}{\rho_{\text{air}} \cdot U \cdot A_{\text{gr}} \cdot C_p}$$

Temperature of the air stream exiting one C.V. and entering next C.V.

$$T_{s_{k,i-1}} := \left| T_{o_{k-1,i-1}} - T_{s_{k-1,i-1}} \right| \cdot \left[1 - \exp\left(\frac{|h_{i-1}|^2 \cdot \alpha \cdot t}{k_s^2}\right) \cdot \left(1 - \operatorname{erf}\left(\frac{h_{i-1} \cdot \sqrt{\alpha \cdot t}}{k_s}\right) \right) \right] + T_{s_{k-1,i-1}}$$

Slab surface temperature at different times

$$q_{s_{k,i-1}} := h_{i-1} \cdot \left| T_{o_{k,i-1}} - T_{s_{k,i-1}} \right| \cdot \exp\left(\frac{|h_{i-1}|^2 \cdot \alpha \cdot t}{k_s^2}\right) \cdot \left(1 - \operatorname{erf}\left(\frac{h_{i-1} \cdot \sqrt{\alpha \cdot t}}{k_s}\right) \right)$$

Heat flow to slab, for every C.V. at time t

$$T_{o_{k,i}} := T_{o_{k,i-1}} - \frac{q_{s_{k,i-1}} \cdot A_{slab}}{\rho_{air} \cdot U \cdot A_{gr} \cdot C_p}$$

Temperature of the air stream exiting one C.V. and entering next C.V.

$$T_{s_{k,i-1}} := \left| T_{o_{k-1,i-1}} - T_{s_{k-1,i-1}} \right| \cdot \left[1 - \exp\left(\frac{|h_{i-1}|^2 \cdot \alpha \cdot t}{k_s^2}\right) \cdot \left(1 - \operatorname{erf}\left(\frac{h_{i-1} \cdot \sqrt{\alpha \cdot t}}{k_s}\right) \right) \right] + T_{s_{k-1,i-1}}$$

Slab surface temperature at different times

$$q_{s_{k,i-1}} := h_{i-1} \cdot \left| T_{o_{k,i-1}} - T_{s_{k,i-1}} \right| \cdot \exp\left(\frac{|h_{i-1}|^2 \cdot \alpha \cdot t}{k_s^2}\right) \cdot \left(1 - \operatorname{erf}\left(\frac{h_{i-1} \cdot \sqrt{\alpha \cdot t}}{k_s}\right) \right)$$

Heat slab to floor, for every C.V. at time t

$$q_{stored_{k,i-1}} := q_{s_{k,i-1}} \cdot A_{slab}$$

Heat removal rate per control volume

$$q_{total} := \sum_{i=2}^{11} \sum_{k=1}^{10} \left[|q_{stored_{k,i-1}}| \cdot 1hr \right]$$

Cooling stored/ heat removed

$$q_{building} := q_{total} \cdot 16$$

Cooling stored/ heat removed for 8 floors , 864 sqm

Night time heat removal from building's thermal mass

Weather data for the cooling season:

| 2007 | Tmean outside | Avg ΔTo |
|-----------|---------------|---------|
| Month | | |
| April | 5.9 | 8.3 |
| May | 14.1 | 12 |
| June | 20 | 11.5 |
| July | 20.6 | 9.4 |
| August | 20.5 | 10.7 |
| September | 17.1 | 11.6 |
| October | 11.6 | 9.7 |
| | | |
| 2008 | Tmean outside | Avg ΔTo |
| Month | | |
| April | 8.2 | 11.4 |
| May | 12.8 | 11 |
| June | 19.7 | 9 |
| July | 21.6 | 9 |
| August | 19.7 | 10 |
| September | 16.9 | 10.4 |
| October | 8.6 | 9.3 |

Properties of the air (for T=20 degC):

$$\rho := 1.2 \frac{\text{kg}}{\text{m}^3} \quad \text{density of air}$$

$$C_p := 1005 \frac{\text{joule}}{\text{kg} \cdot \text{degC}} \quad \text{specific heat capacity}$$

Heat transfer rate at which heat may be removed for the building thermal mass:

$$T_{\text{icsp}} := 25 \text{degC} \quad \text{cooling setpoint}$$

$$q_{\text{night}_i} := M \cdot C_p \cdot |T_{\text{icsp}} - T_{o_i}|$$

$$q_{\text{night}_i} := \text{if} \left[|T_{o_i} > 8 \text{degC}| \cdot |T_{o_i} < 25 \text{degC}|, q_{\text{night}_i}, 0 \right] \quad \text{temperature condition (3 night schedules)}$$

Total energy removed from the building's thermal mass during the evening may be used to offset internal gains on the subsequent day:

$$\Delta t := 10 \text{hr} \quad \text{workday time period}$$

$$q_{\text{nighttotal}} := \sum_{i=19}^{23} q_{\text{night}_i} \cdot 1 \text{hr} + \sum_{i=0}^6 q_{\text{night}_i} \cdot 1 \text{hr}$$

$$q_{\text{avgcool}} := \frac{q_{\text{nighttotal}}}{\Delta t}$$

workday time period

total heat removal during nighttime

average internal gain that may be offset the day after

Temperature outside:

$$\text{degC} := 1$$

$$T_{om} := 14.1 \text{degC} \quad \text{daily mean outside temperature}$$

$$\Delta T_o := 12 \text{degC} \quad \text{range of } T_o = (\text{max.} - \text{min.})$$

$$n := 1, 2, 3 \quad \text{harmonic index}$$

$$i := 0, 1, \dots, 23 \quad \text{time index}$$

$$w_n := 2 \cdot \frac{\pi \cdot n}{24} \frac{\text{rad}}{\text{hr}} \quad \text{fundamental frequency (period = 1 day)}$$

$$t_i := i \cdot \text{hr} \quad \text{time}$$

$$T_{o_i} := T_{om} + \frac{\Delta T_o}{2} \cdot \cos \left(w_n \cdot t_i - 5 \cdot \frac{\pi}{4} \right) \quad \text{outdoor temperature}$$

Mass flow rate:

$$U := 1.5 \frac{\text{m}}{\text{sec}} \quad \text{velocity of air stream}$$

$$A := 1.4 \text{m}^2 \quad \text{grilles opening area}$$

$$A_{\text{total}} := A \cdot 2 \cdot 8 \quad \text{total inlet grilles area for 2 facades, 8 floors}$$

$$M := \rho \cdot U \cdot A_{\text{total}} \quad \text{air mass flow rate}$$